

UV Remote Sensing

Larry J. Paxton

Larry.paxton@jhuapl.edu

240 228 6871

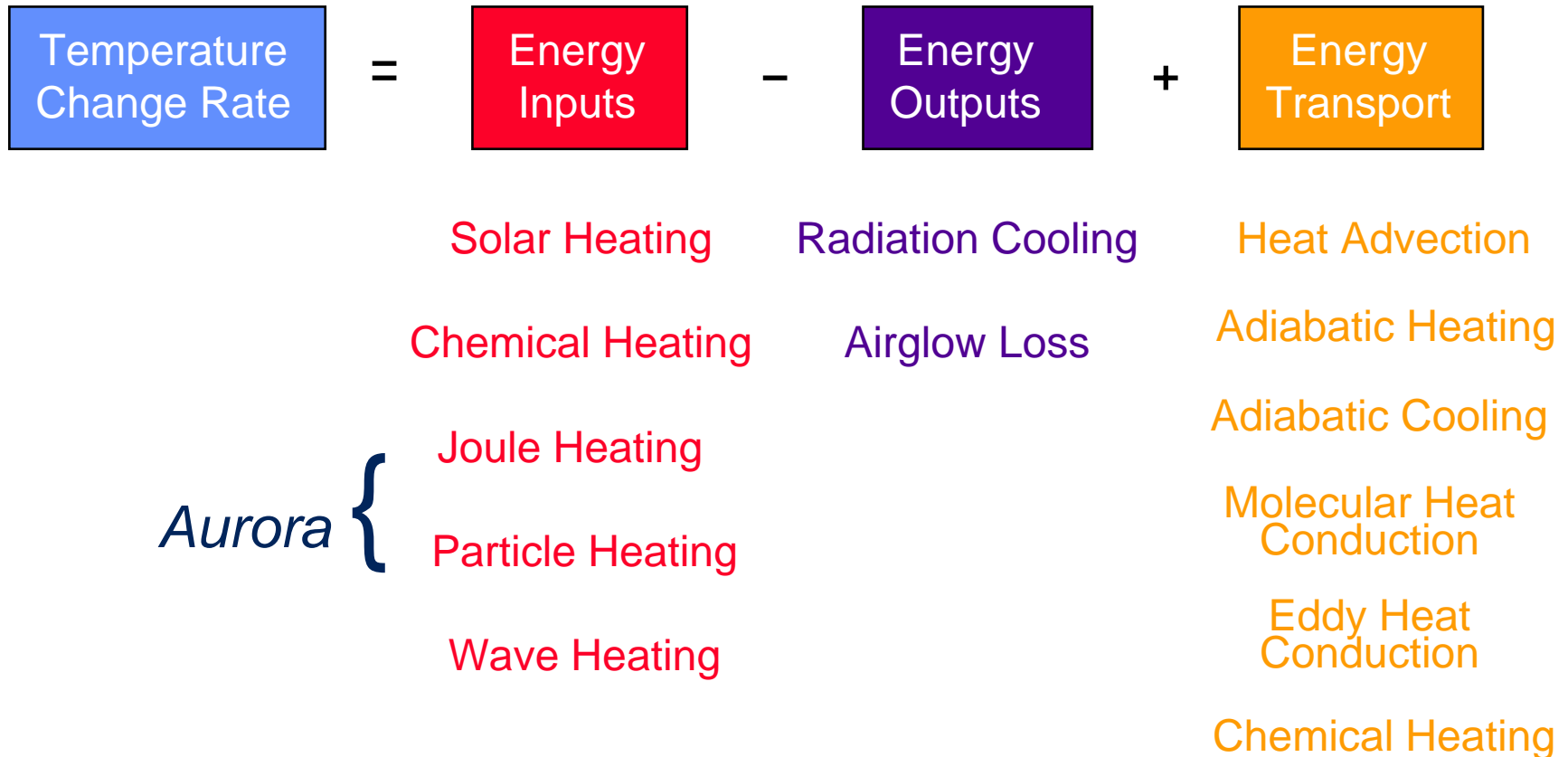
The logo for the Applied Physics Laboratory (APL) at Johns Hopkins University, consisting of the letters 'APL' in a large, bold, blue, sans-serif font.

The Johns Hopkins University
APPLIED PHYSICS LABORATORY

We Seek an Understanding of the Atmosphere of the Earth and Other Planets

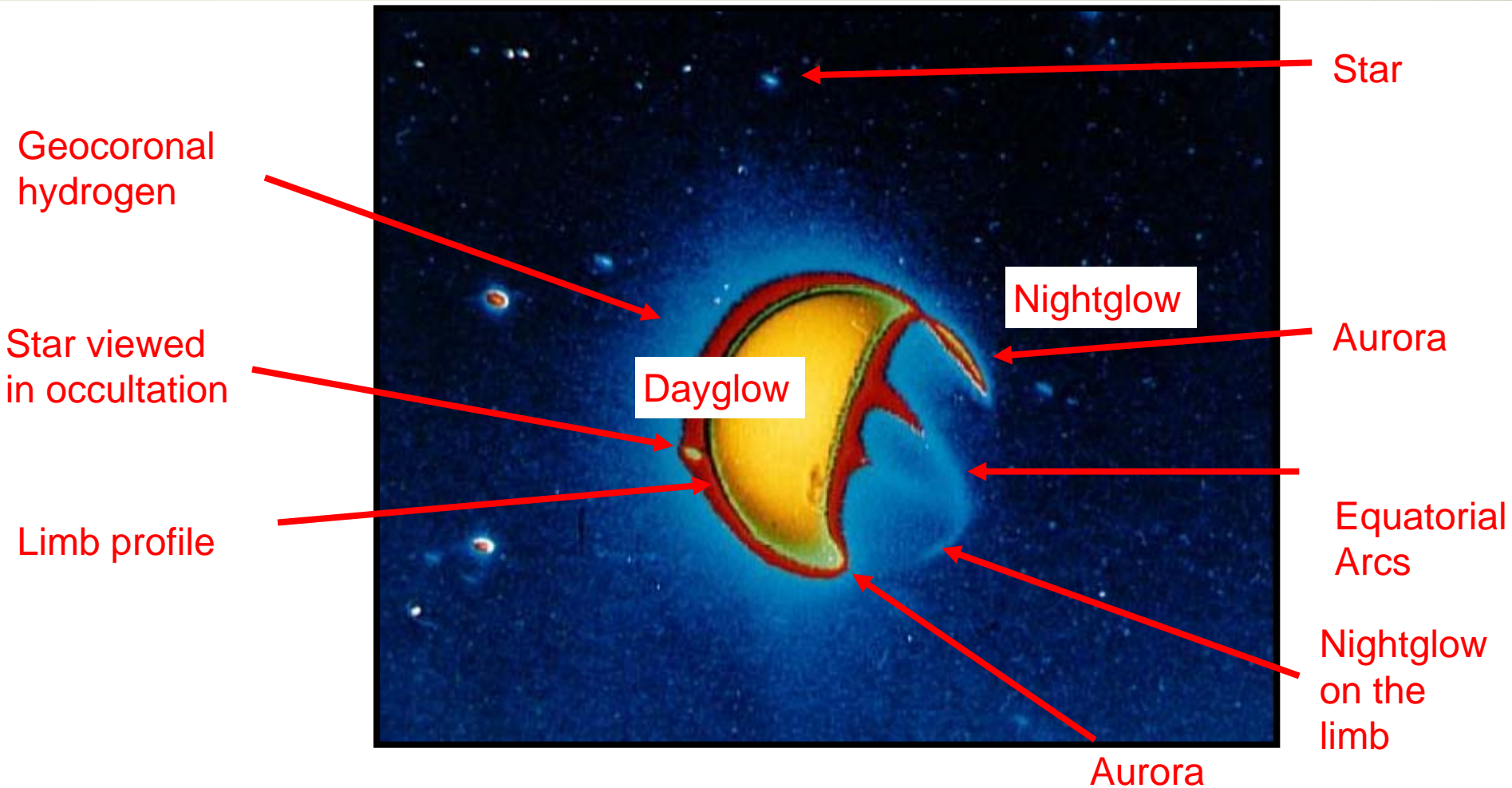
- **UV remote sensing provides us an important technique for understanding, as well as testing our understanding of, the connections between the upper atmosphere and**
 - **The Sun**
 - **The magnetosphere**
 - **The ring current and plasmasphere**
 - **The lower atmosphere**
- **as well as the connections between the ionosphere and the thermosphere.**
- **TIMED is the first mission to make a systematic exploration of the coupled-ionosphere thermosphere system.**
 - **What is the state of the IT system?**
 - **What are the drivers and what is the response?**
- **In this talk I will focus on the Far Ultraviolet (115 to 180 nm) because we have instruments routinely making observations at these wavelengths.**
- **FUV data has quantitative as well as qualitative information.**

To Understand the IT system We Have to Understand the Energy Balance



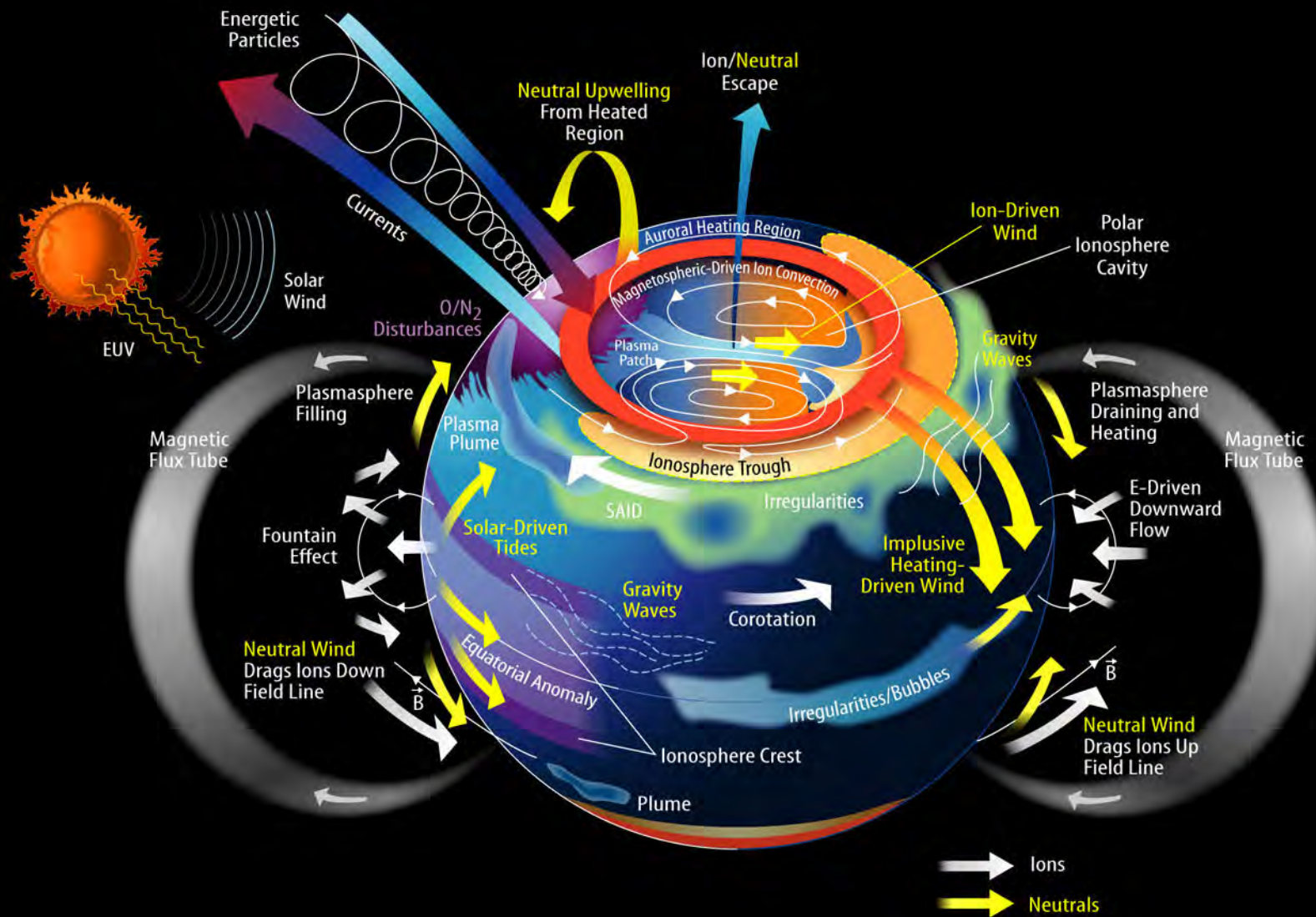
Many of these processes have optical signatures.

The Earth in the FUV: The Subject of this Talk



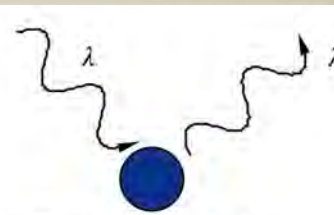
First FUV image of the Earth- taken from the Moon by the Apollo 16 crew
Carruthers and Page, 1972

The Near-Earth Space Environment is Externally Forced and Many of These Processes Have UV Signatures

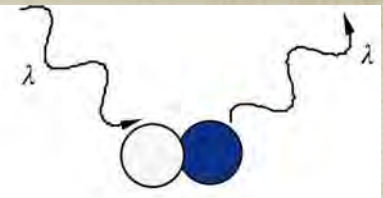


The processes that give rise to the emissions

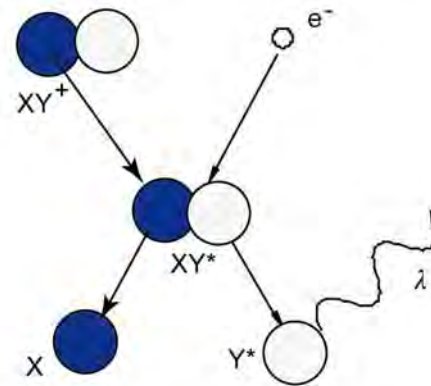
- From laboratory studies and more than half a century of sounding rocket observations and almost a century of ground-based spectroscopy, we know the mechanisms that produce the signatures seen in the Earth's optical spectrum.
- There are still many cross sections, processes, and reaction rates that are poorly known because they are difficult to measure in the lab.



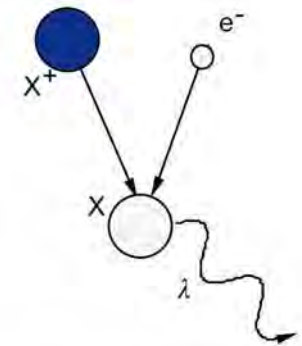
Resonant Scattering



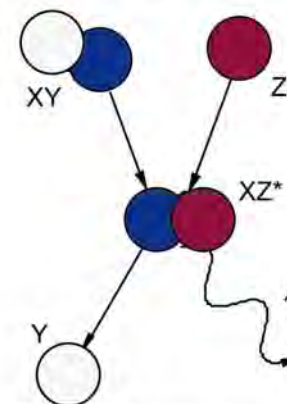
Fluorescent Scattering



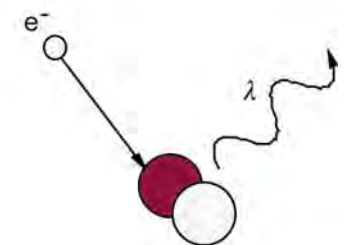
Dissociative Recombination



Radiative Recombination



Chemiluminescence



Electron Impact Excitation

Molecular Spectra Arise From Transitions Between Electronic States

- The N₂ Lyman-Birge-Hopfield bands (a ¹Π_g - X ¹Σ_g⁺) are an electric dipole forbidden transition but is allowed for magnetic dipole and electric quadrupole emission.
- The upper state, a, is excited by photoelectron impact excitation.

“blue” line

LBH

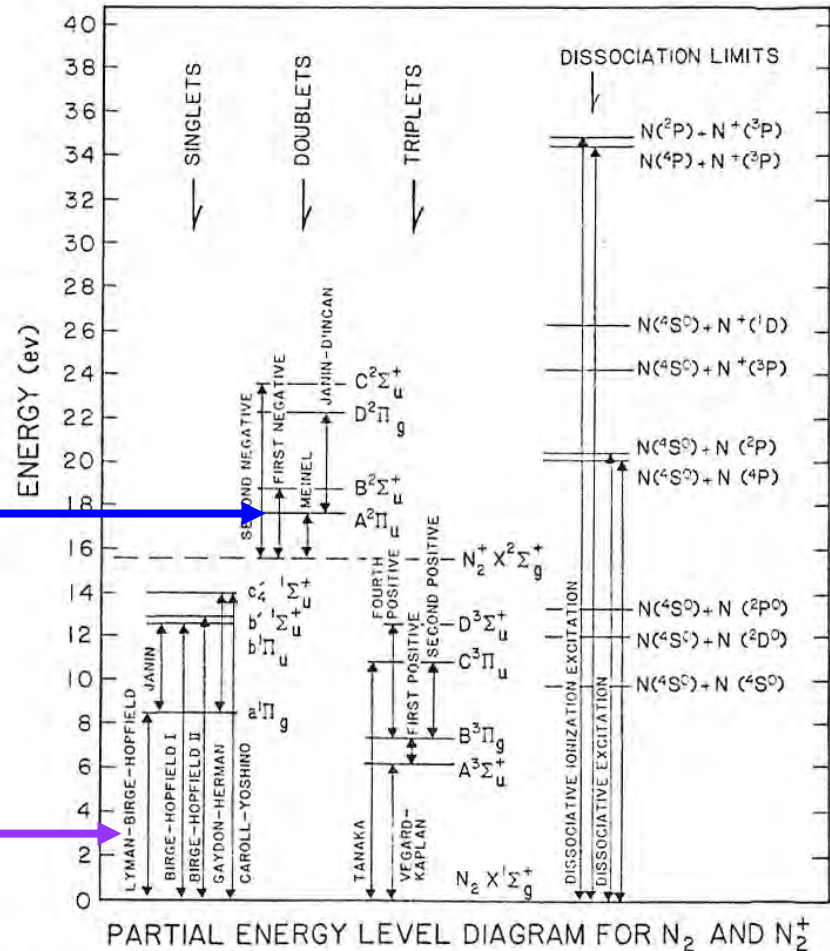


Fig. 39. Partial energy level diagram for N₂ and N₂⁺. Adapted from Ajello (1969).

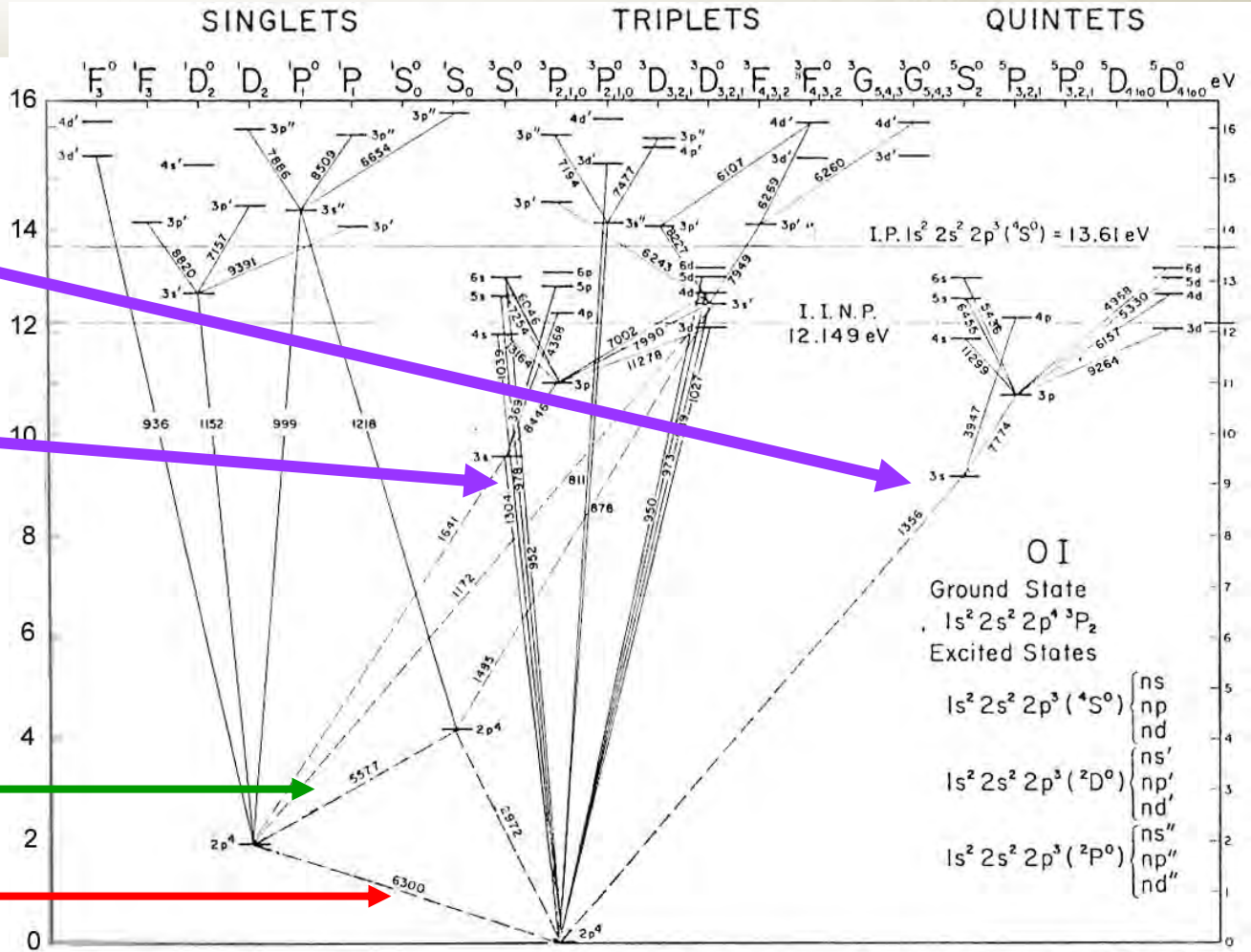
Atomic Transitions Adequately Understood

The OI 135.6 $2p^4 \ ^3P - 3s \ ^5S$ is spin forbidden and produces a doublet.

The OI 130.4 $2p^4 \ ^3P - 3s \ ^3S$ transition is allowed and produces a triplet.

Note the green line

And the red line



Partial energy level diagram of atomic oxygen. Forbidden transitions are indicated by dashed lines. Adapted from Tinsley (1972).

Radiative Transfer Theory is the Key to a Quantitative Understanding of Optical Observations

I is the spectral radiance (specific intensity) – photons $\text{cm}^{-2} \text{s}^{-1} \text{Hz}^{-1} \text{steradian}^{-1}$

$$\frac{dI}{ds} = -\chi I + \varepsilon$$

← Volume emissivity or number of photons $\text{cm}^{-3} \text{s}^{-1} \text{Hz}^{-1} \text{steradian}^{-1}$ added to the beam

↑ Probability per cm at a given frequency of the photon being scattered out of the beam – the extinction coefficient

↑ Change in intensity along a path length

From the Radiative Transfer Equation we can Derive Beer's Law

$$\frac{dI}{ds} = -\chi I + \varepsilon$$

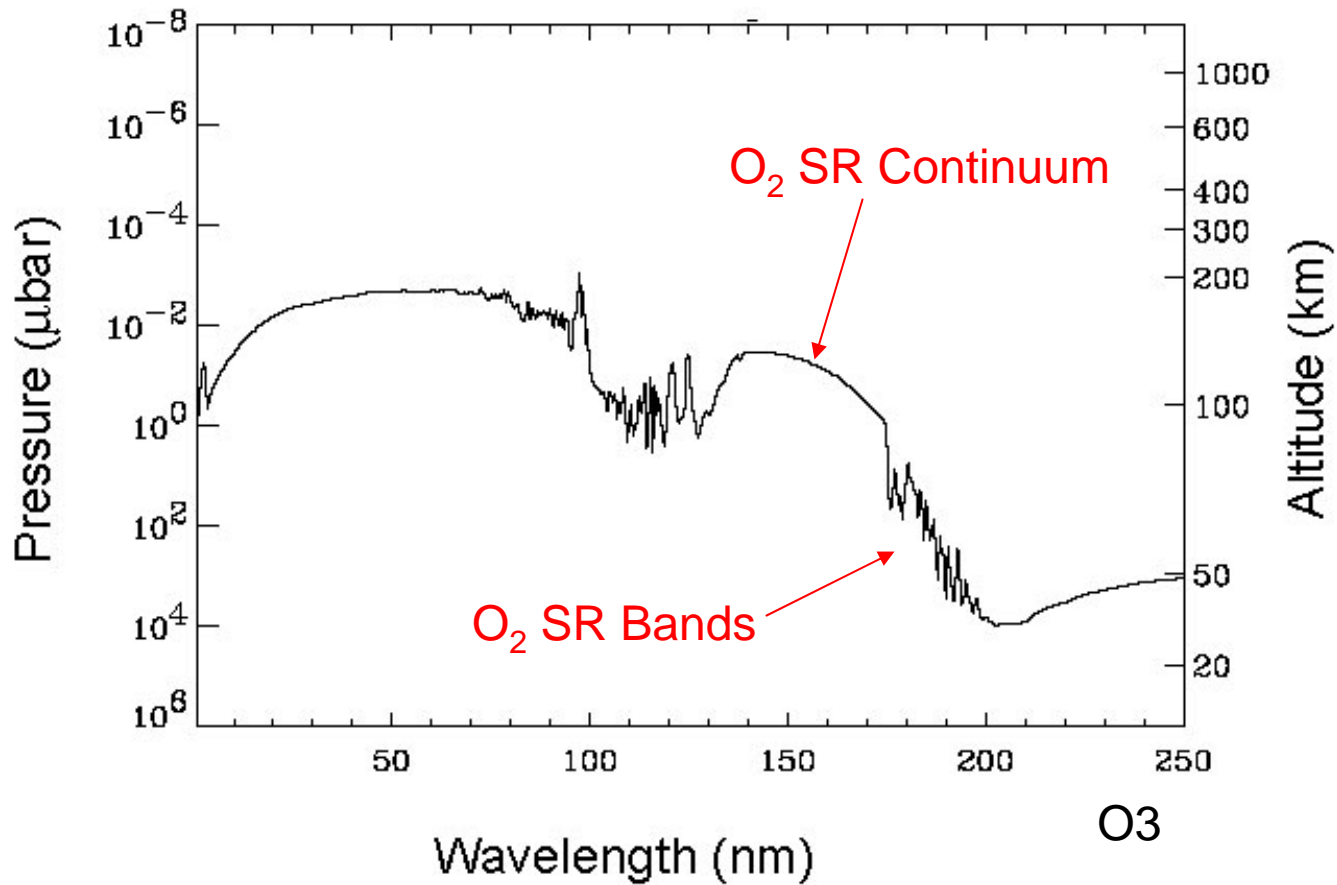
let $\varepsilon = 0$ and ignore resonant scattering then

$$I[r, \hat{n}, \nu] = I[\infty, \hat{n}, \nu] \exp[-\tau_a[\infty, r]]$$

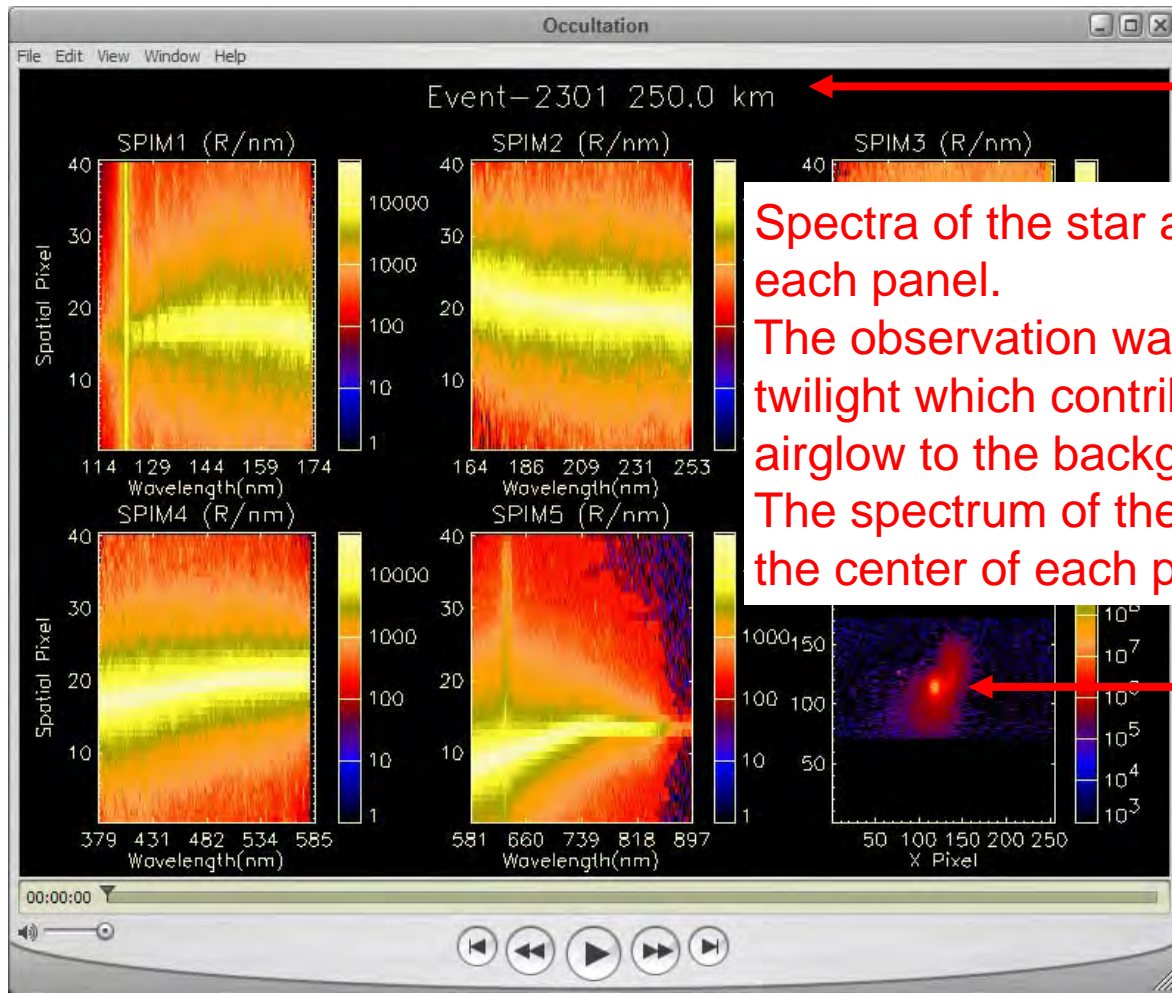
Where the absorption optical depth, t_a is given by

$$\tau_a[r', r, \nu] = \int_{s[r']}^{s[r]} \sigma_a[\nu] n[r] ds$$

Point at Which the Vertical Optical Depth Equals 1



Stellar Occultation Observation Illustrates the Principals of a Limb Observation, Absorption, Airglow, and Refraction.



Tangent altitude

Spectra of the star are shown in each panel.

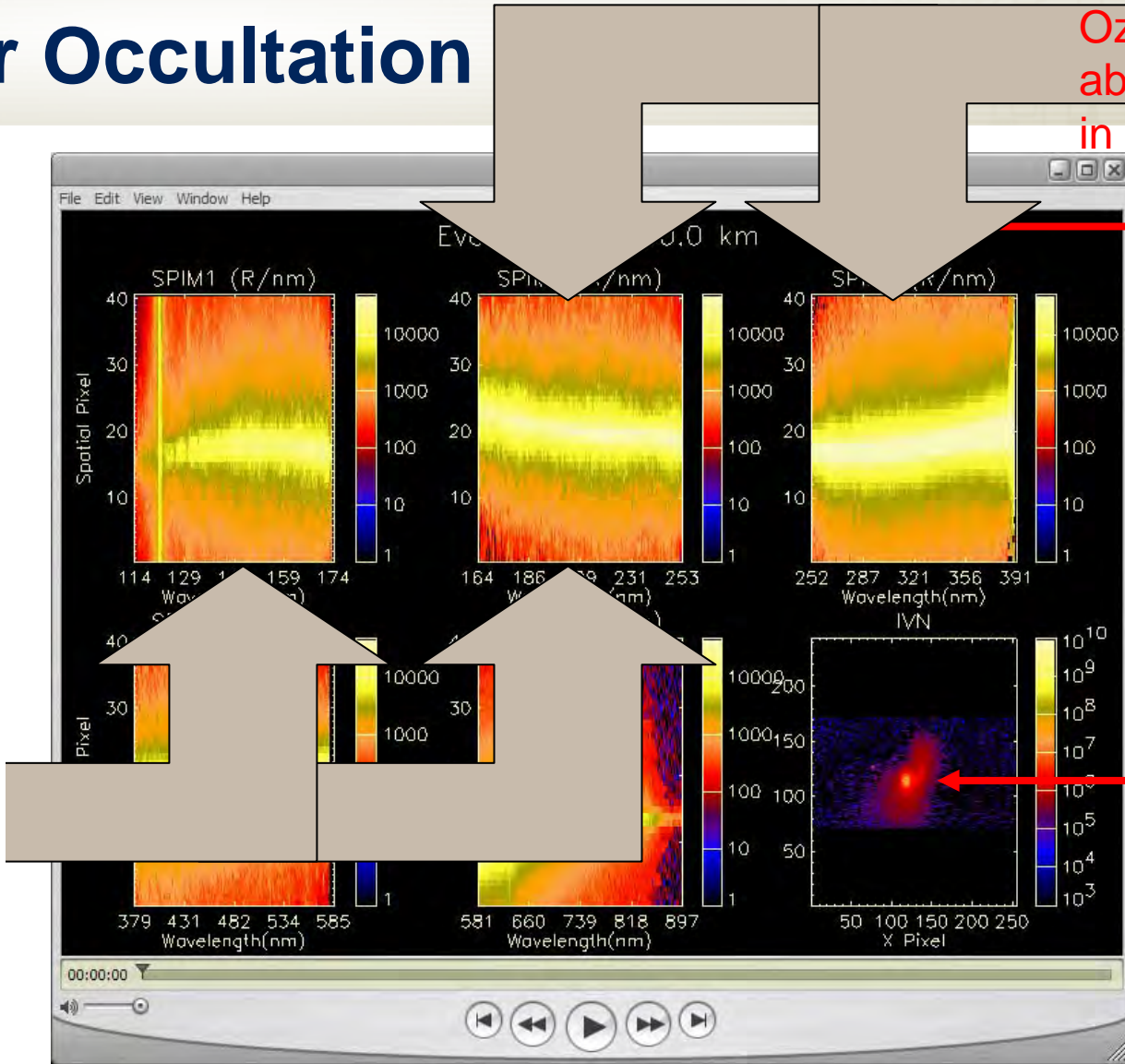
The observation was made at twilight which contributes some airglow to the background.

The spectrum of the star is in the center of each panel.

Image of star in a coaligned telescope

Stellar Occultation

FUV spectra are shown in SPIM1 and SPIM 2. Oxygen absorption is seen here.

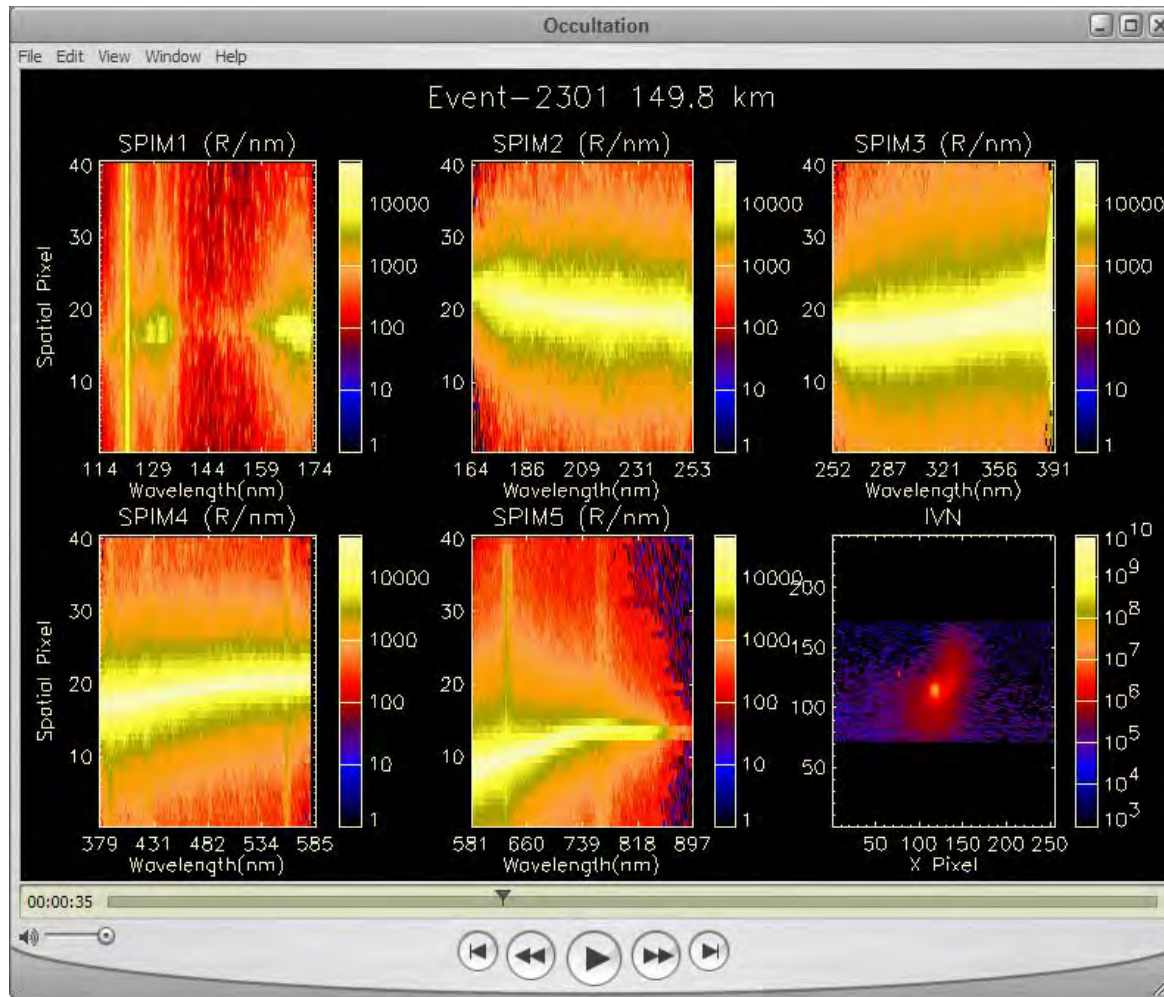


Ozone absorption seen in SPIM2 and 3

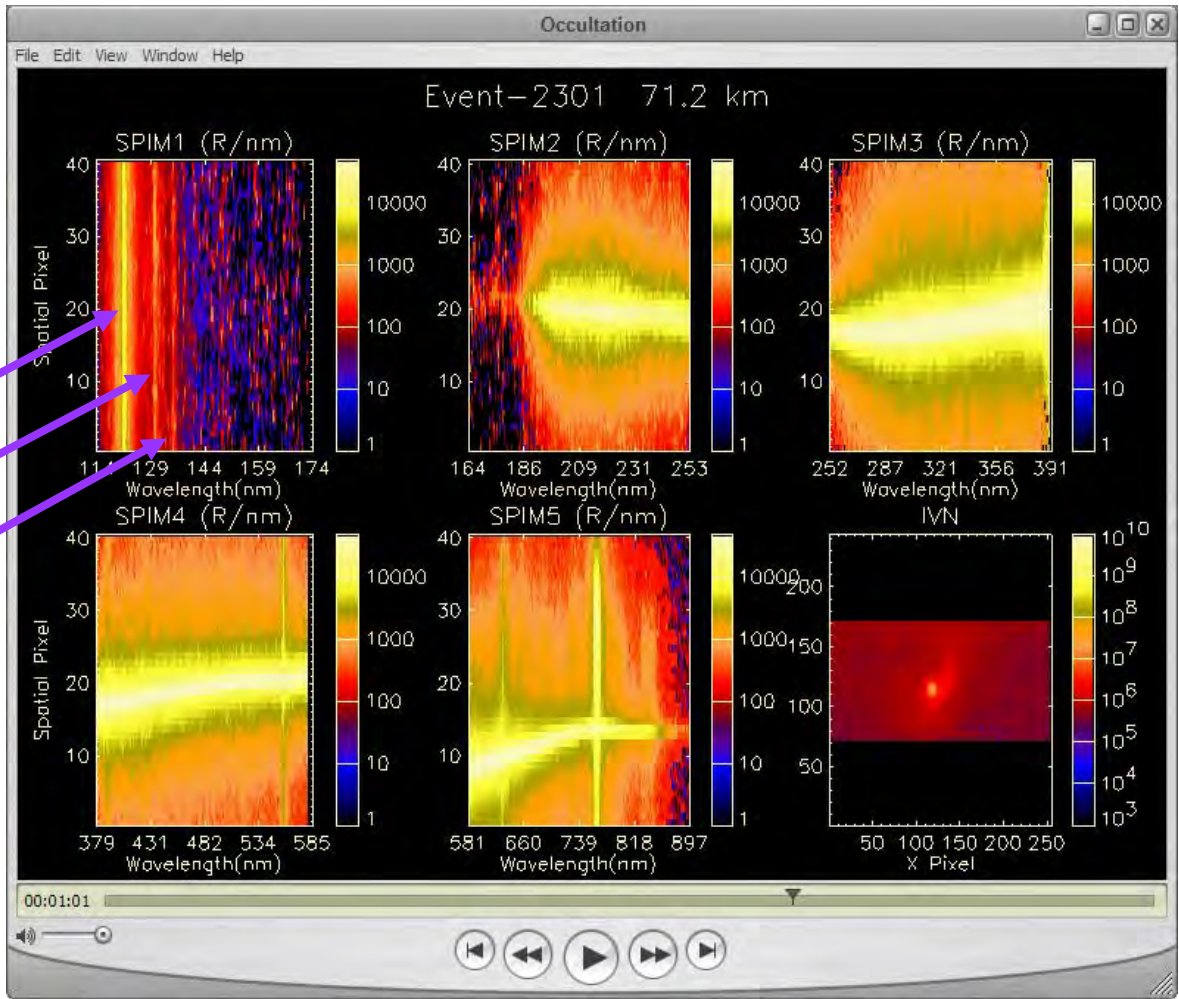
At the top of the atmosphere

Image of star in a coaligned telescope

FUV Spectrum shows O₂ Absorption -150 km

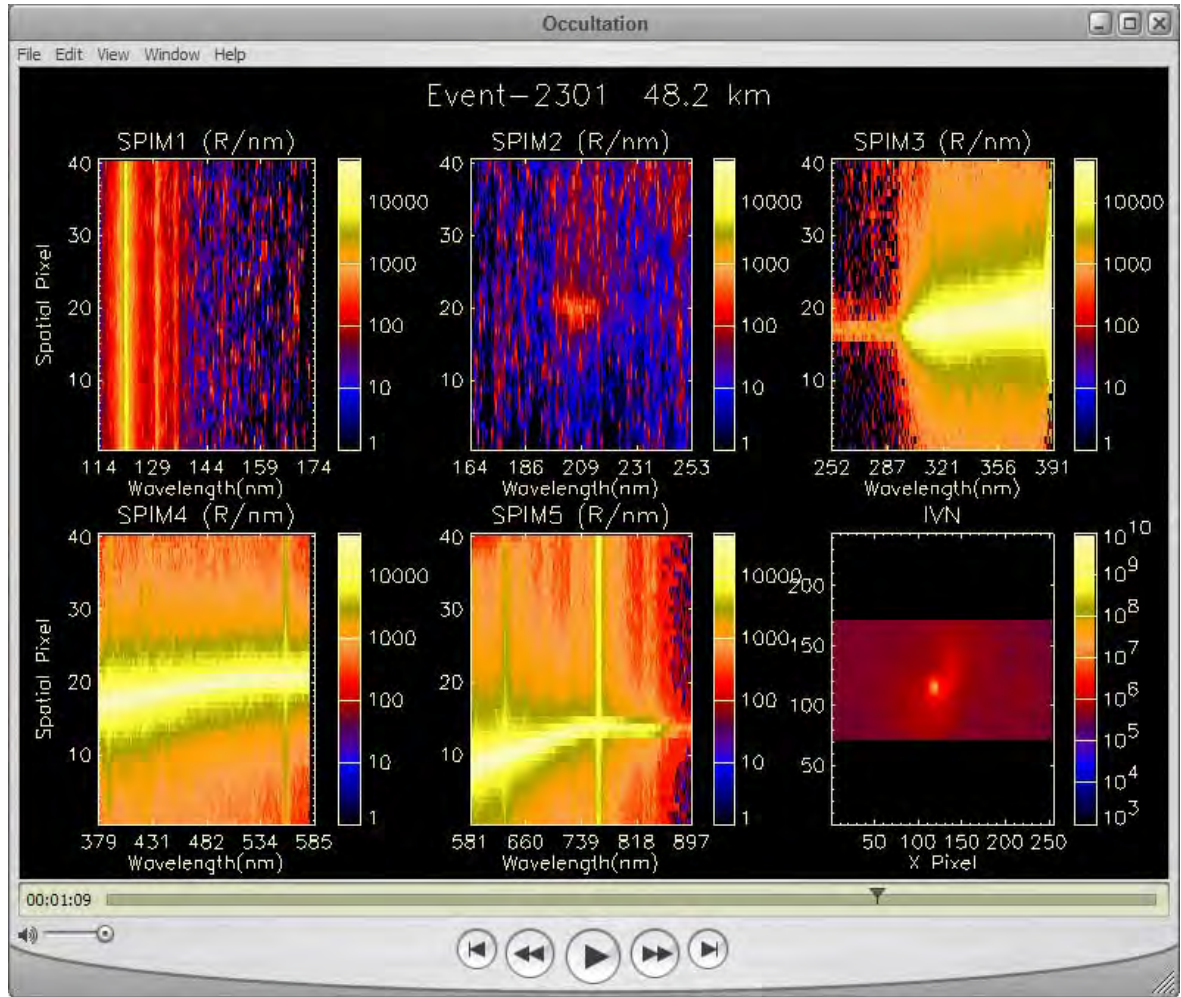


Stellar FUV is gone – only foreground airglow remains – 71 km

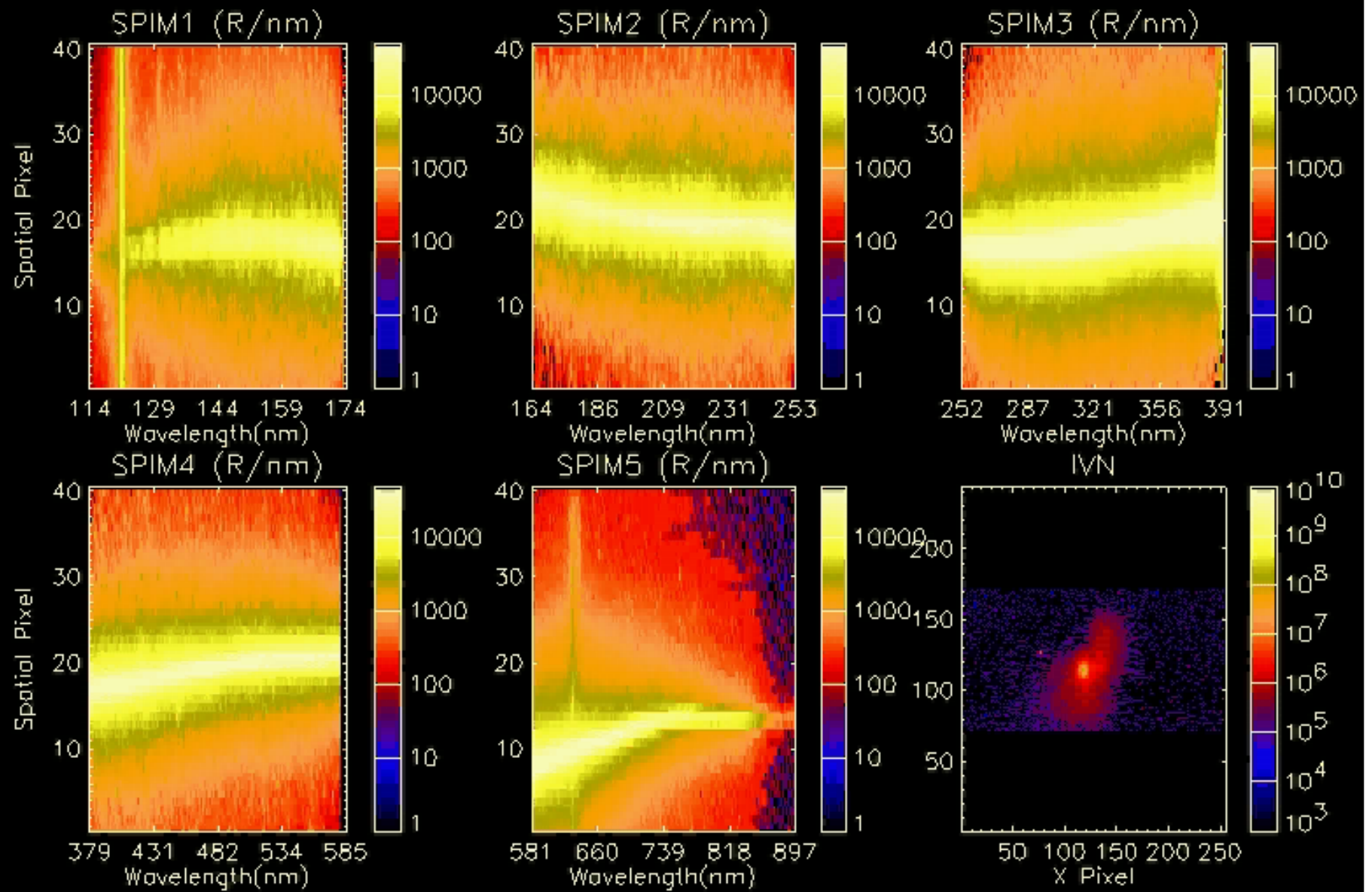


HI 121.6
OI 130.4
OI 135.6

MUV Airglow is gone and stellar spectrum is severely attenuated -48 km



Event-2301 250.0 km



Click on the image to view the movie

And Now for Something Completely Different....

The General Form of the Radiative Transfer Equation Includes Multiple Scattering

Formal solution of the RT equation

$$I[\mathbf{r}, \hat{\mathbf{n}}, \nu] = I[\infty, \hat{\mathbf{n}}, \nu] \exp[-\tau[\infty, \mathbf{r}, \nu] - t_a[\infty, \mathbf{r}]] + \int \varepsilon[\mathbf{r}, \hat{\mathbf{n}}, \nu] \exp[-\tau[\mathbf{r}, \nu] - t_a[\mathbf{r}, \mathbf{r}']] ds$$

Solving the integral form of the emission rate

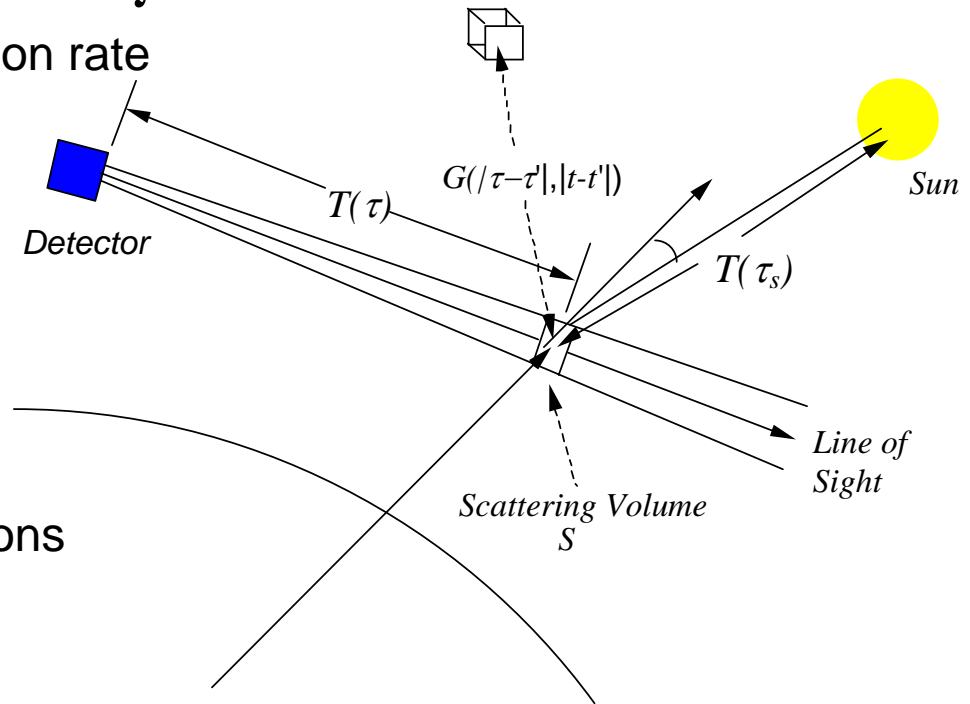
$$I[\vec{r}, \hat{\mathbf{n}}] = \frac{1}{4\pi} \int S[\tau'] T[\tau'] d\tau'$$

where

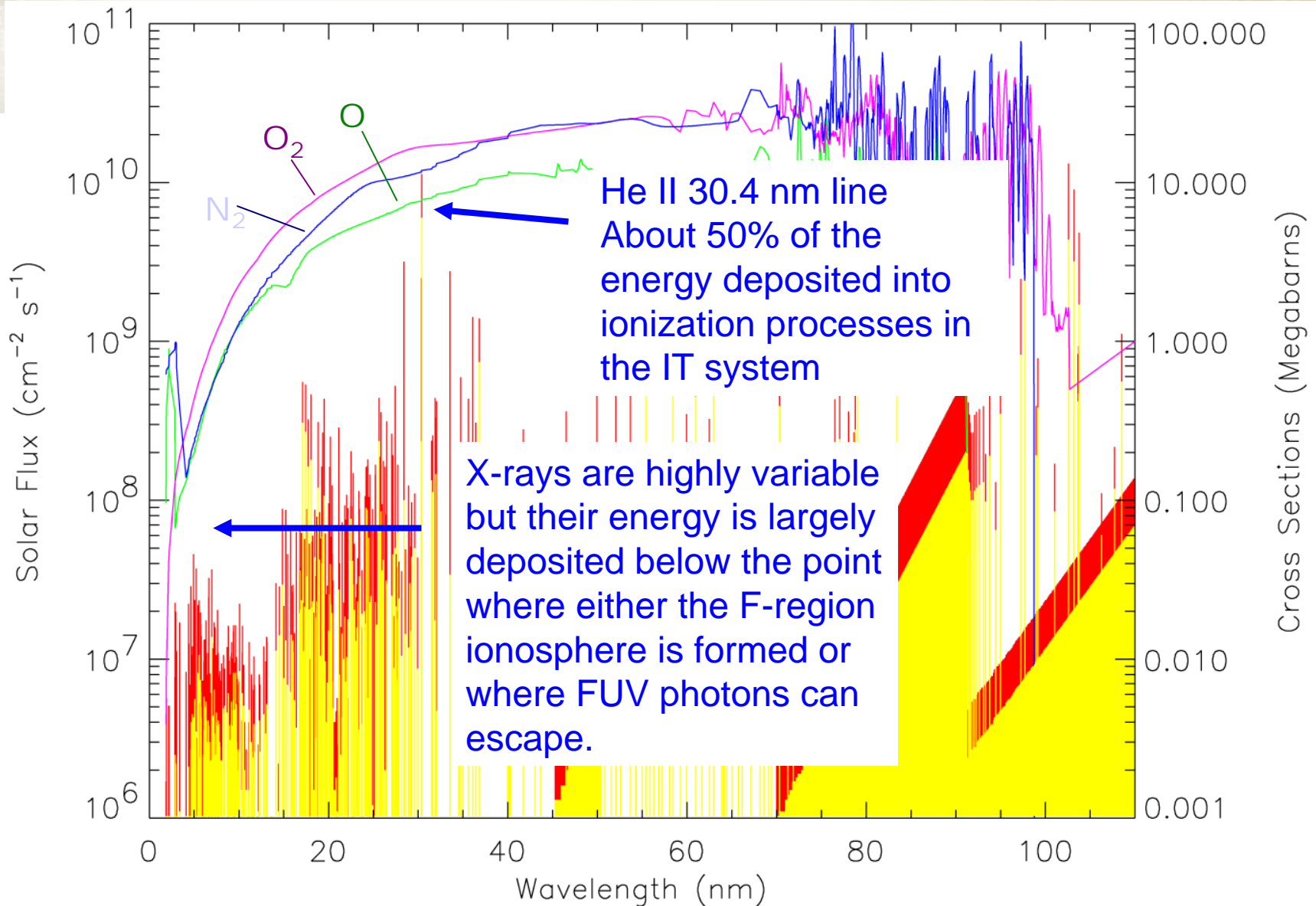
$$S[\tau] = S_0[\tau] + \int \frac{d\Omega'}{4\pi} \int S[\tau'] G[\tau', \tau] d\tau'$$

$$S_0 = \frac{4\pi\varepsilon_0[\vec{r}]}{\sigma_0 n[\vec{r}]} = \frac{g[\vec{r}]}{\sigma_0} \quad \text{for photoelectrons}$$

$$S_0 = \frac{4\pi\varepsilon_s[\vec{r}]}{\sigma_0 n[\vec{r}]} = \pi F \sqrt{\pi} \Delta \nu_D T(\tau_s) \quad \text{for solar resonant scattering}$$



Solar EUV and Atmospheric Cross Sections – Red is for Solar Maximum



Photoelectron Flux Calculations Show the Dependence on the Neutral Atmosphere

$$\frac{d\phi^+}{ds} = \frac{-1}{\langle \cos \theta \rangle} \sum_k n_k [\sigma_a^k + p_e^k \sigma_e^k] \phi^+ + \frac{1}{\langle \cos \theta \rangle} \sum_k n_k p_e^k \sigma_e^k \phi^- + \frac{q}{2} + \frac{q^+}{\langle \cos \theta \rangle}$$

$$-\frac{d\phi^-}{ds} = \frac{-1}{\langle \cos \theta \rangle} \sum_k n_k [\sigma_a^k + p_e^k \sigma_e^k] \phi^- + \frac{1}{\langle \cos \theta \rangle} \sum_k n_k p_e^k \sigma_e^k \phi^+ + \frac{q}{2} + \frac{q^-}{\langle \cos \theta \rangle}$$

mean pitch angle

Inelastic cross section

Elastic scattering cross section

contribution from direct photoionization

probability

photoelectron production in the range to due to cascading from higher energy photoelectrons undergoing inelastic collisions

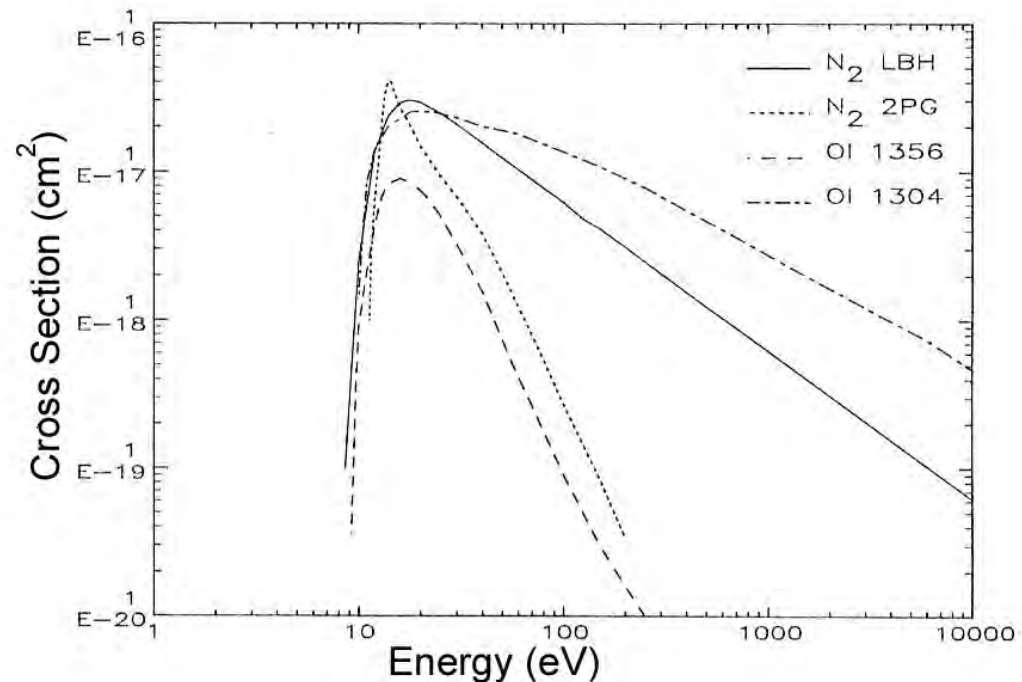
$$\sigma_a^k = \sum_j \sigma_{aj}^k$$

$$q^+(\varepsilon, s) = \sum_k n_k(s) \sum_{\substack{j \\ E > \varepsilon}} \{ p_{aj}^k(E) \sigma_{aj}^k(E \rightarrow \varepsilon) \phi^-(E, s) + [1 - p_{aj}^k(E)] \sigma_{aj}^k(E \rightarrow \varepsilon) \phi^+(E, s) \}$$

$$q^-(\varepsilon, s) = \sum_k n_k(s) \sum_{\substack{j \\ E > \varepsilon}} \{ p_{aj}^k(E) \sigma_{aj}^k(E \rightarrow \varepsilon) \phi^+(E, s) + [1 - p_{aj}^k(E)] \sigma_{aj}^k(E \rightarrow \varepsilon) \phi^-(E, s) \}$$

The Location of the Peak in the Cross Sections for Emission Due to Electron Impact is Important

- With a peak near 15 eV and an ionization energy for the major thermospheric constituents of around 15 eV, a photon has to have an energy of at least about 30 eV to be able to create a photoelectron that has a significant probability of exciting these FUV emissions.
- A 30 eV photon has a wavelength of about 40 nm.
- How far do these photons penetrate into the atmosphere?
- If they create a photon, can that photon escape?
- Are there many photons at those wavelengths and how does the solar spectrum vary with time?



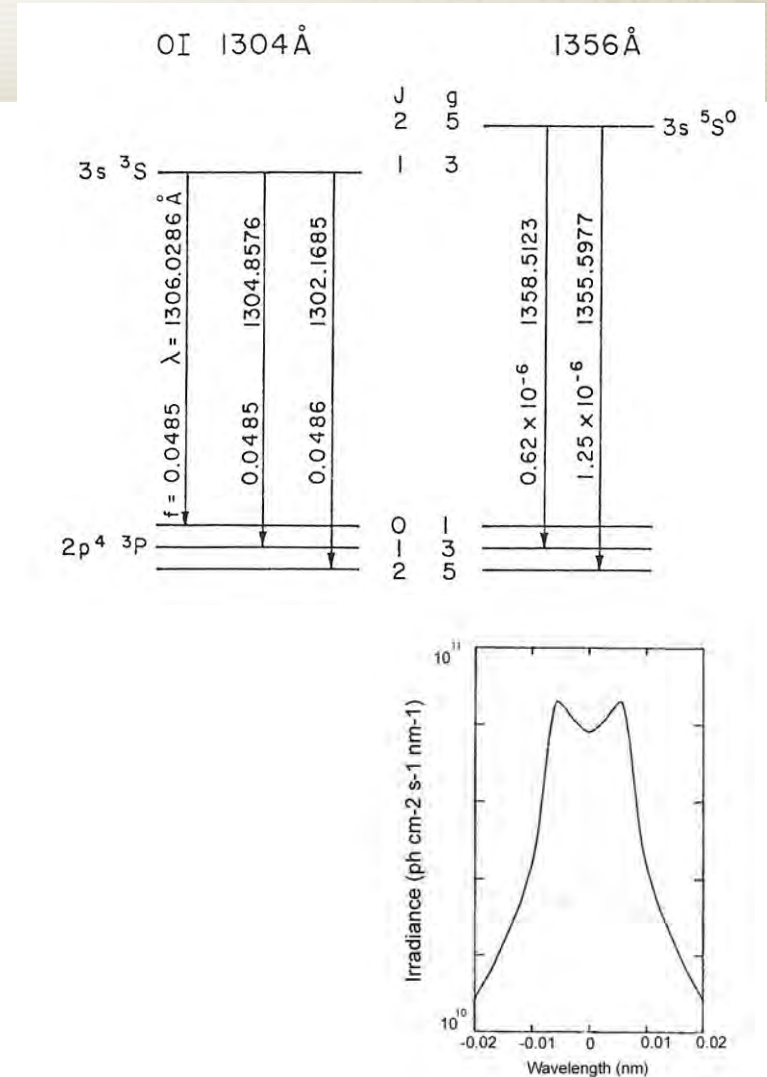
The atomic oxygen lines show self absorption effects

$$\sigma_T = \int \sigma[\nu] d\nu = \frac{\pi e^2}{mc} f_{12} = \frac{h\nu_0}{4\pi} B_{12}$$

$$\sigma_0 = \frac{\sigma_T}{\sqrt{\pi} \Delta\nu_D} \quad \text{Line center cross section}$$

The line center optical depth is about 1 for OI 135.6 emissions but 100,000 for OI 130.4 above the $\tau=1$ point in the pure absorber.

The emissions at 130.4 show the effect of multiple scattering.

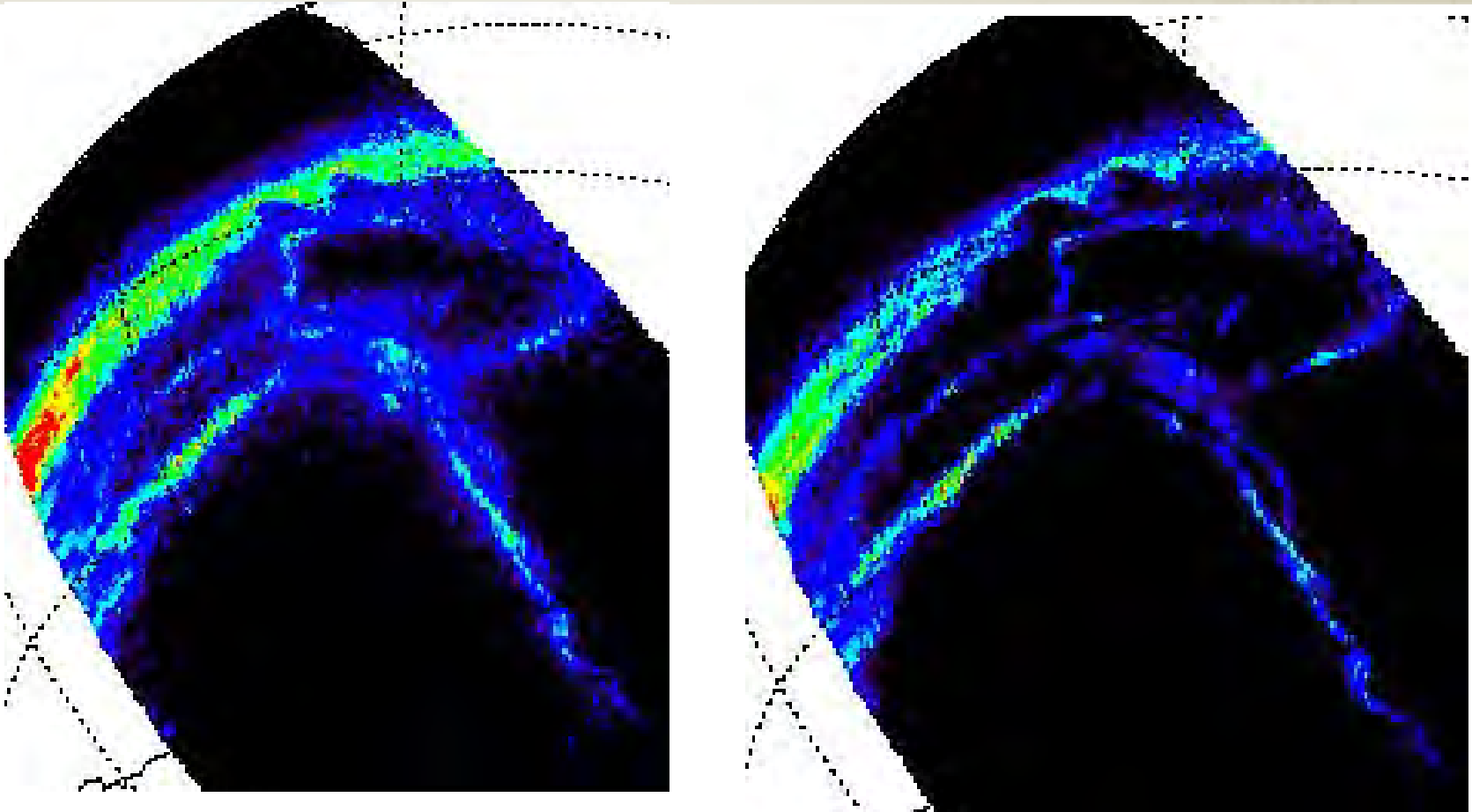


Solar 130.4 nm line

From Meier, 1991



130.4 nm Images Show the Effect of Multiple Scattering



- Narrowest features are 25 km across.
- September 10, 2005 over the south pole near midnight MLT.

FUV Spectrum of the Earth

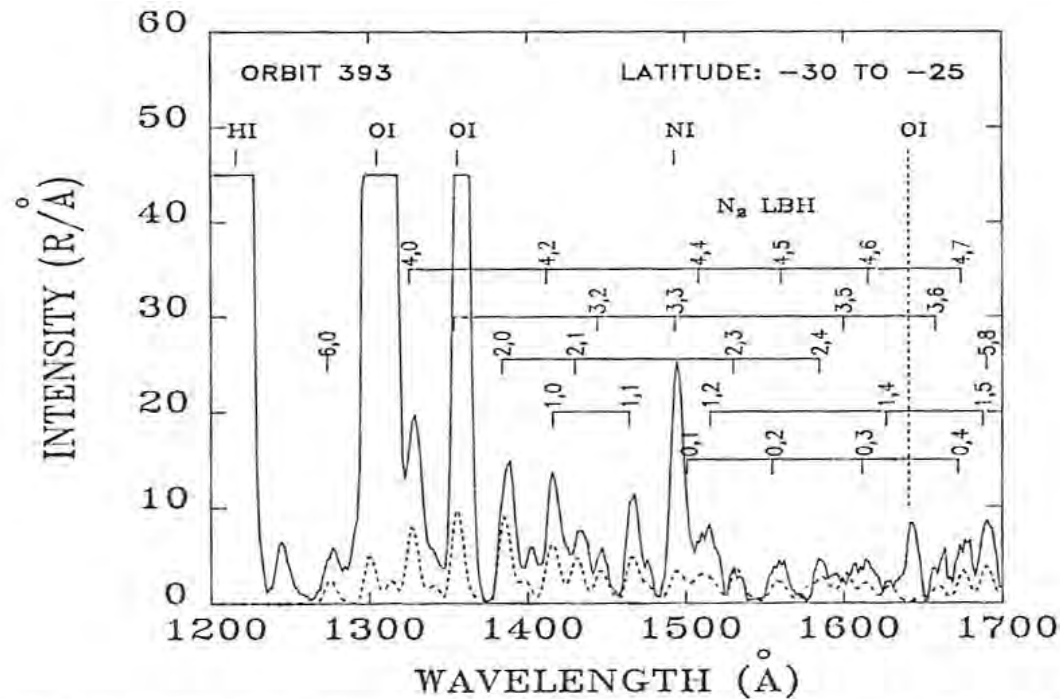
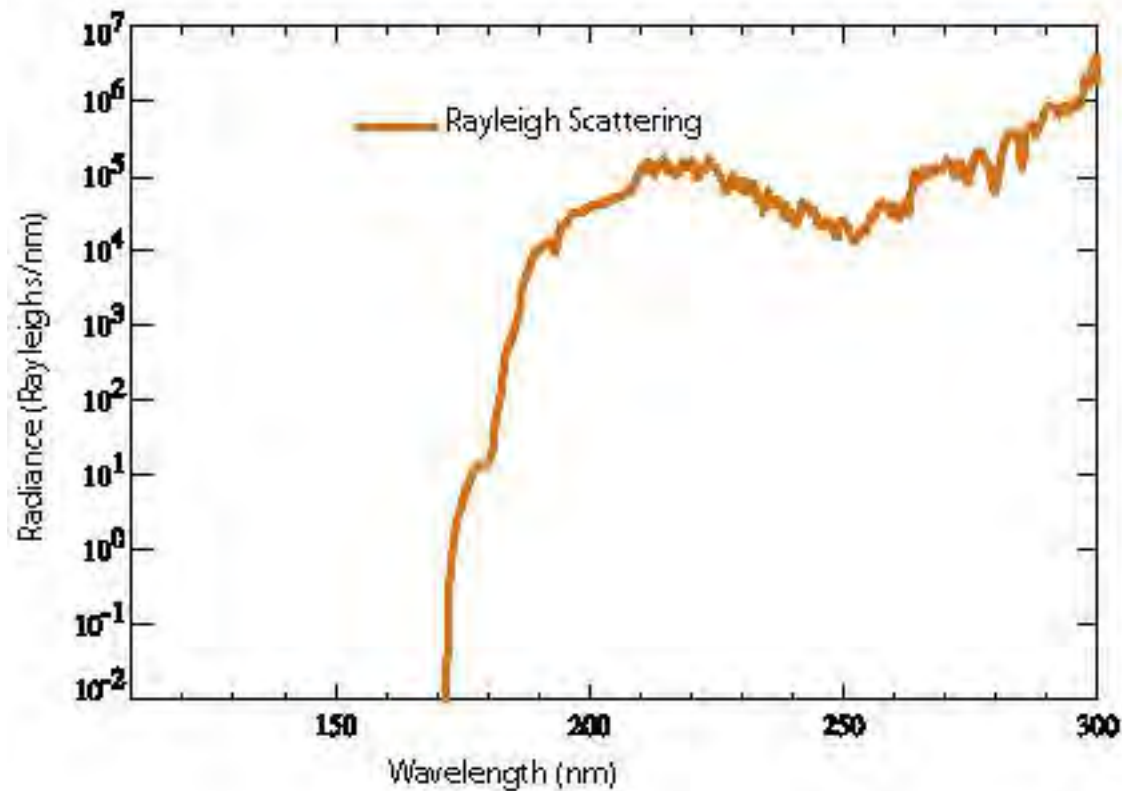


Fig. 6a. S3-4 FUV dayglow spectrum (solid line) on 9 April, 1978 for nadir viewing from 205 km (Conway *et al.*, 1988; Huffman *et al.*, 1980). The spectral resolution is 7 \AA . The dashed curve is the predicted N_2 LBH band band spectrum using a photoelectron model appropriate to the observation conditions and a Franck-Condon theoretical spectrum (R. Conway, private communication, 1988). No O, H, emission features were included in the theory. The excess emission seen in the S3-4 N_2 data is the result of spacecraft glow (Conway *et al.*, 1987, 1988). The bright H I and O I features in the S3-4 data have been truncated.

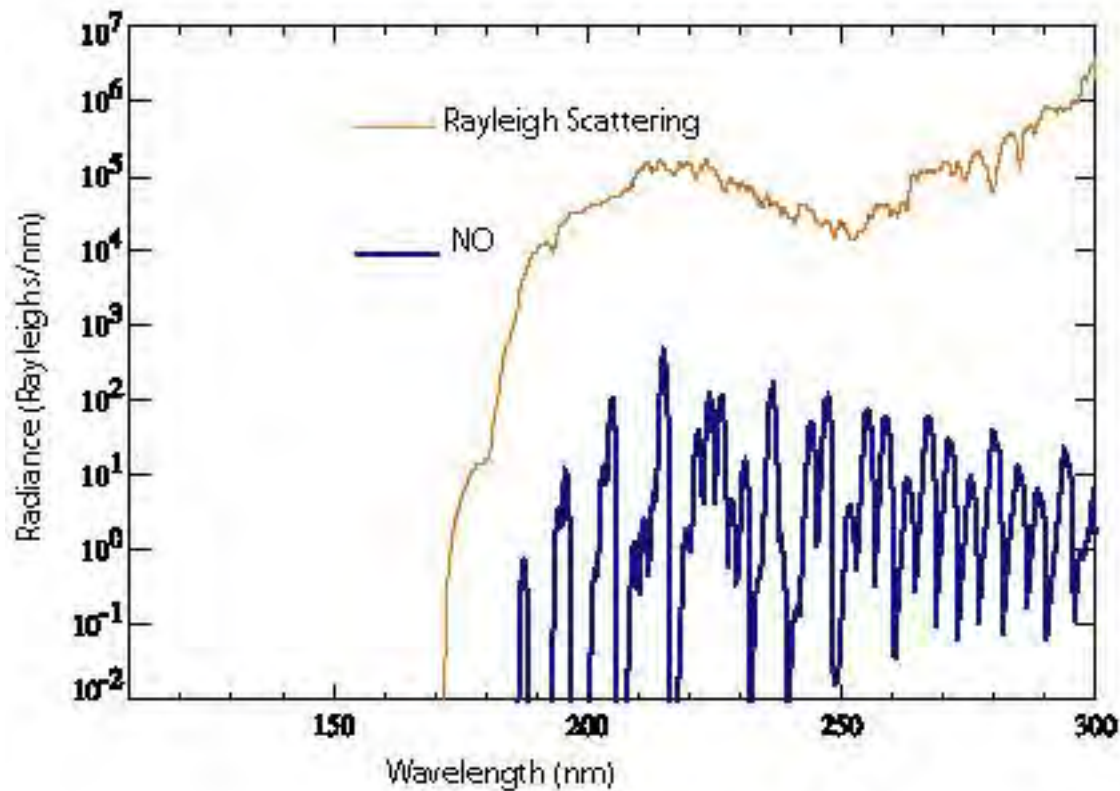
The Ability to Model the Spectrum is a Key Enabler for Quantitative Studies

- The ability to model the spectrum, and account for all the processes that contribute to emission, are key to the ability to design instruments as well as to recover quantitative information.
- The modeling effort requires an understanding of the scattering properties of the atmosphere, chemistry and excitation process.
- RT models build on decades of laboratory work in the measurement of cross sections for photon and particle processes.
 - There still are cross sections that need to be measured and processes that are poorly understood.
 - Some of these can only be addressed by using the atmosphere as a natural laboratory.
 - Lifetimes of processes may dictate a chamber size that is impractical.

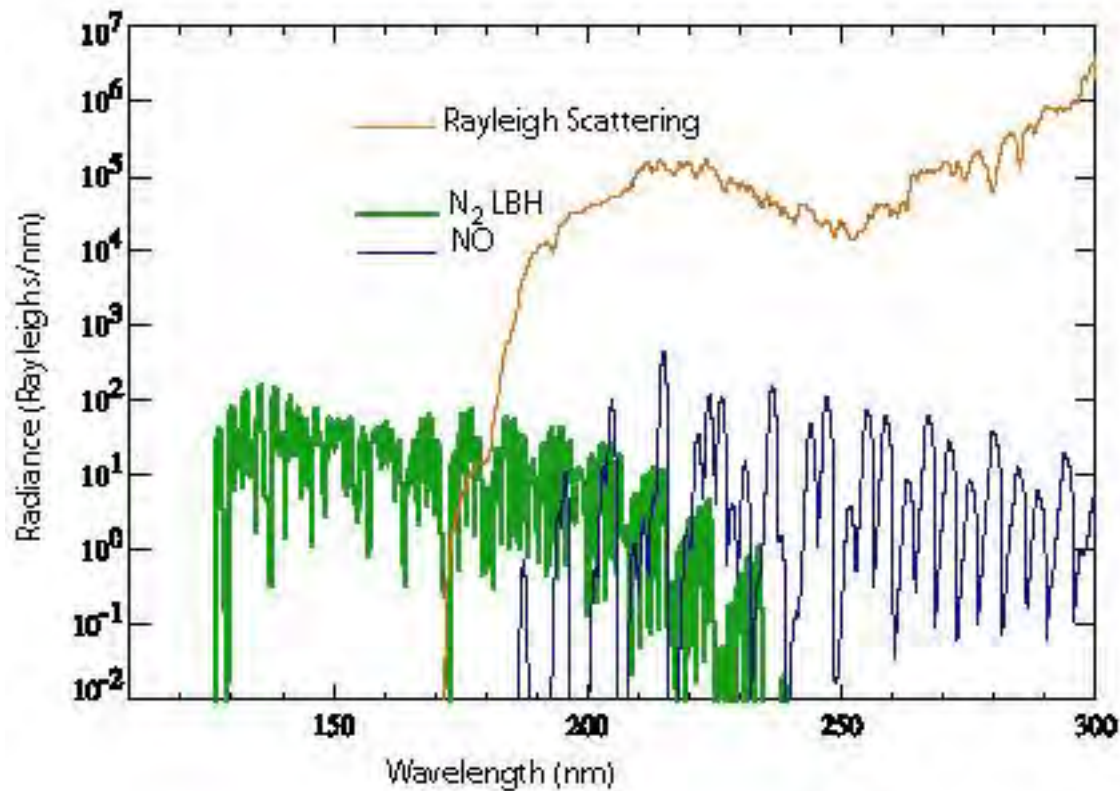
The Ability to Model the Spectrum is a Key Enabler for Quantitative Studies



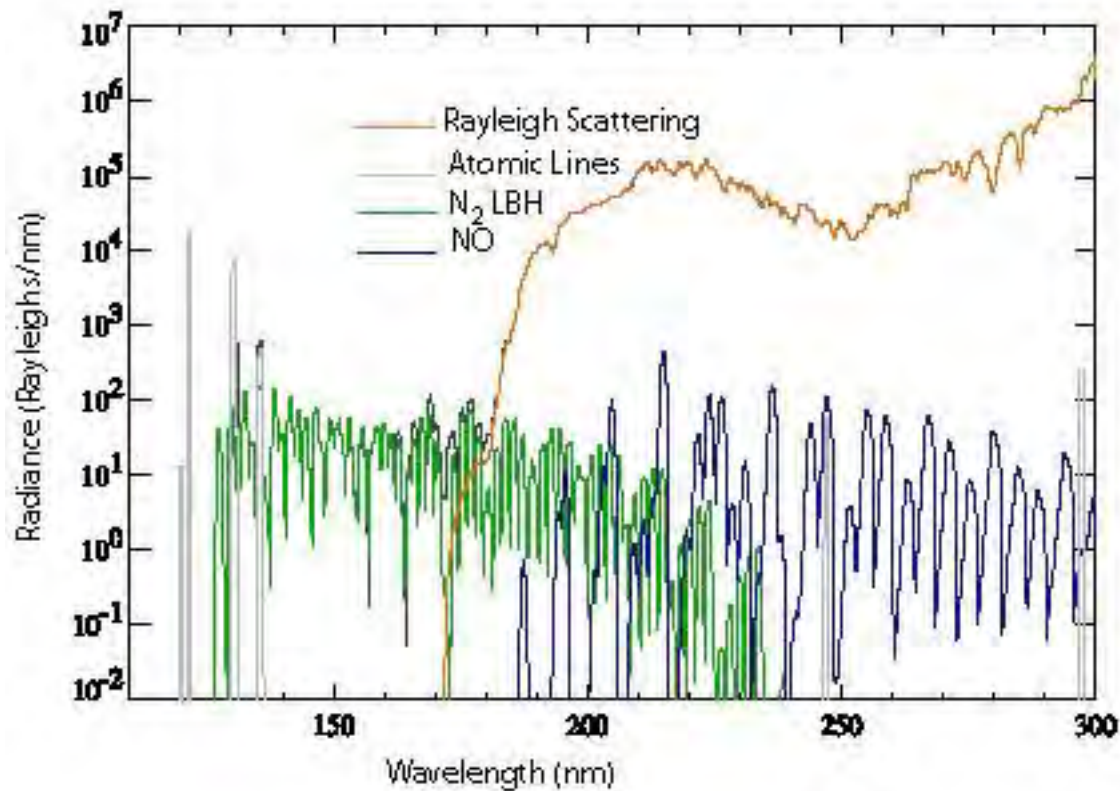
The Ability to Model the Spectrum is a Key Enabler for Quantitative Studies



The Ability to Model the Spectrum is a Key Enabler for Quantitative Studies



The Ability to Model the Spectrum is a Key Enabler for Quantitative Studies



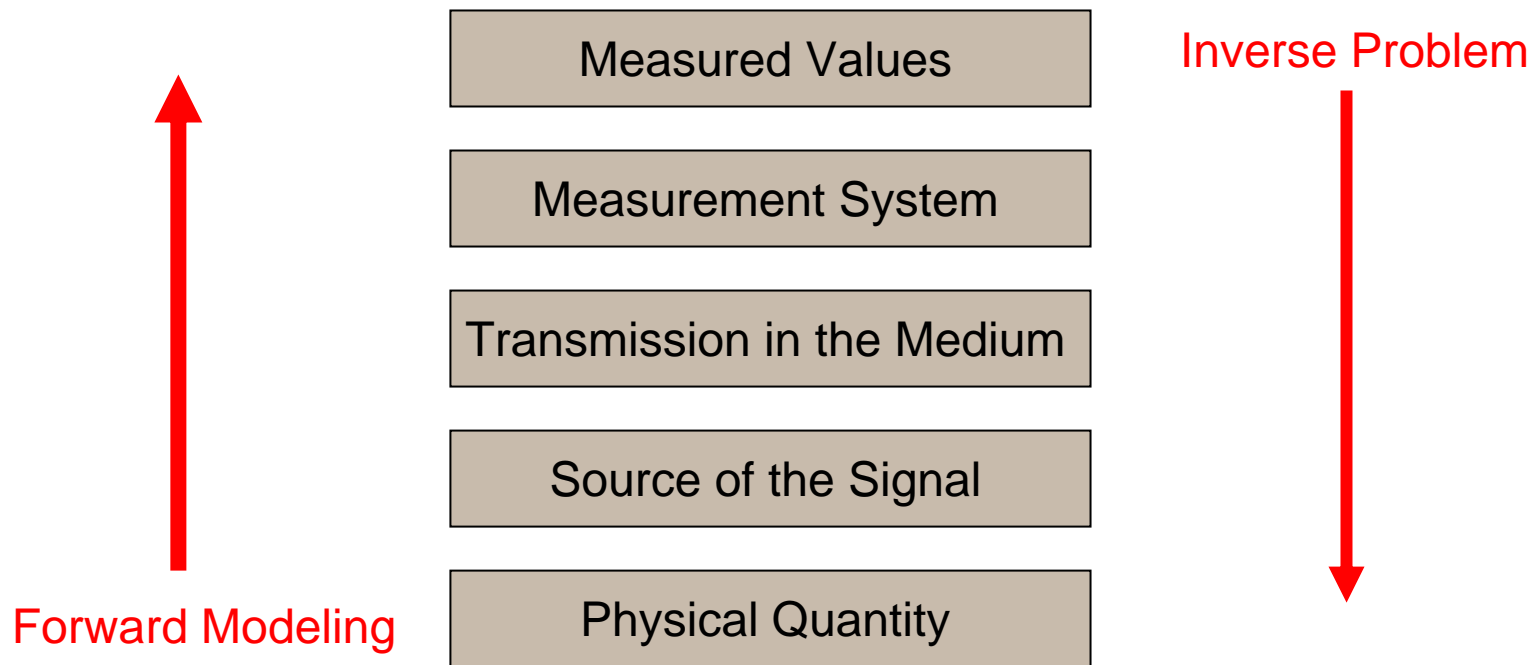
FUV Spectral Region Exhibits the Signatures of Space Weather in the Upper Atmosphere

- FUV spectral features were identified and interpreted during 30 years of rocket and spacecraft missions.

	HI (121.6 nm)	OI (130.4 nm)	OI (135.6 nm)	N ₂ (LBHs)	N ₂ (LBHI)
Dayside Limb	H profiles and escape rate ¹	Amount of O ₂ absorption ¹	O altitude profile	Amount of O ₂ as seen in absorption	N ₂ , Temperature
Dayside Disk	Column H	Amount of O ₂ absorption ¹	Used with LBHs to form O/N ₂	N ₂ , Solar EUV	Solar EUV
Nightside Limb	H profile and escape rate	Ion/ENA precipitation	EDP HmF2 NmF2 T _{plasma}	Ion/ENA precipitation characteristic energy	Ion/ENA precipitation characteristic energy
Nightside Disk	Geocorona and Ion/ENA precipitation	Ion/ENA precipitation	$\int n_e^2 ds$ (line of sight) and $\int n_e dz$ (vertical TEC) Ion/ENA precipitation	Ion/ENA precipitation	Ion/ENA precipitation
Auroral Zone	Region of proton precipitation	Auroral Boundary and amount of column O ₂ present ¹	Region of electron and (possibly) proton precipitation	Used with LBHI to form E _o and the ionization rate and conductance information	Measure of the effective precipitating flux, used with LBHI to form E _o and the ionization rate and conductance information

Remote Sensing is Indirect: How Do We Retrieve Information?

- Inverse techniques are relatively new in their application to IT problems.
- Both forward modeling and inverse processes use the same building blocks.



From Our Ability to Simulate the Scene and the End to End Performance We Can Design an Instrument

$$\frac{C}{t} = A\Omega E \int 4\pi I(\lambda) \phi(\lambda) d\lambda$$

Where

- C = counts
- t = integration period
- A = collecting area
- Ω = field of view
- E = efficiency
- $\phi(\lambda)$ = normalized spectral shape
- $4\pi I$ = Intensity in Rayleighs
where 1 Rayleigh = 10^6 ph/cm²/s into 4π steradians

Increasing A increases the mass (and cost) of the instrument

Increasing Ω decreases the spectral resolution

Increasing t improves statistics (by the square root) but degrades resolution (linearly)

Increasing the bandpass improves statistics but can degrade the products

The Trade Space for the Optical Design is Constrained by Many Factors

$$\frac{C}{t} = \frac{\int 4\pi I(\lambda)\phi(\lambda)d\lambda}{4\pi} \left(\frac{h}{f}\right) \left(\frac{m}{d}\right) A_g T Q_e D_e$$

Where

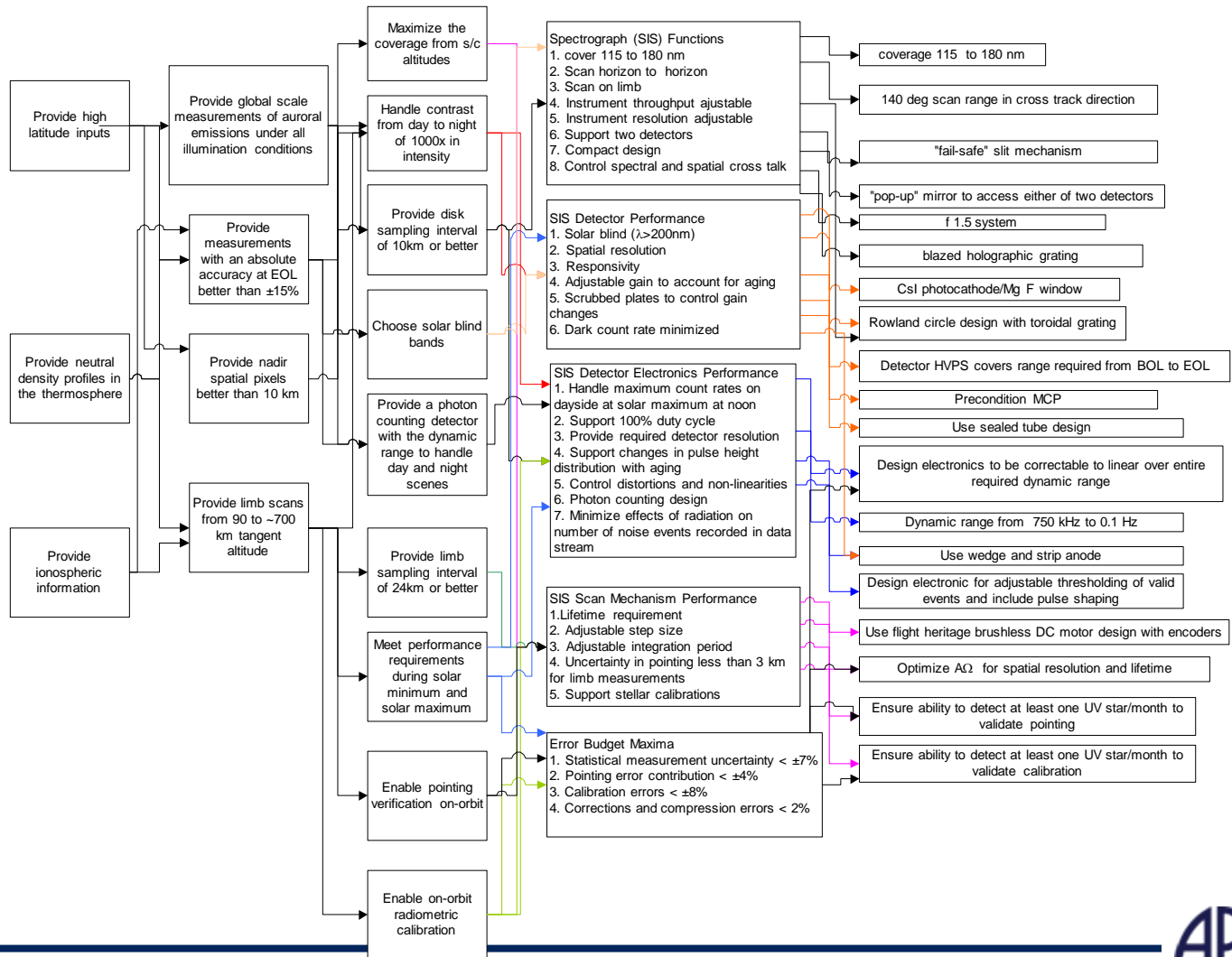
h	= slit height
f	= focal length
m	= grating order
d	= grating ruling density
A_g	= filled area of the grating
T	= transmission (product of all reflectivities)
Q_e	= quantum efficiency of the photocathode
D_e	= detector electronics efficiency

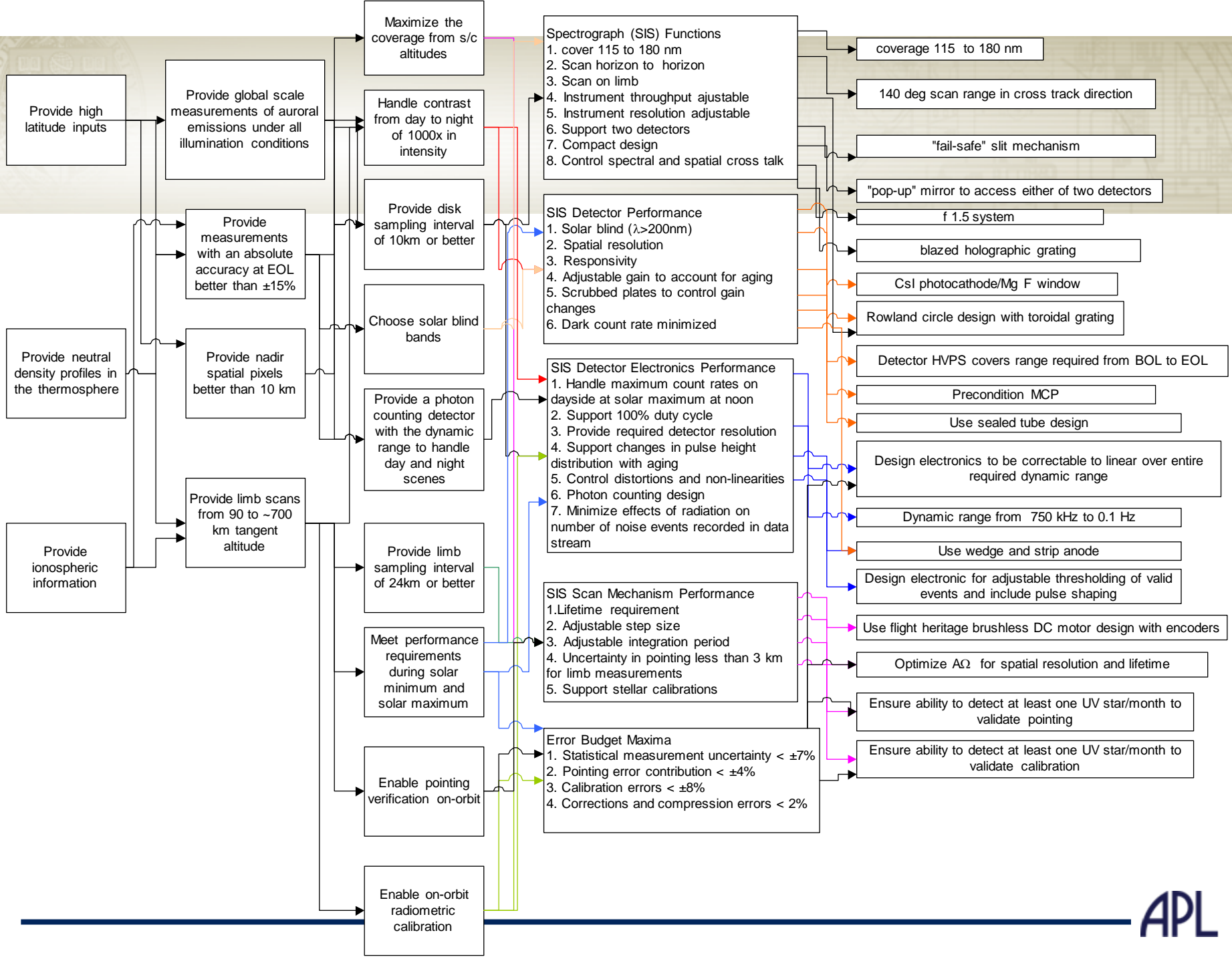
You need to make the slit (instantaneous FOV) as large as possible while keeping the focal length short. You'd like to operate with a coarsely ruled grating in high order with as large a grating as possible while minimizing reflections and still getting adequate imaging properties. A high Q_e is desirable but may lead to a shorter lifetime as may an amplification that leads to high counting efficiency.

In Both Forward Modeling and Inversions the Instrument Needs to be Well Characterized and Designed with a Measurement in Mind

What is the variability of the IT system?

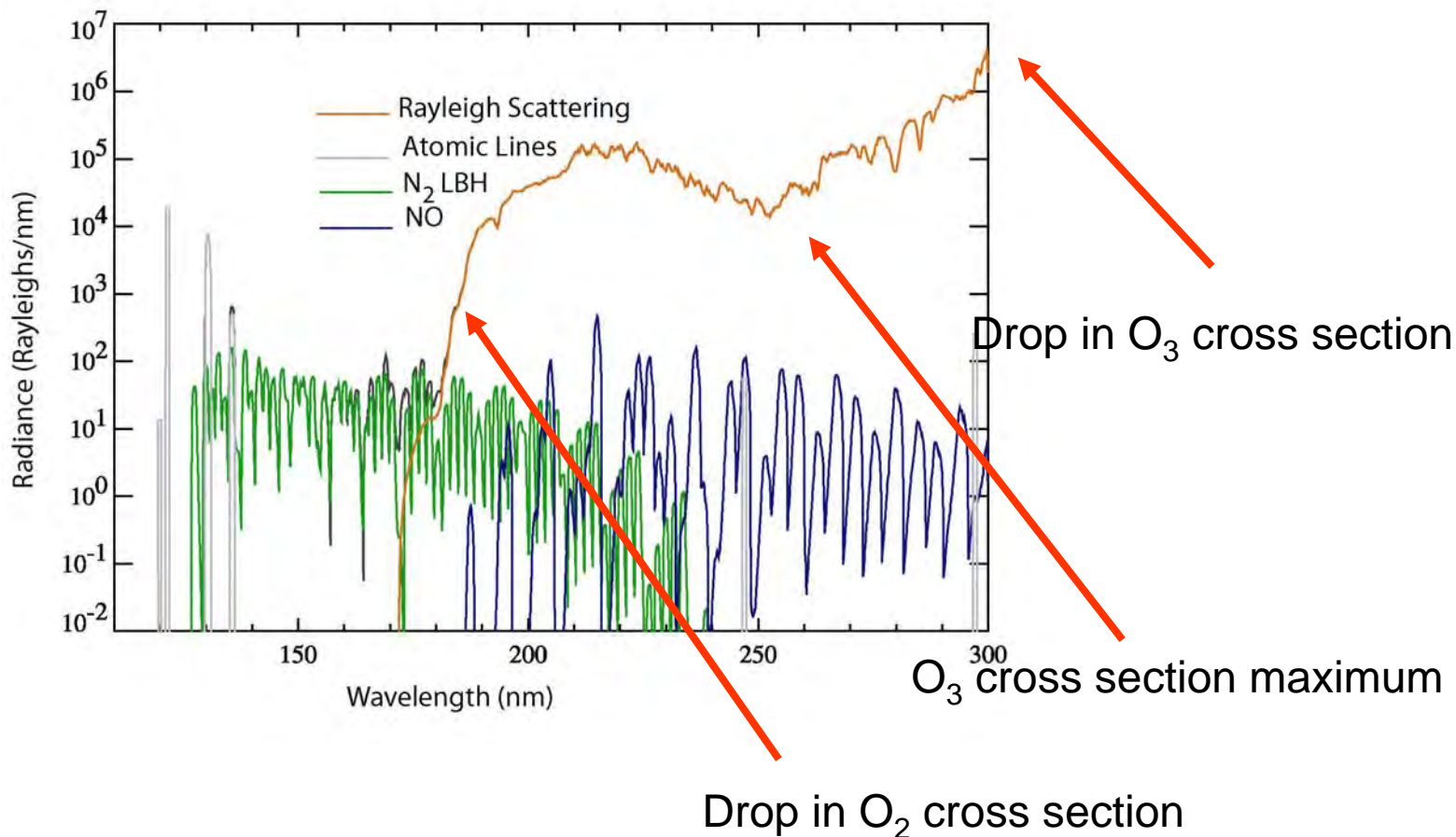
What are the energy inputs into the IT?





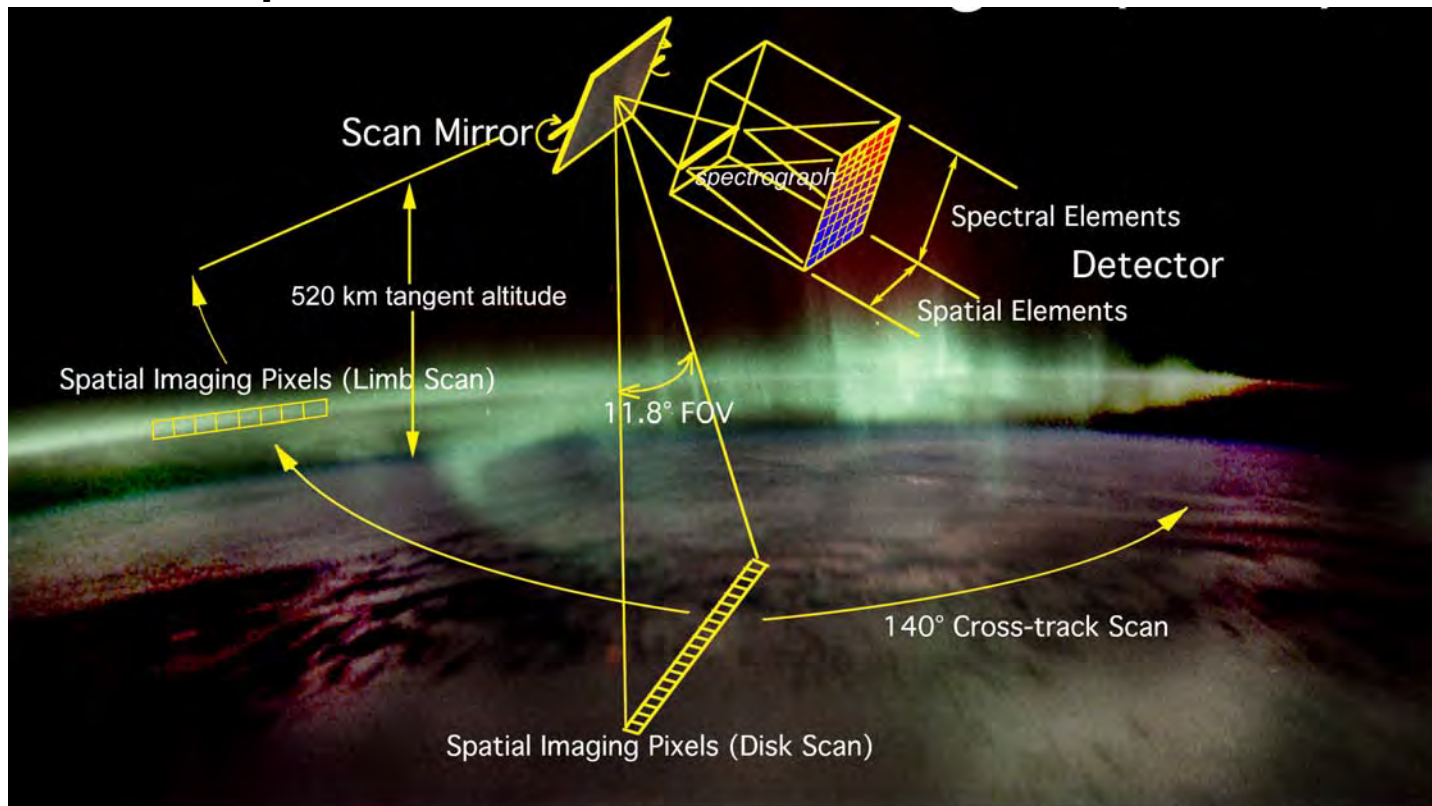
The Dayglow Spectrum of the Earth Drives the Specification of the Out of Band Response

The Factor of 1000 Contrast Between Day and Night Drives the Electronics and the Optics

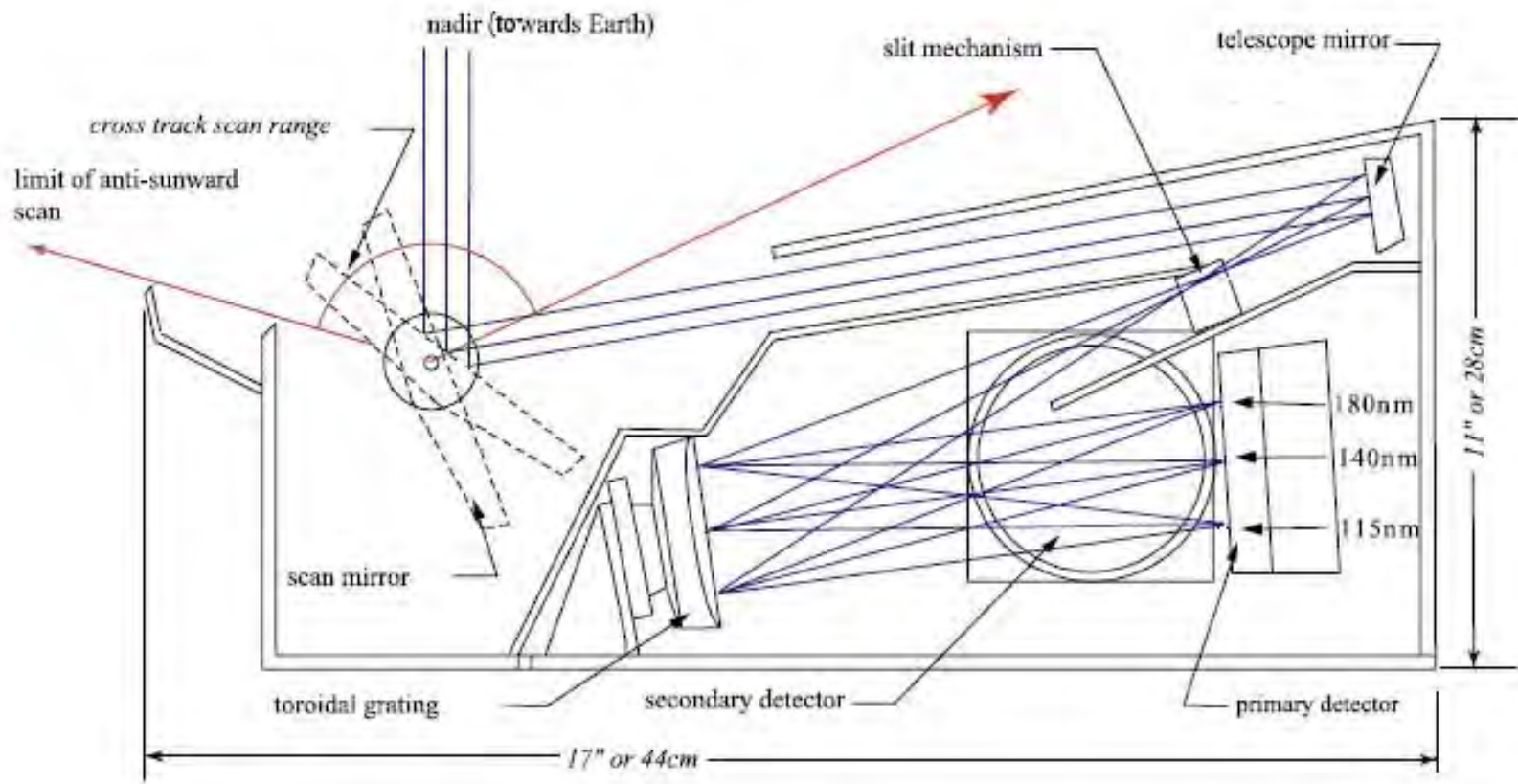


GUVI/SSUSI Uses a Spectrographic Imager to Produce 3D Images

- GUVI/SSUSI scans across the disk and onto the limb
 - Column density information on the disk
 - Imagery for context and boundary location
 - Altitude profiles on the limb



Optical Design Maximizes End-to-End Throughput While Minimizing Package Size and Complexity



DE-0000E_10

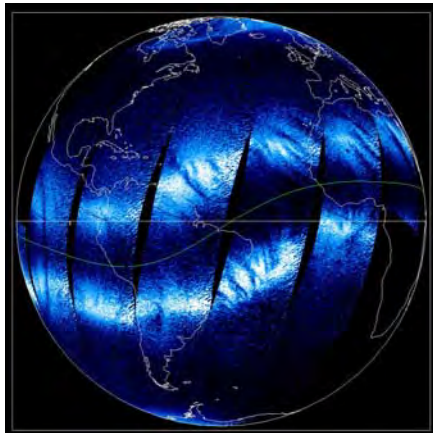
These Instruments are Small, for an Optical Instrument, Relatively Inexpensive

- Modern FUV instruments operate with photon counting electronics.
- An image intensifier converts incoming photons into a cloud of electrons that is localized on a position sensitive anode.
- That position is equivalent to knowledge of wavelength and spatial pixel.



GUVI Produces Key Parameters that Provide Unique Insight into the IT

Dayside	Nightside	AURORAL Region
O/N2	Electron Density Profile	Boundary
Qeuv	Bubble location and extent	Energy and flux
Neutral Density Profile	ENA precipitation	Imagery (day or night)
O+ above airglow profile		



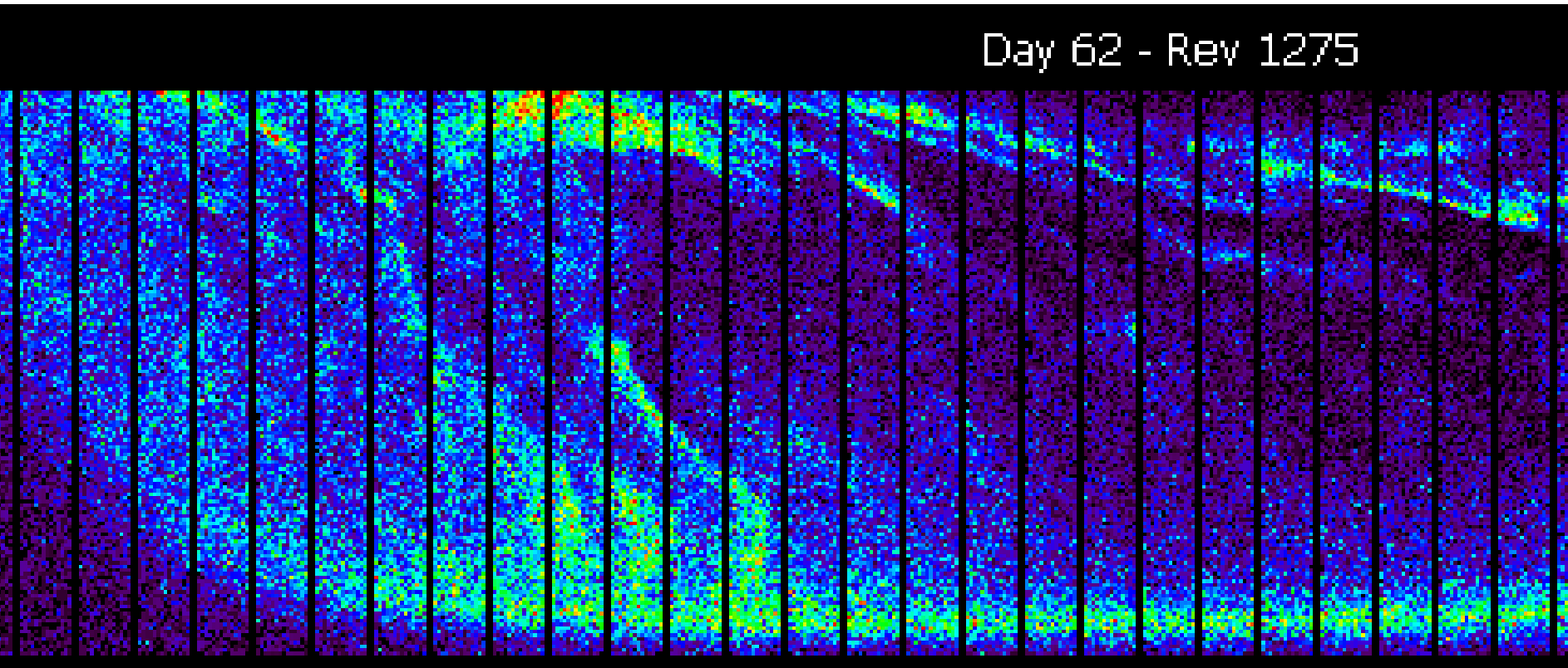
GUVI Image of the night-time ionosphere and ionospheric irregularities.



GUVI Image of the aurora over the US during the day in the middle of a large geomagnetic storm.

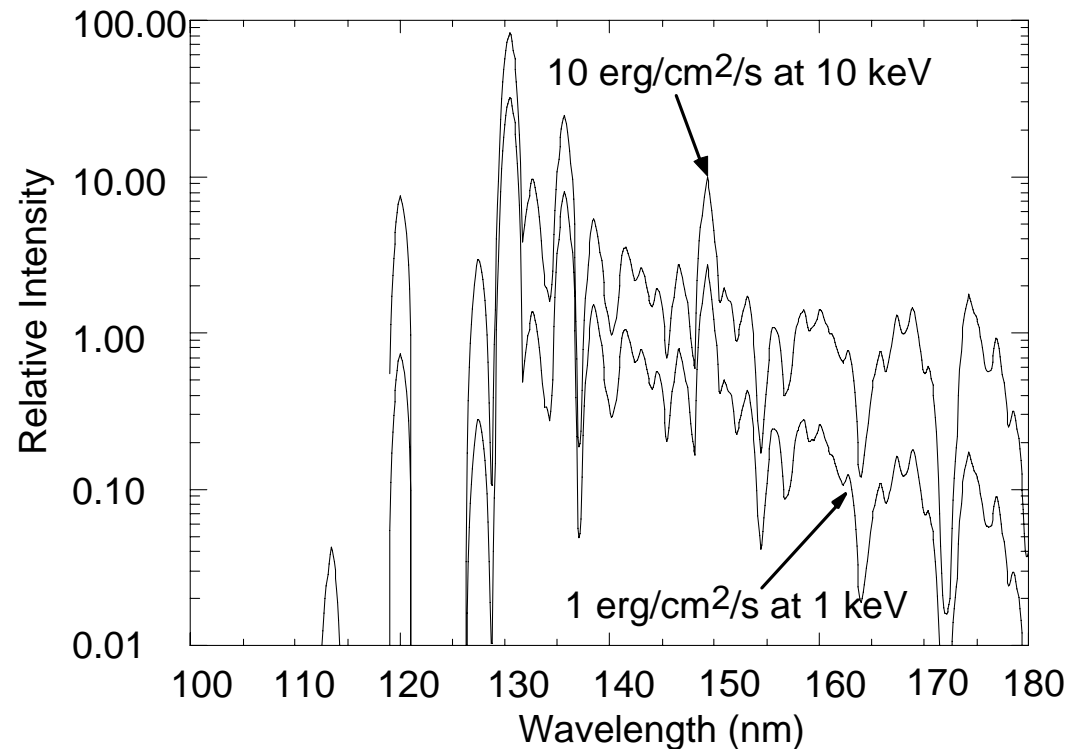
GUVI has a 7km (at nadir) spatial resolution

This is a series of individual scans in the 135.6 nm oxygen emission feature. The integration period for each pixel is 0.1 s.



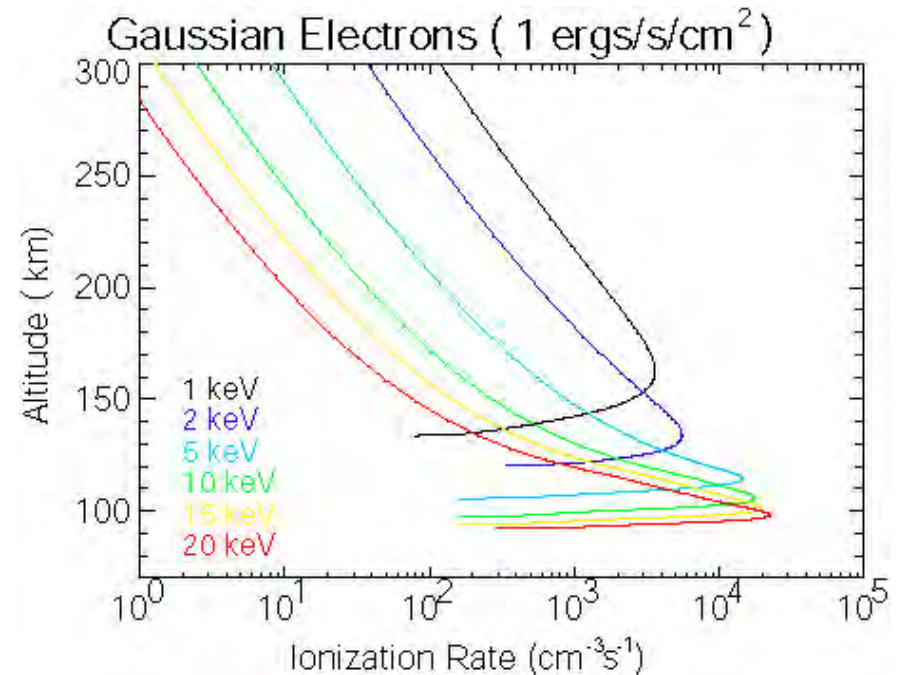
The Auroral Products are Produced Using Look-up Tables Based on Forward Calculations

- The auroral algorithm uses the fact that O_2 absorption peaks at about 145 nm.
- The harder the spectrum (higher $\langle E \rangle$) the lower the ionization (and subsequent secondary electrons) peak will occur.
- The ratio of the N_2 LBH bands where this absorption is important to the where it is negligible is a good indicator of the energy of the incoming particles from about 2 keV to 15 keV.
 - Outside of that range the determination is less accurate.
 - But it probably doesn't matter for most applications.



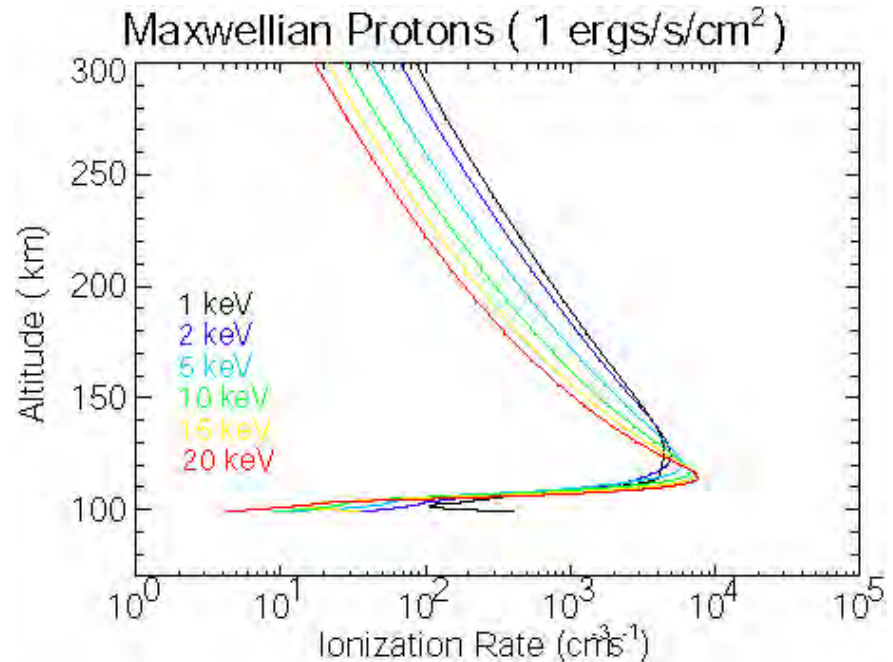
The Auroral Products are Produced Using Look-up Tables Based on Forward Calculations

- The auroral algorithm uses the fact that O_2 absorption peaks at about 145 nm.
- The harder the spectrum (higher $\langle E \rangle$) the lower the ionization (and subsequent secondary electrons) peak will occur.
- The ratio of the N_2 LBH bands where this absorption is important to the where it is negligible is a good indicator of the energy of the incoming particles from about 2 keV to 15 keV.
 - Outside of that range the determination is less accurate.
 - But it probably doesn't matter for most applications.



Proton Precipitation Can Also Be Important

- The proton energy and flux cannot be unambiguously determined from the measurement of HI 121.6.
- GUVI measures the total emission in the line.
- The protons can, however, be treated as being effectively electrons as determined by the ratio of LBHs/LBHI.
- This introduces a small error under the usual circumstances.



Note that for protons there is much less spread in the altitude of the peak in the ionization rate than for electrons.

E-region Quantities from GUVI “colors”

LBHs/LBHI

$\langle E \rangle$

$\langle E \rangle$ vs. LBHs/LBHI

LBHI

Q

LBHI/ I_{model}

$$P = 1.8 \times 10^{10} Q \text{ ions cm}^{-2} \text{ s}^{-1}$$

NmE

HmE

σ and Σ

Where

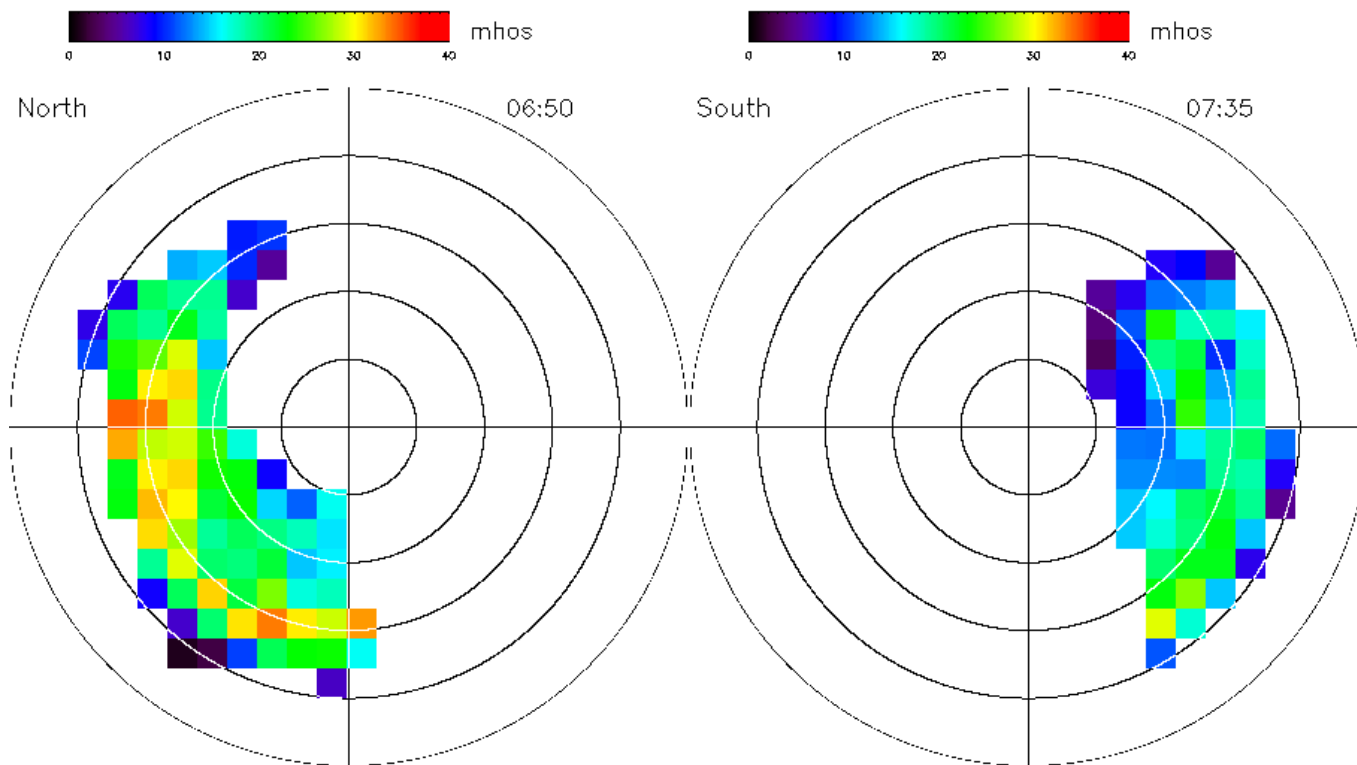
$$\Sigma_P = \frac{40 \langle E \rangle \sqrt{Q}}{16 + \langle E \rangle^2}$$

$$\frac{\Sigma_H}{\Sigma_P} = 0.45 \langle E \rangle^{0.85}$$

Robinson et al., 1987 formulation is currently being used.

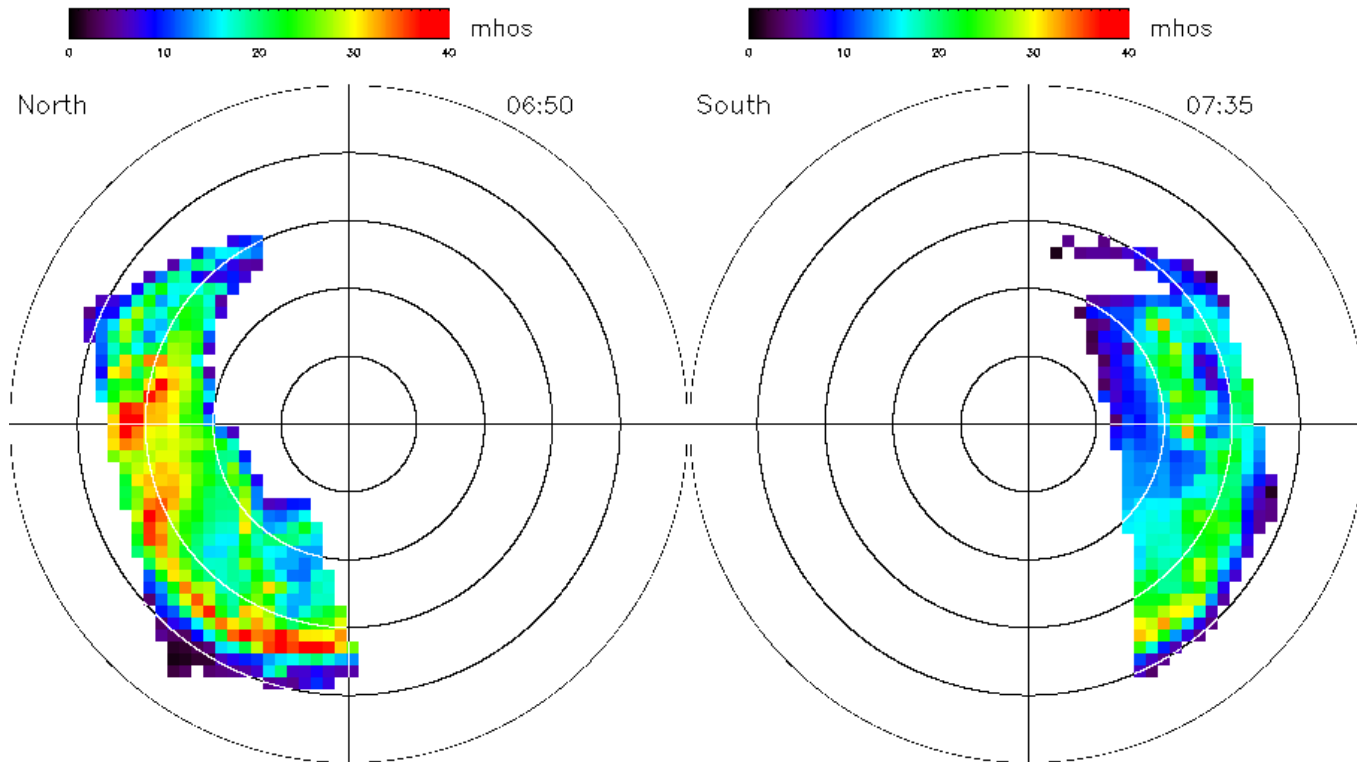
What Resolution Captures the Physics? 500km?

GUVI SigmaP Data Orbit#: 18594 May 15, 2005 (135)



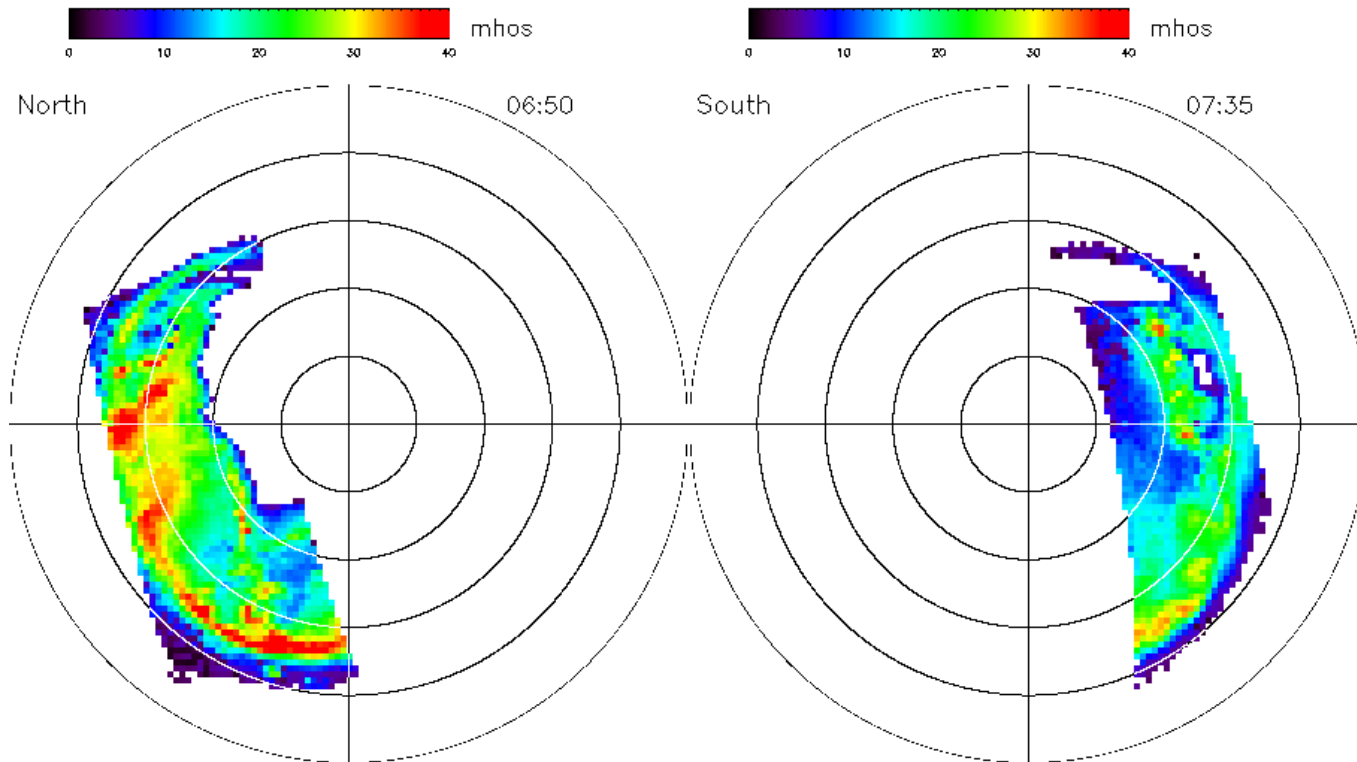
What is the Resolution Captures the Physics? 200km?

GUVI SigmaP Data Orbit#: 18594 May 15, 2005 (135)



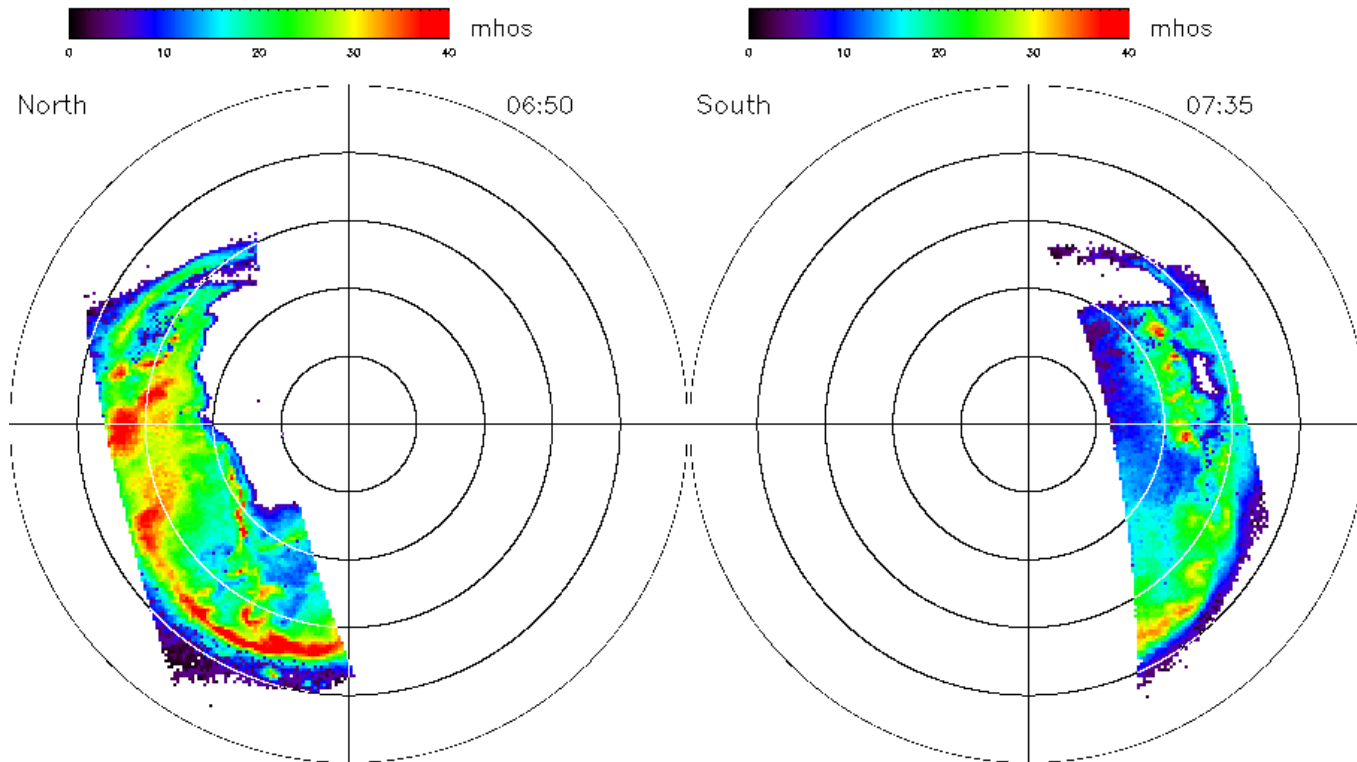
What is the Resolution Captures the Physics? 100km?

GUVI SigmaP Data Orbit#: 18594 May 15, 2005 (135)



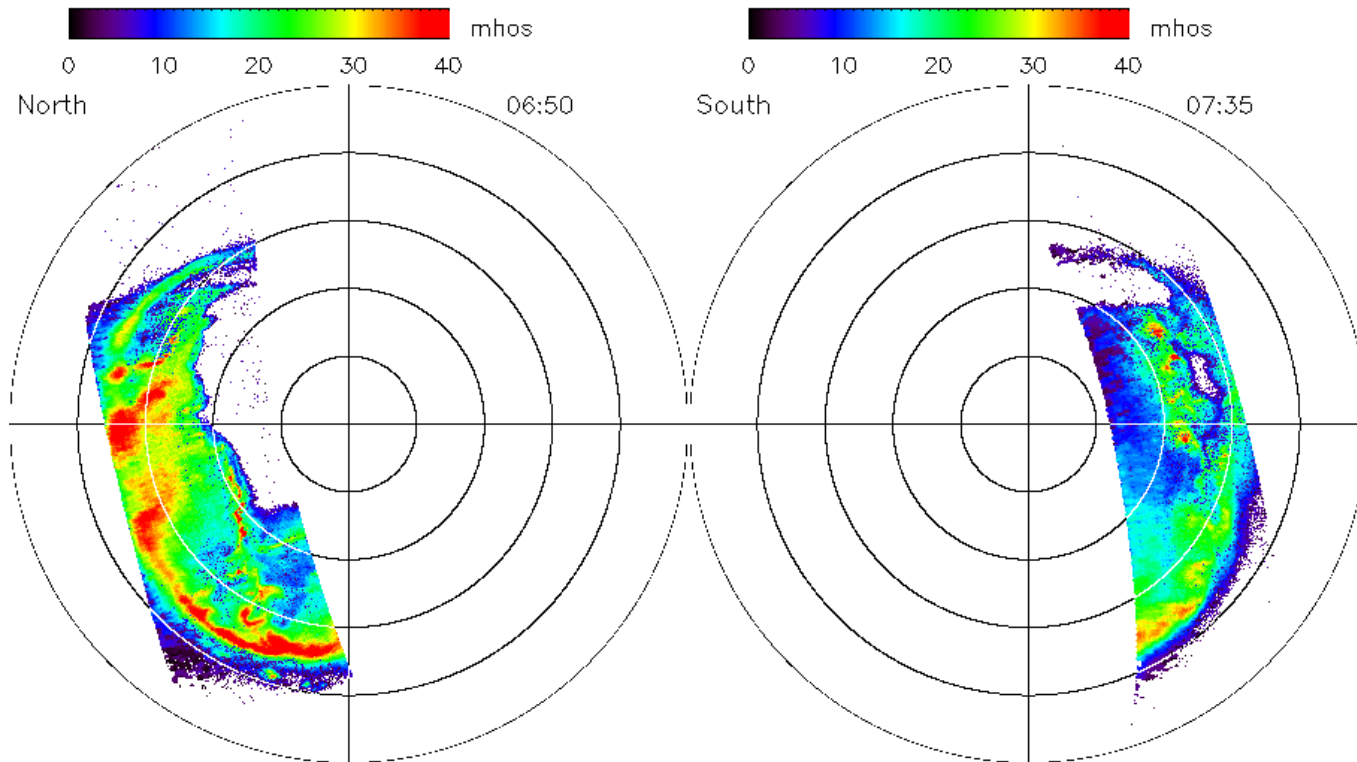
What is the Resolution Captures the Physics? 50km?

GUVI SigmaP Data Orbit#: 18594 May 15, 2005 (135)



What is the Resolution Captures the Physics? 25km?

GUVI SigmaP Data Orbit#: 18594 May 15, 2005 (135)

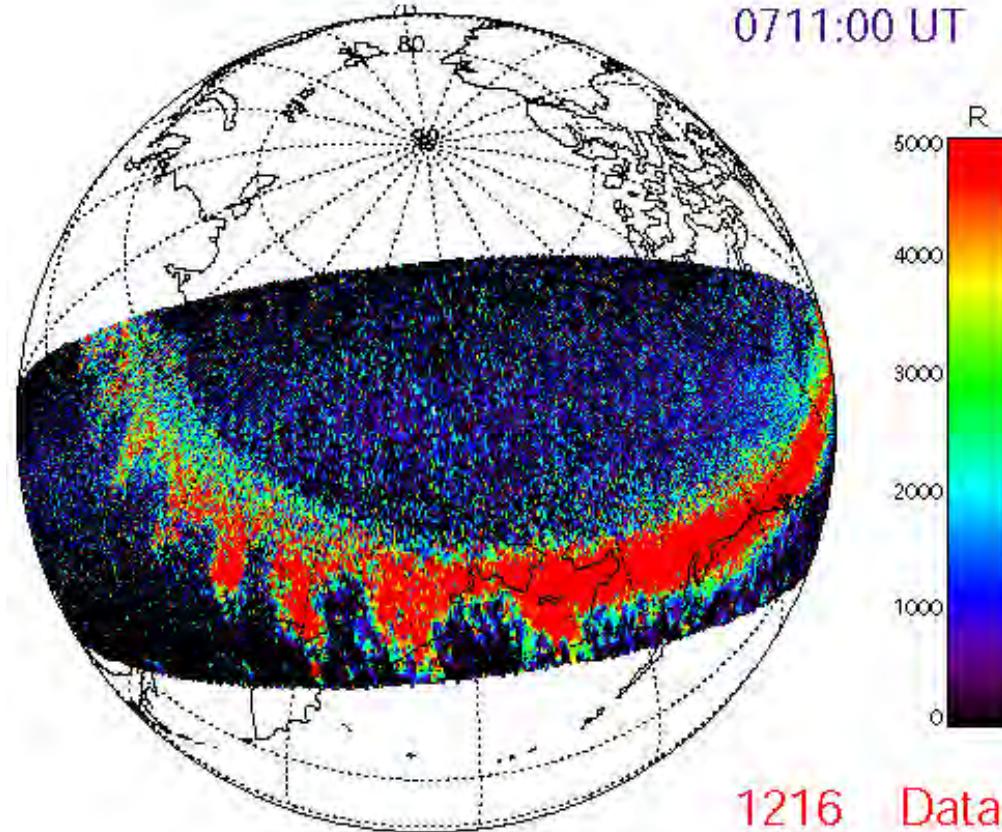


GUVI Detects Proton Precipitation

- We can begin to get an understanding of the spatial variability and scales of proton precipitation.
- Protons are not always a small contributor nor are they smooth.

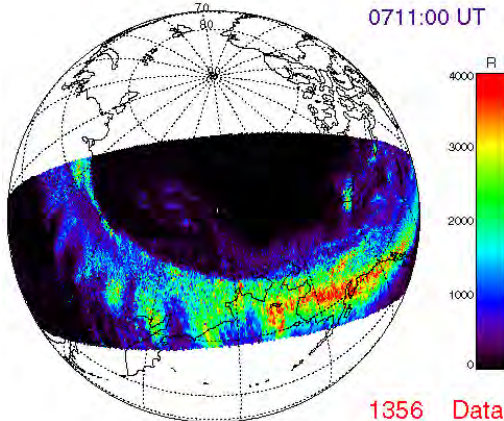
GUVI L1B September 11, 2005

0711:00 UT



GUVI L1B September 11, 2005

0711:00 UT



1356 Data

Orbit #: 20358

Orbit #: 20358

The Ionosphere Responds to Solar Inputs

- The ionosphere will respond to changes in the details in the solar flux and to changes in neutral composition and wind fields.
- How accurately can we predict the ionosphere on a global basis?
- UV remote sensing can provide us with a missing part of that picture.

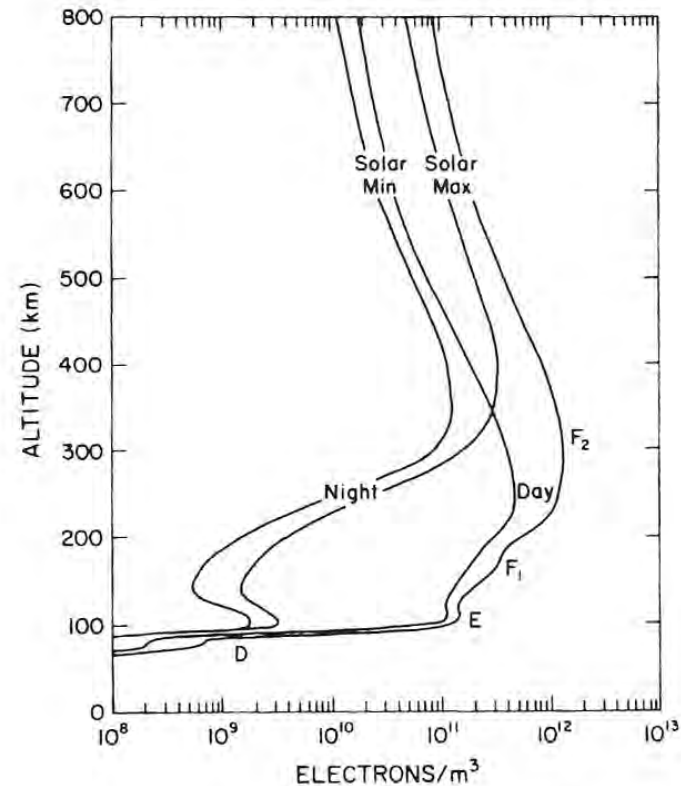
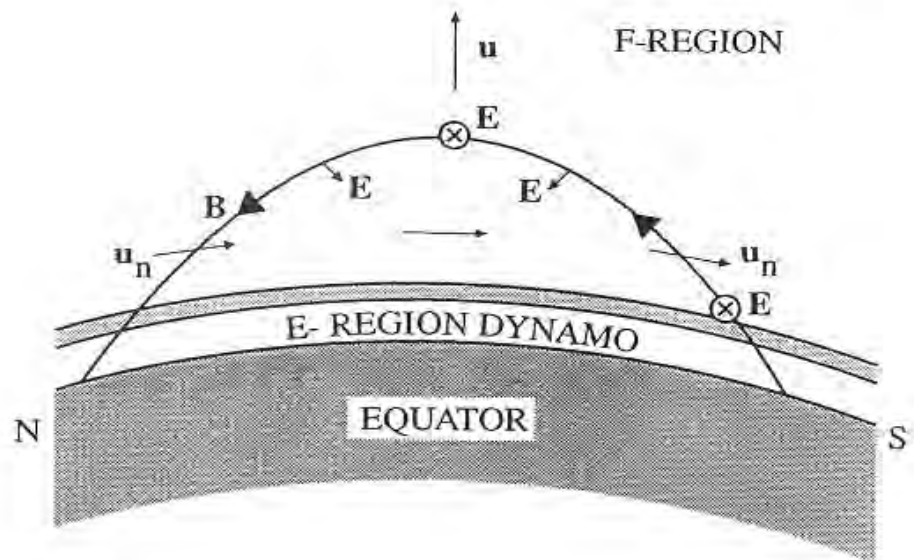


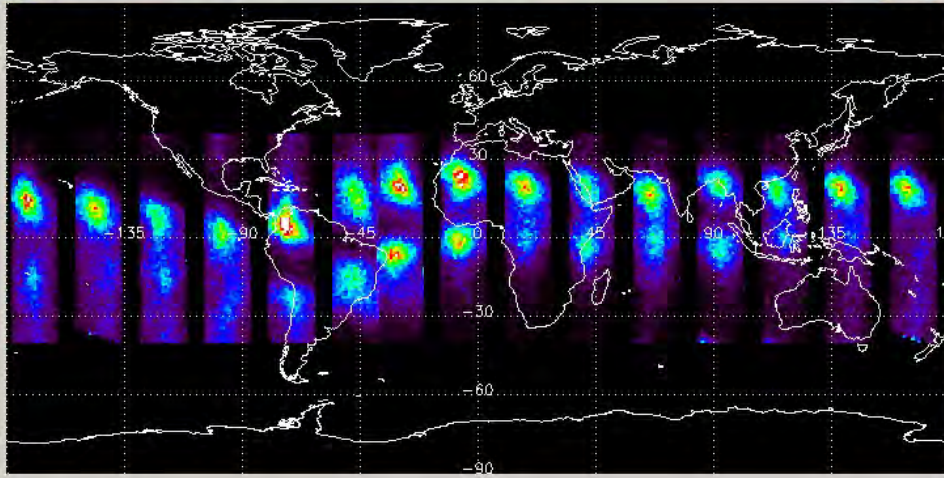
Fig. 5.1. Typical midlatitude ionospheric electron density profiles for sunspot maximum and minimum conditions at daytime and night-time. The different altitude regions in the ionosphere are labelled with appropriate nomenclature. (From Richmond, 1987.)

The Equatorial Ionosphere Shows the Global Coupling of the IT System

- Neutral winds in the low latitude E-region generate dynamo E-field as ions are dragged across B-field.
- Dynamo E-field is transmitted to F-region altitudes.
- Meridional neutral winds induce field-aligned plasma drifts at F-region altitudes.
- Corotational E-field causes the plasma to $E \times B$ drift to the east with the corotation speed.

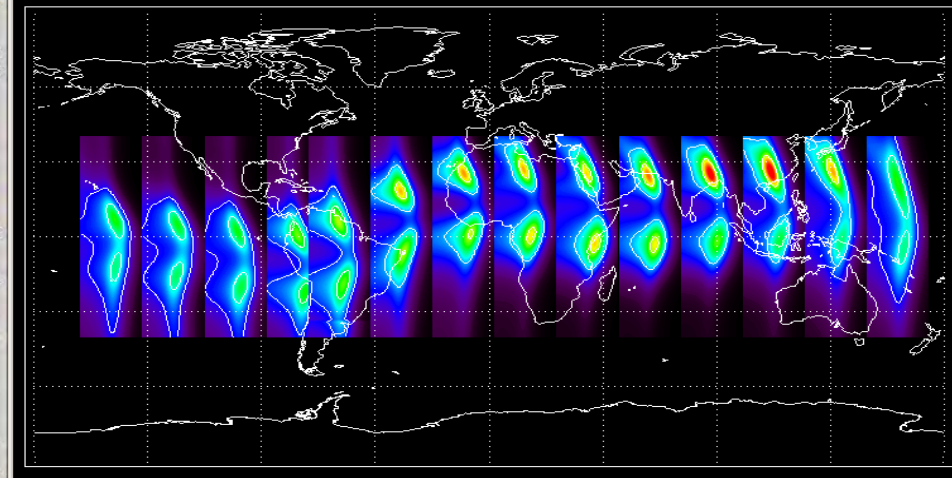


Images of the Nightside Ionosphere Show Differences Between “Weather” and “Climate”



GUVI

- A day of GUVI limb profiles compared to predictions from RIBG, an ionospheric climate model.
- The altitude axis runs horizontally and the plots are positioned at the equator-crossing point for an orbit.
- The climatological model embodies a different effective neutral wind and a different ExB drift than the observations.

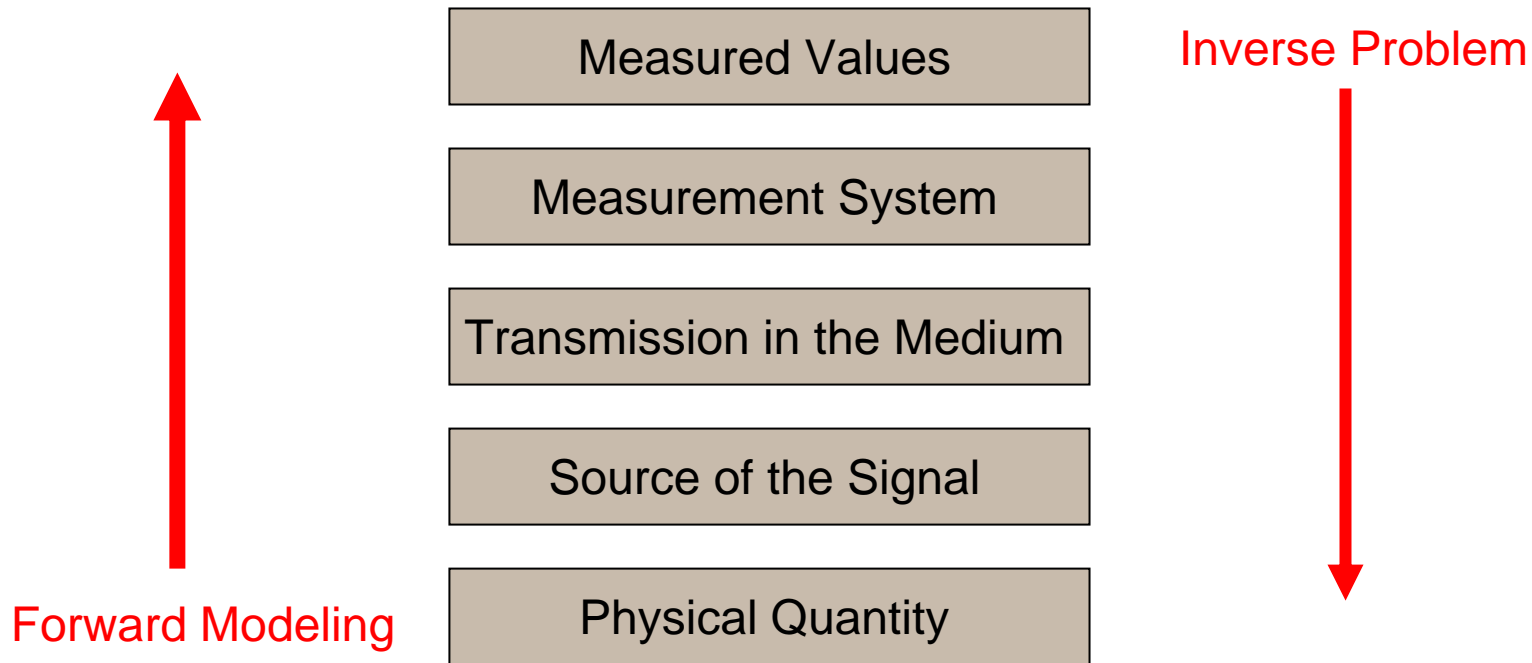


RIBG

From P. Straus

Remote Sensing is Indirect: How Do We Retrieve Information?

- Inverse techniques are relatively new in their application to IT problems.
- Both forward modeling and inverse processes use the same building blocks.



Discrete Inverse Theory Can Be Applied to the Nightside OI 135.6 nm Observations to Produce Electron Density Profiles

Measured Intensity

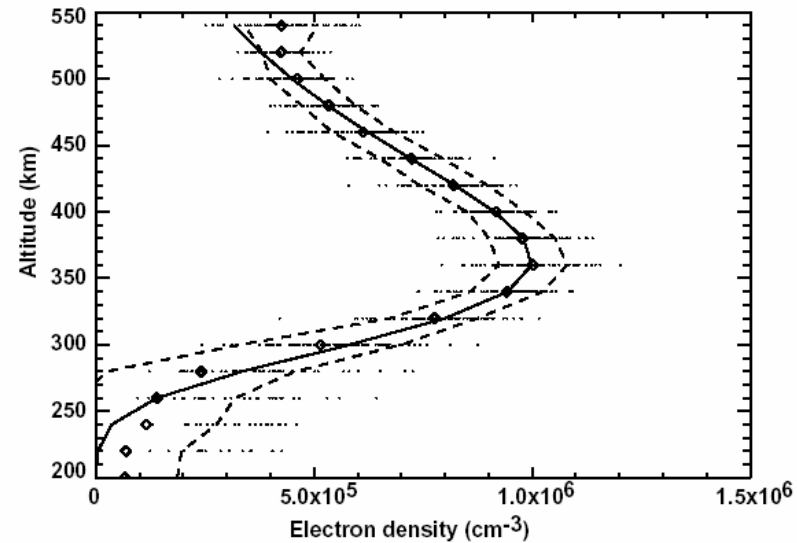
$$\mathbf{B} = \mathbf{W}\boldsymbol{\eta} ([e])$$

Geometric weighting function

Volume emission rate

$$\boldsymbol{\eta} = (\mathbf{W}_a^T \mathbf{C}_{ma}^{-1} \mathbf{W})^{-1} \mathbf{W}_a^T \mathbf{C}_{ma}^{-1} \bar{\mathbf{B}}_m$$

Covariance of the measurements



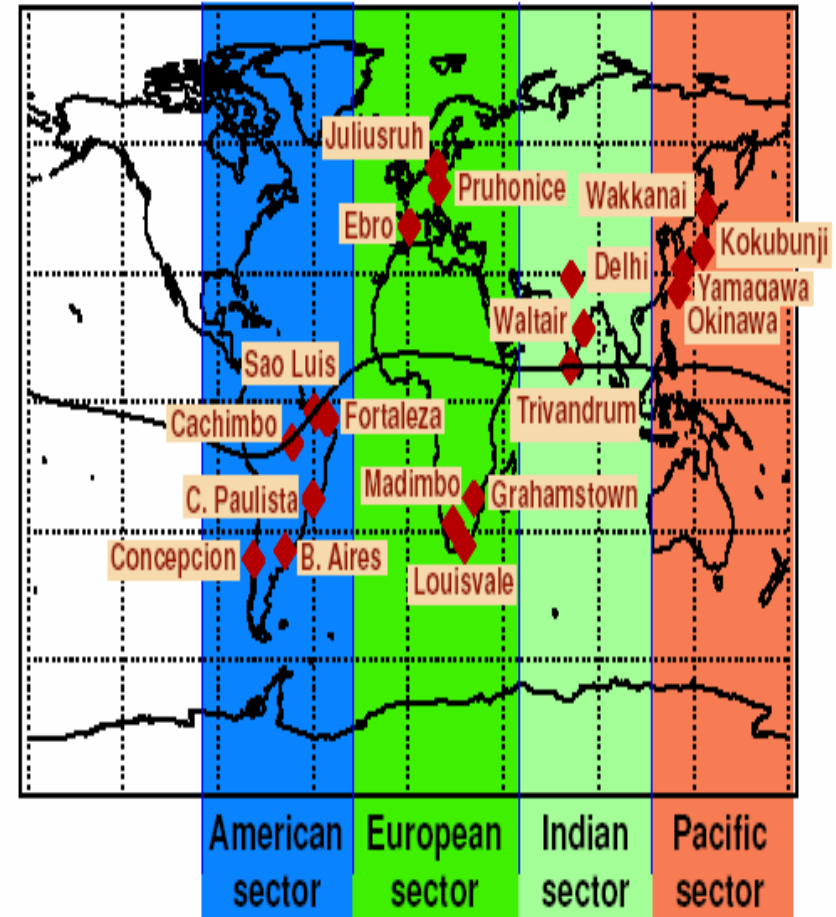
From the volume emission rate we can determine the O⁺ density (or electron number density if we assume $n_e = n_{O^+}$)

$$\eta = \alpha n_e n_{O^+} \approx \alpha n_e^2$$

$$\alpha = 7.3 \times 10^{-13} \text{ cm}^3 \text{ s}^{-1}$$

Comparison of GUVI NmF2 to Ionosonde

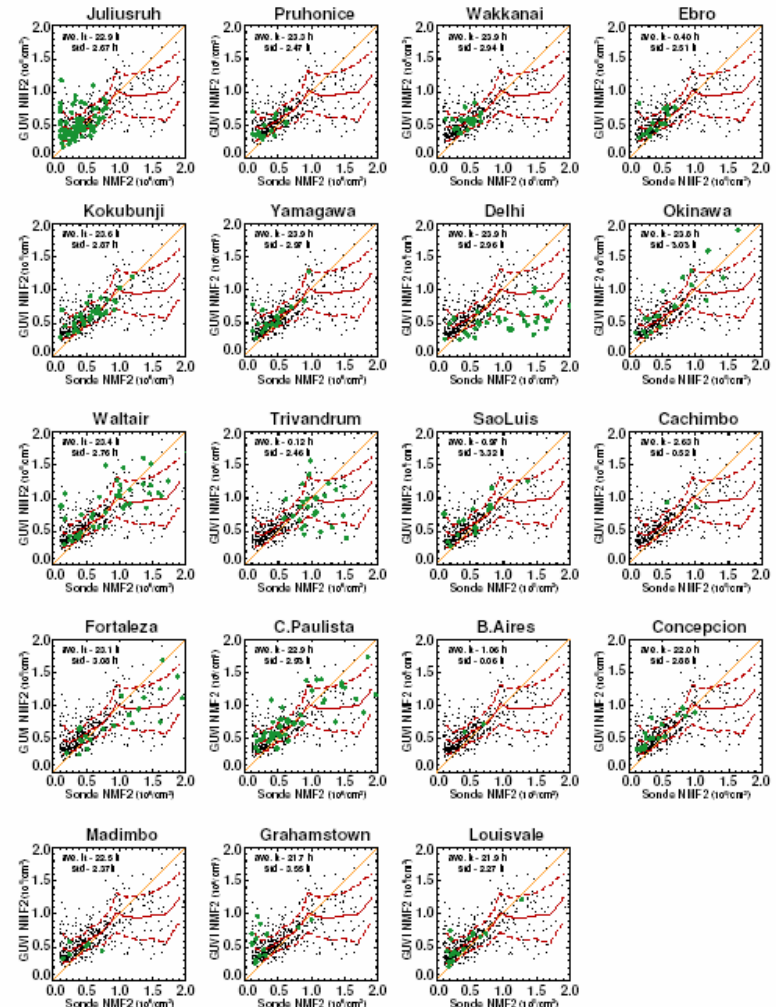
- A systematic comparison of GUVI data with hand-scaled data from ionosondes has been carried out.
- The comparison indicates that GUVI can retrieve an accurate measure of NmF2.
- Note that HmF2 is also a product of the GUVI retrievals as well as a TO+C (Total O+ Column).
- The TOC product may be useful as a method of elucidating variations in the plasmasphere from TEC measurements.
- A very important “discovery” is that some stations appear to show a systematic bias when compared to GUVI data.



DeMajistre, Paxton, and Bilitza, 2006.

Comparison of GUVI NmF2 to Ionosonde

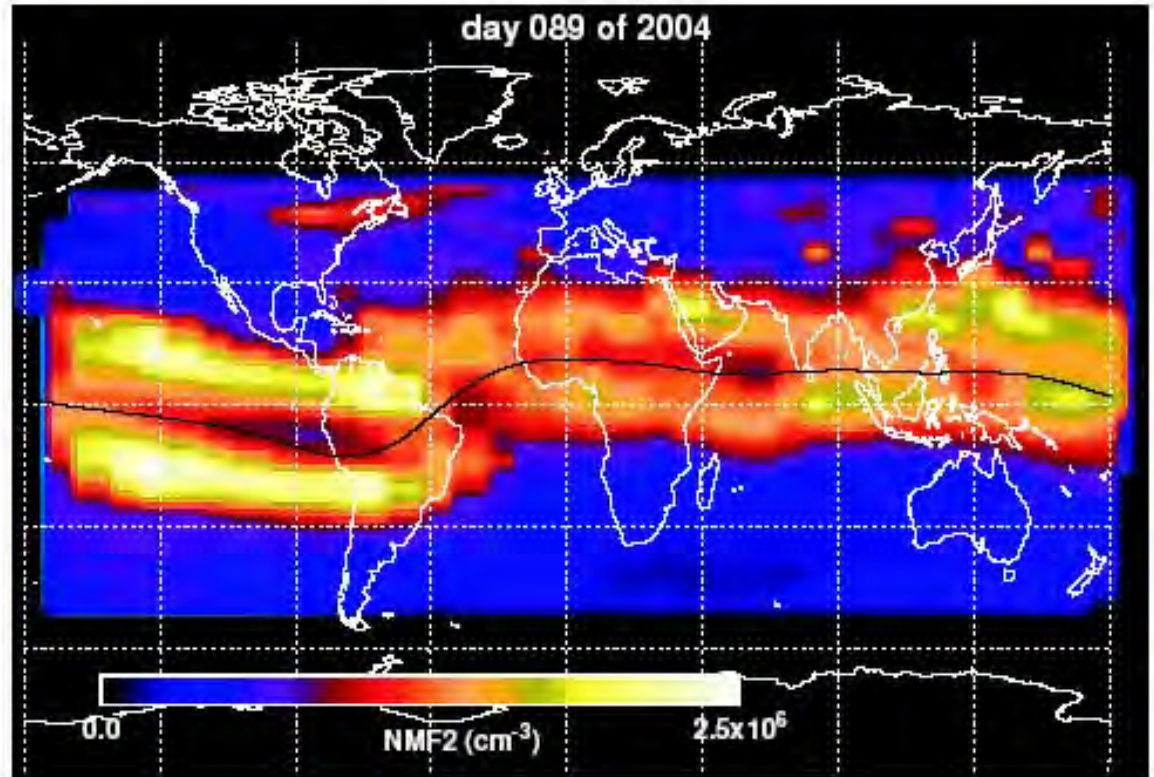
- A systematic comparison of GUVI data with hand-scaled data from ionosondes has been carried out.
- The comparison indicates that GUVI can retrieve an accurate measure of NmF2.
- Note that HmF2 is also a product of the GUVI retrievals as well as a TO+C (Total O+ Column).
- The TOC product may be useful as a method of elucidating variations in the plasmasphere from TEC measurements.
- A very important “discovery” is that some stations appear to show a systematic bias when compared to GUVI data.



DeMajistre, Paxton, and Bilitza, 2006.

Retrievals Allow Us to Map Ionospheric Parameters on a Global Basis (at Fixed LST)

- GUVI NmF2 values for one day (2004/89) for a local solar time near midnight.
- The Equatorial Arcs are clearly visible.
- The important feature is that the parameters can be retrieved on a global basis and are not limited to locations of ground stations or subject to constraints of models as are the GPS TEC maps.

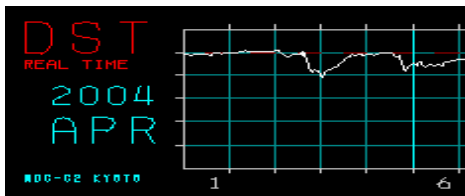
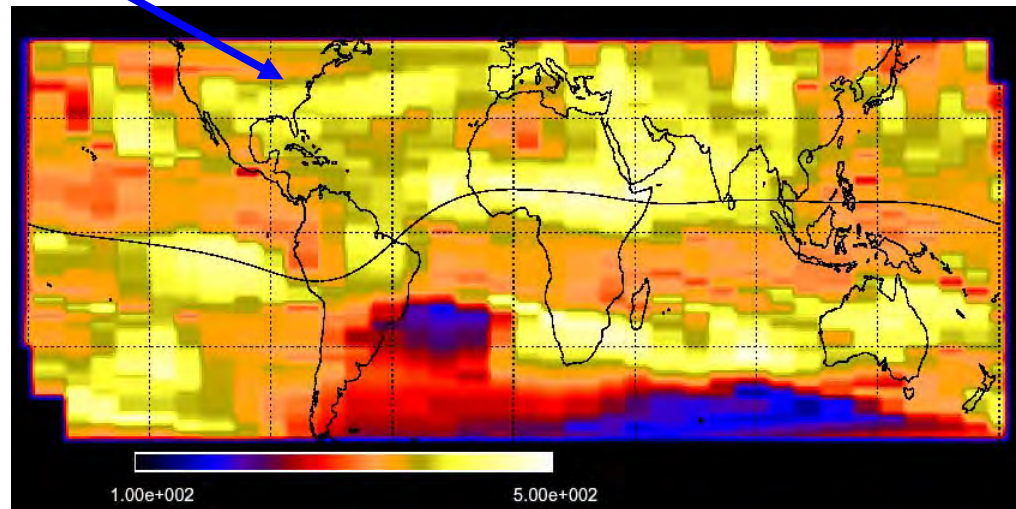
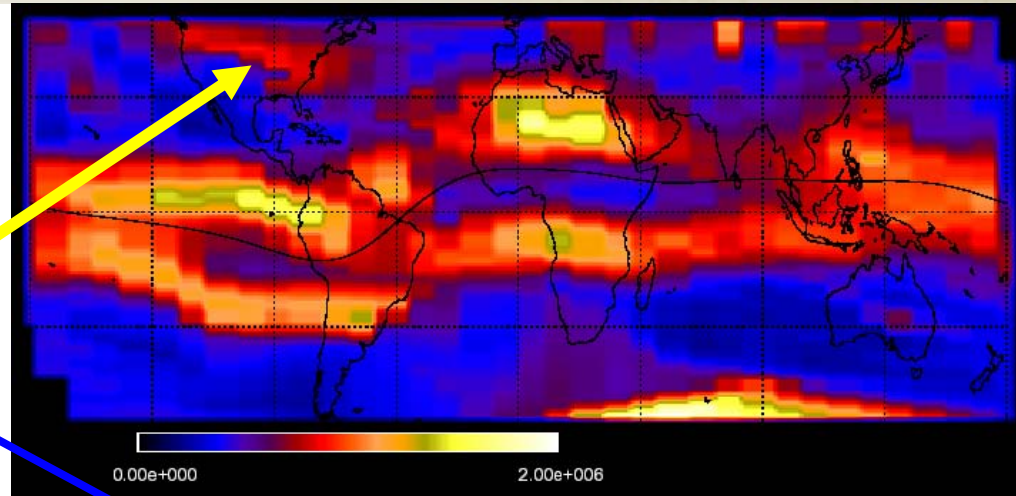


EDP Can Be Sliced in Different Ways

During the March-April 2004 CAUSES Campaign there were a series of interesting events that

Note general uplift including uplift over Millstone Hill and SED events.

A slow CME (3/31) initiated a disturbance in geospace over North America extending over Europe.



GUVI is Able to Map the Occurrence of Ionospheric Irregularities

Hendersen has done a study of the location, and magnitude of the crests in the EIA as well as bubble locations.

Once a database has been produced we can begin to ask questions about mechanisms and our models for processes we have little direct information about such as what the underlying sources of the bubbles might be.

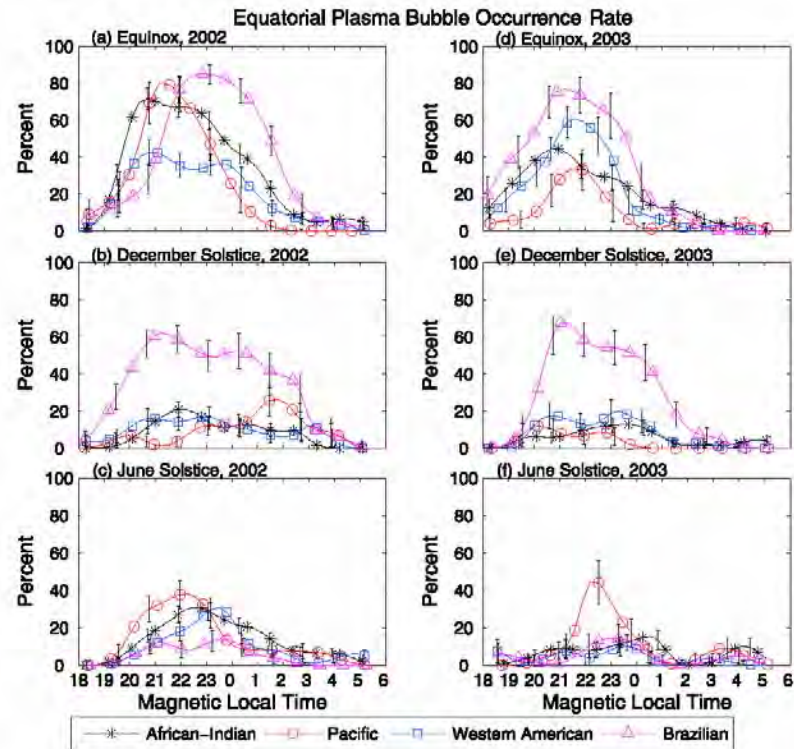


Figure 4. Percent probability of EPB occurrence (P_{EPB}) mean (solid lines) and standard error (error bars) as a function of MLT, season, year, and longitude sector. Data are divided into the following longitude sectors: African-Indian (0° – 150° E, 73° – 221° ME), Pacific (150° – 210° E, 221° – 281° ME), western American (210° – 300° E, 281° – 12° ME), and Brazilian (300° – 360° E, 12° – 73° ME).

From Hendersen et al, 2004

Coordinated Studies With Ground and Space Assets Enhance our Knowledge

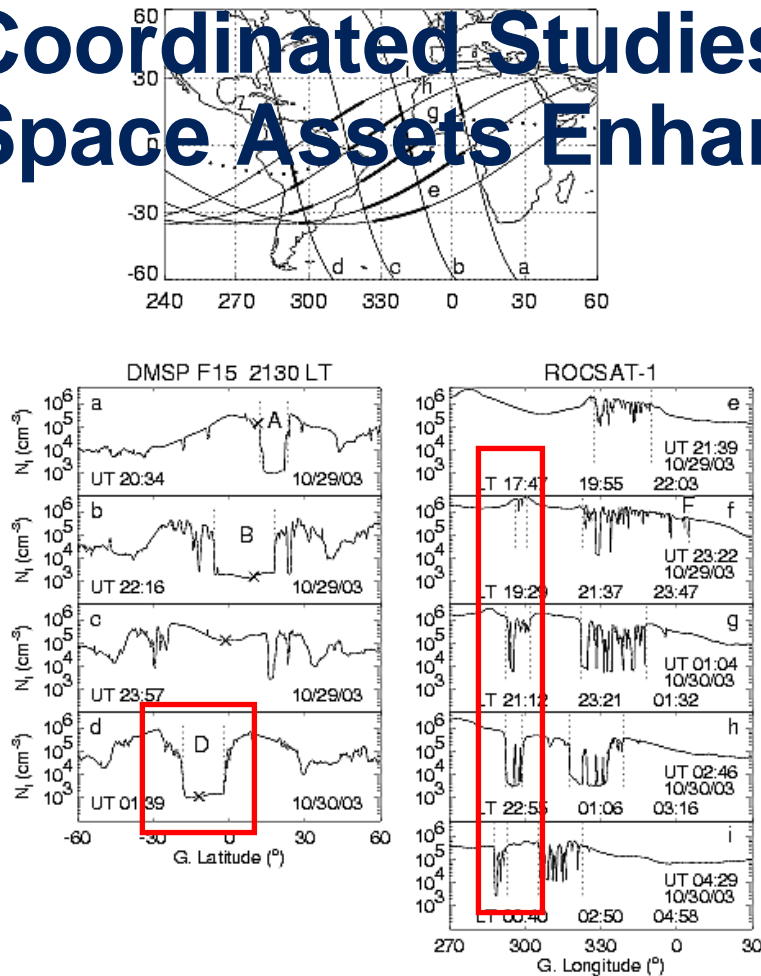


Fig. The ROCSAT passes across the magnetic equator did not show any evidence of the formation of the equatorial ionization trough. The background density between the depletions is $>10^5 \text{ cm}^{-3}$.

October 29, 2003

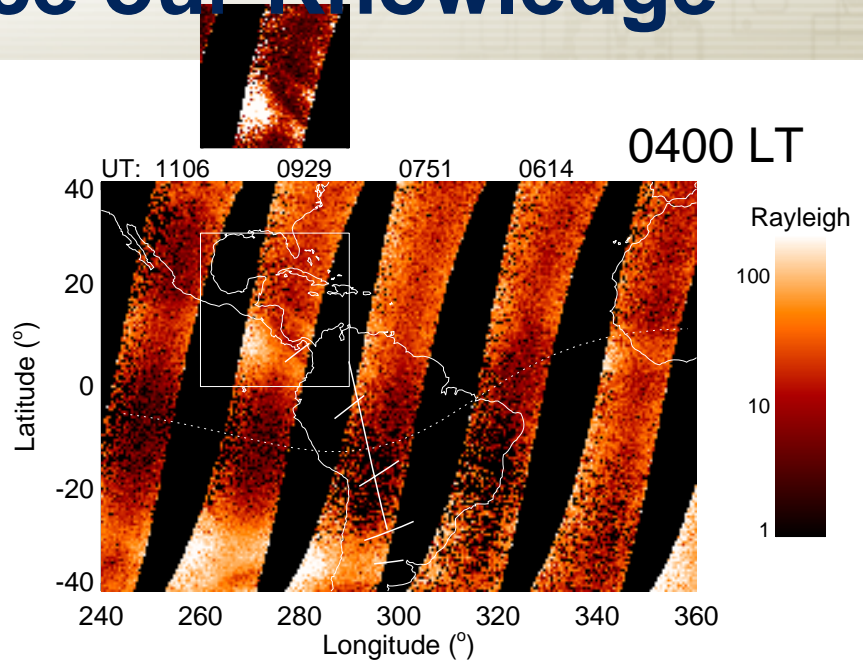
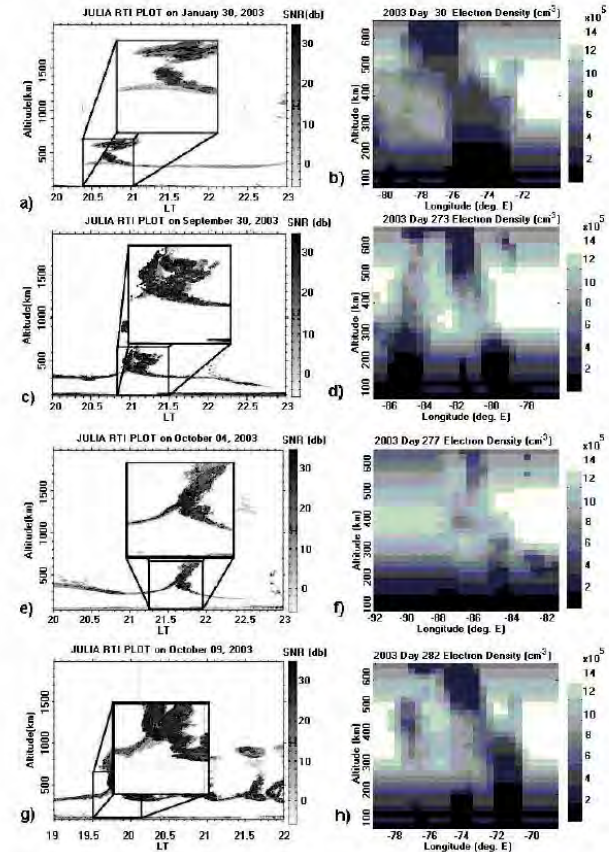
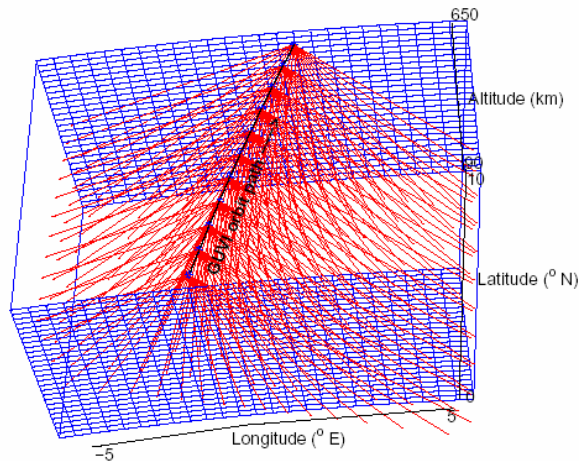


Fig. TIMED/GUVI detected depleted OI 135.6-nm emission at the locations of the plasma depletions. Elongation of the depletions along **B**-field lines and the simultaneous observations of the depletions at different altitudes support the association of the large depletions with smaller scale depletions or bubbles.

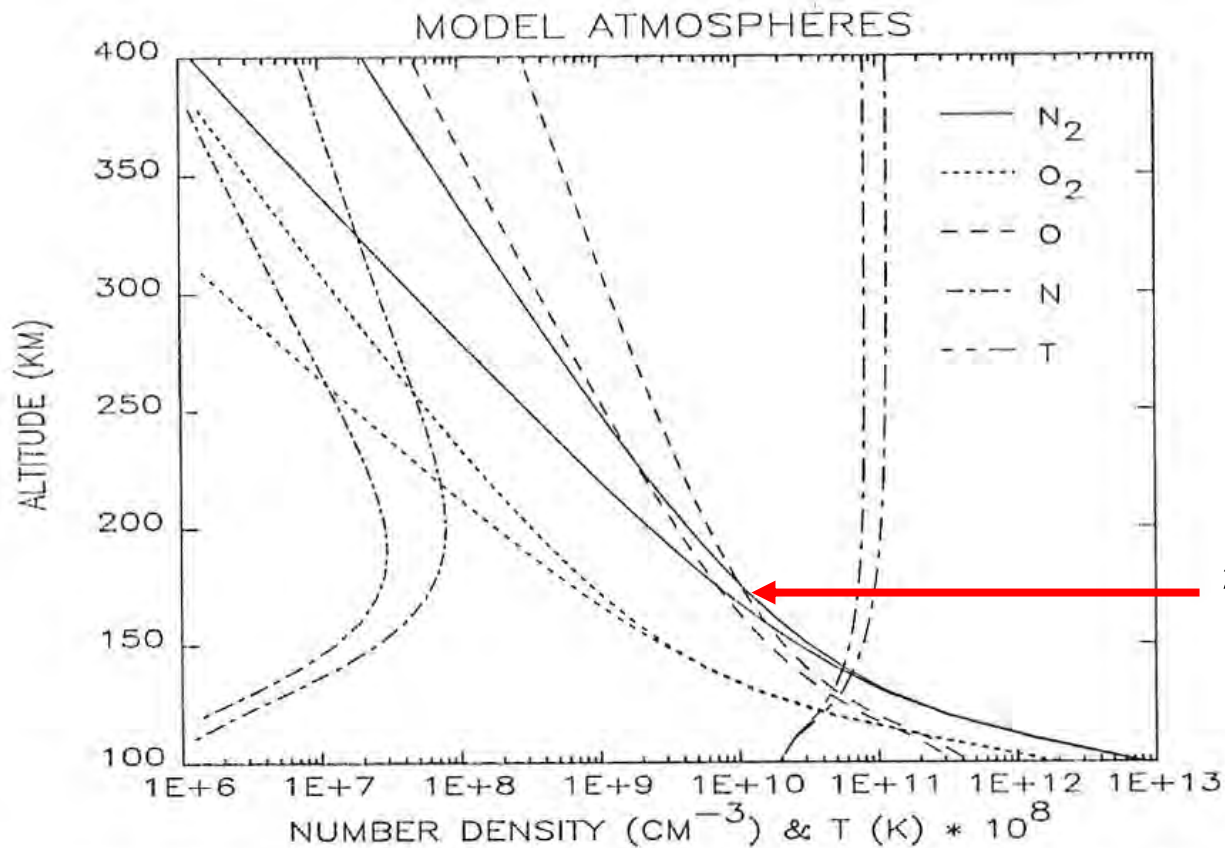
Inversion Techniques can be Applied to GUVI Disk Data to Yield Vertical Structure

Inversion techniques can be applied to a number of problems including the use of disk observations to produce height information. These inversions and comparisons (Comberiate et al., 2005; 2006) have been demonstrated to be consistent with optical and radar observations.



Comparison of inversion of GUVI data with Julia radar images of EsF from Comberiate et al 2006

The Landscape of the Neutral Atmosphere



$$\eta_{\text{N}_2} = \int_z^{\infty} [\text{N}_2] dz = 10^{17} \text{ cm}^{-2}$$

Fig. 30. Atmospheric composition from the MSIS-86 model at solar min (left curves) and max (right curves). The conditions chosen to represent min and max are given in Table VI. Temperature has been multiplied by 10^8 to be on scale.

Tracing the Thermospheric Response Using the O/N₂ Ratio

- The ratio of 135.6 to LBH column emission rates has a close connection to ratio of corresponding column densities.
- GUVI uses 135.6/LBH ratio to obtain O to N₂ column density ratio (designated as O/N₂).
- O/N₂ changes as the depth of N₂ changes
- The process is to pick an N₂ depth and examine the uniqueness of 135.6/LBH to O/N₂ at this depth.
- Strickland and Paxton (1992) first looked at this and found a strong correlation between calculated intensities and changes in thermospheric composition.
- Strickland, Evans, and Paxton (1995) have determined that the least spread in O/N₂ for a given value of 135.6/LBH occurs near an N₂ depth of 10¹⁷ cm⁻² (near 170 km). The standard deviation is less ~ 1%.

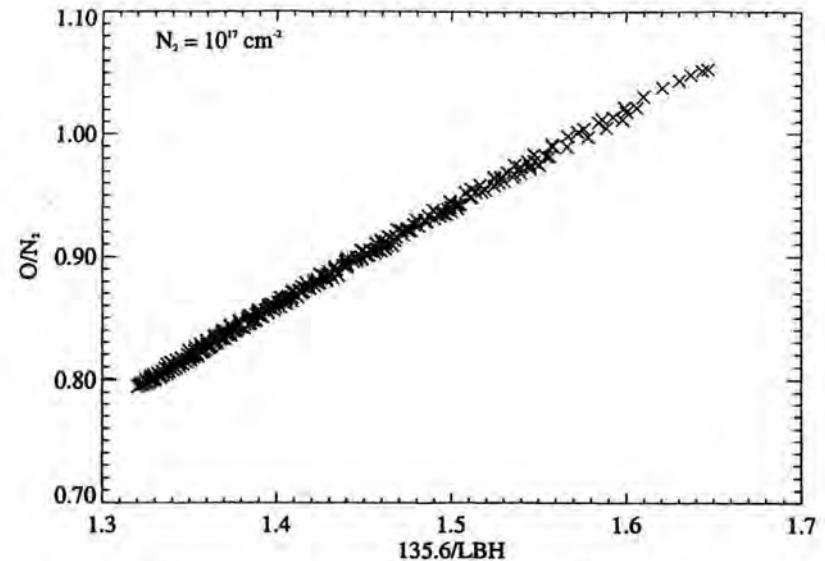
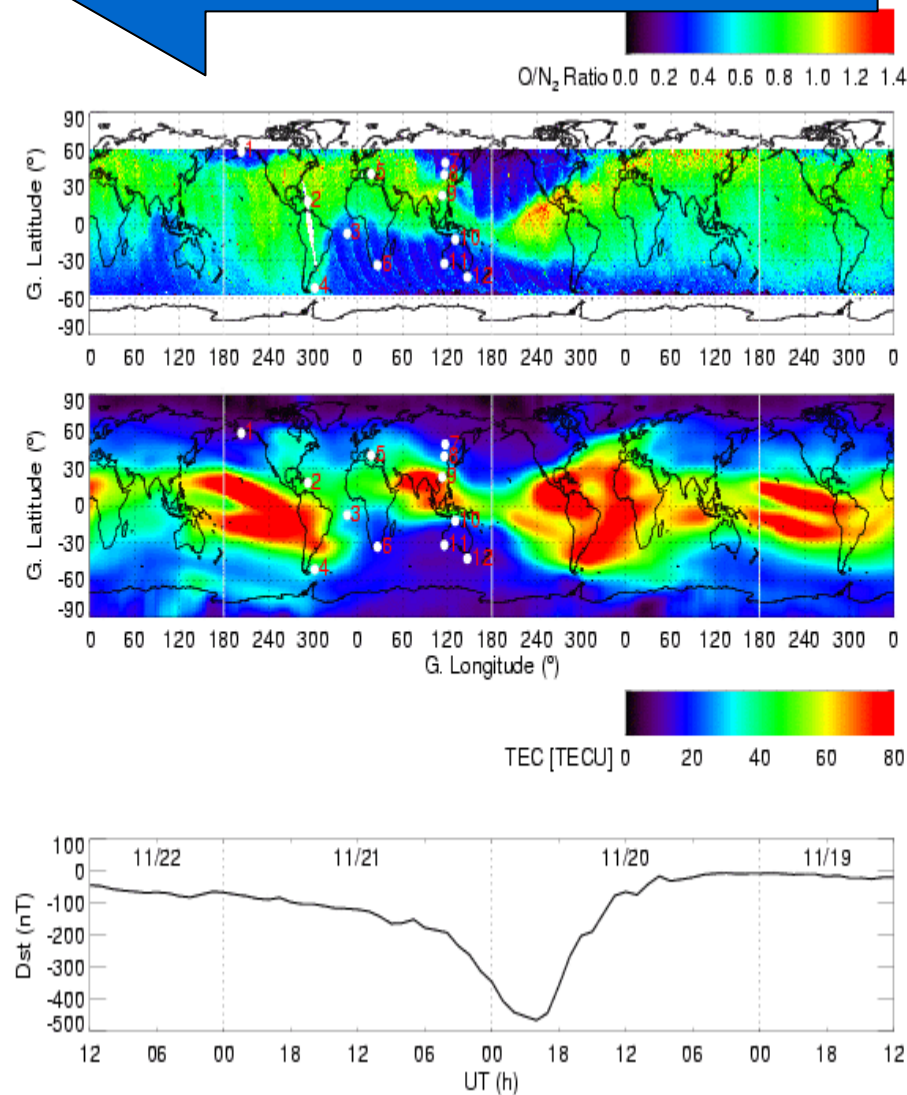


Figure 9. O/N₂ versus 135.6/LBH at an N₂ reference depth of 10¹⁷ cm⁻² for the 324 unscaled TIGCM atmospheres. The results show that a nearly proportional relationship exists with uncertainty consistent with that shown in Figure 7b.

Nov. 20, 2003

Time increases this way

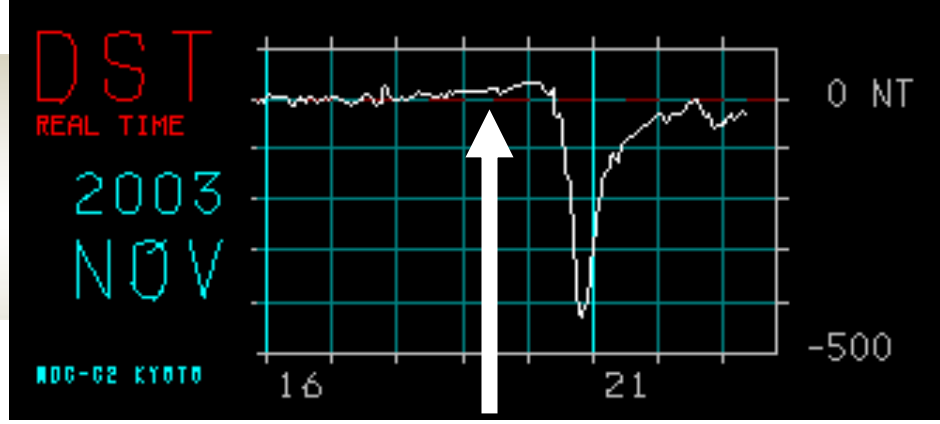
GUVI O/N_2 is well correlated with the negative phase of an ionospheric storm.



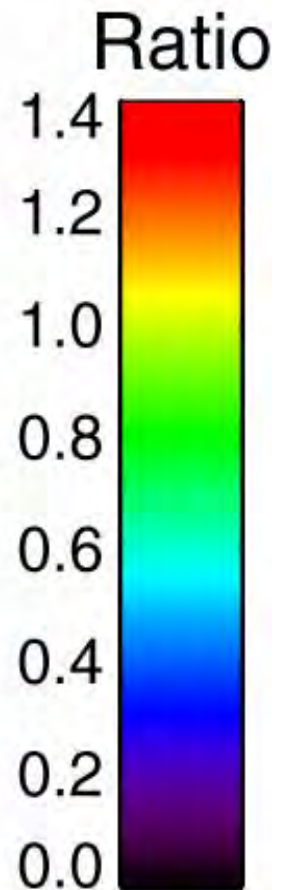
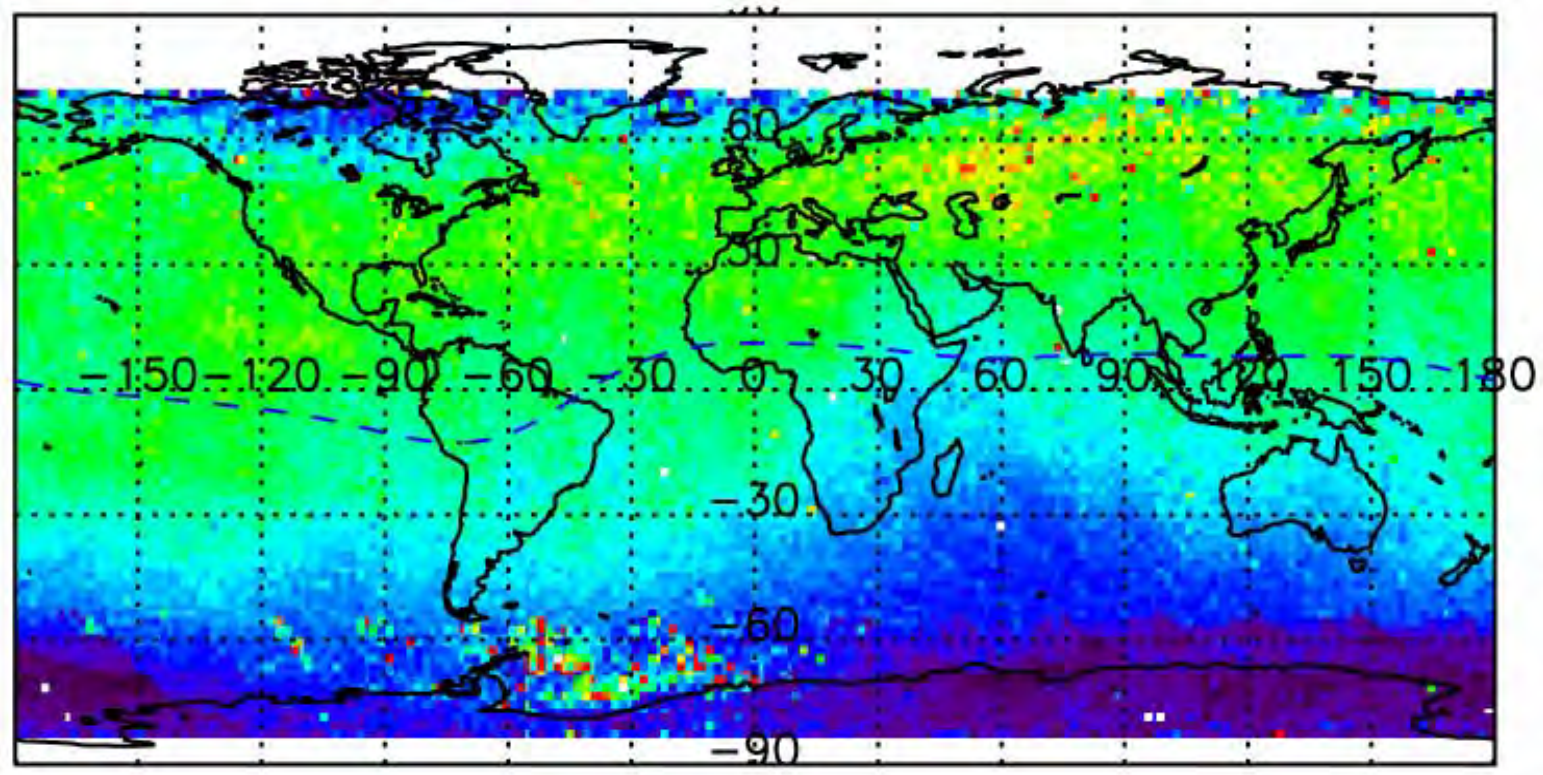
O/N_2 ratio
(TIMED/GUVI)

GPS TEC
(JPL)

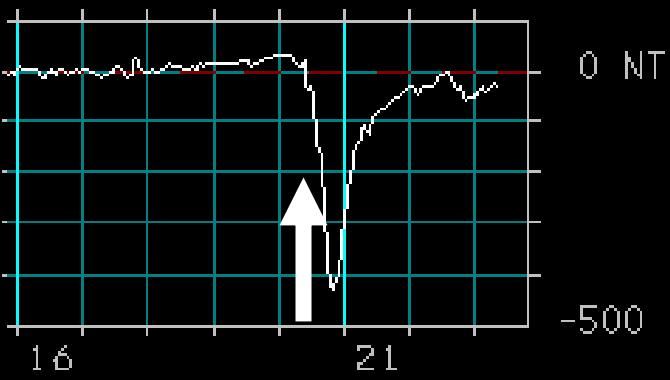
Dst



GUVI O/N₂ Ratio Nov 19, 2003

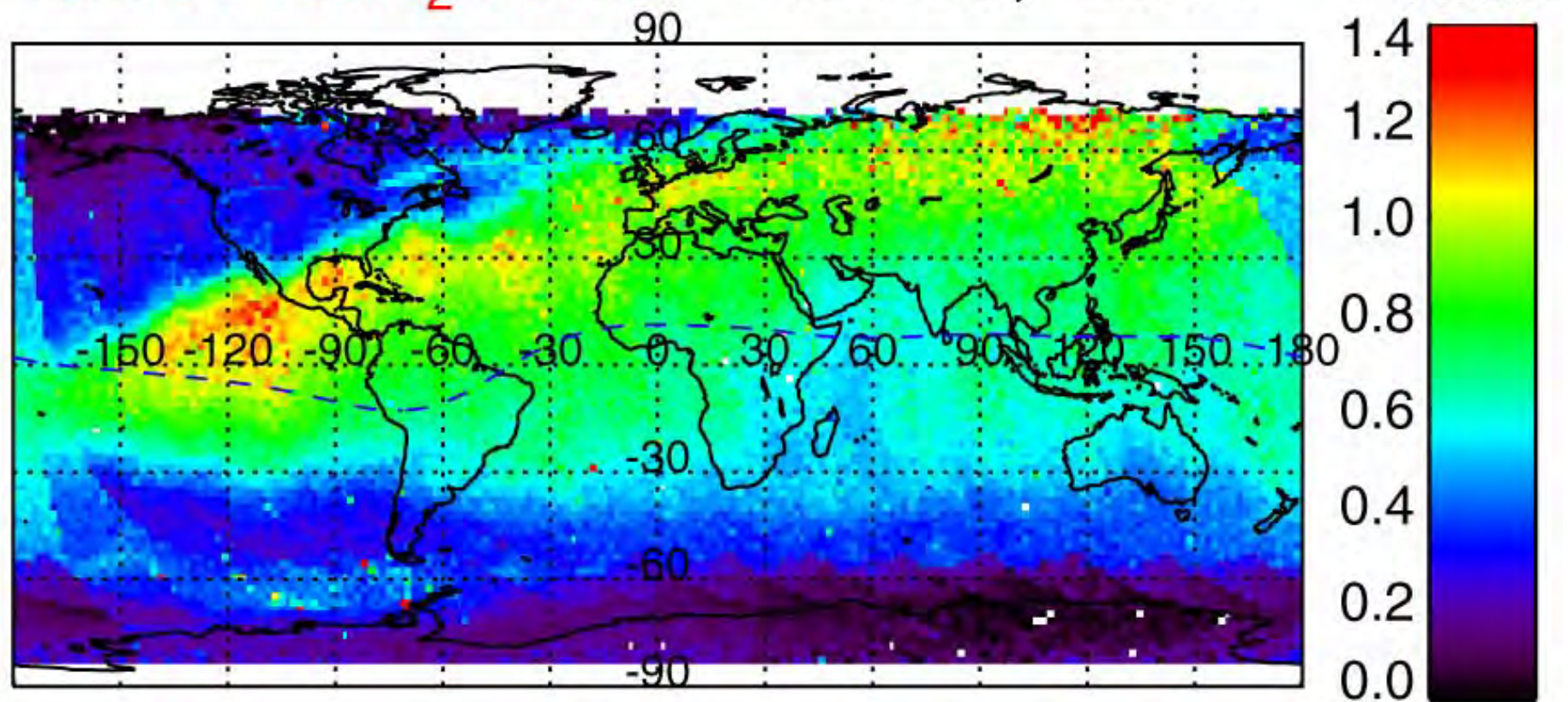


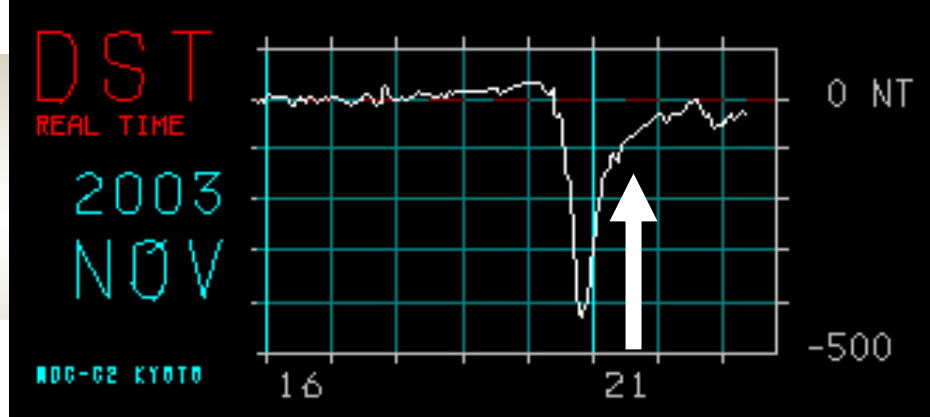
DST
REAL TIME
2003
NOV
MOC-02 KYOTO



GUVI O/N₂ Ratio

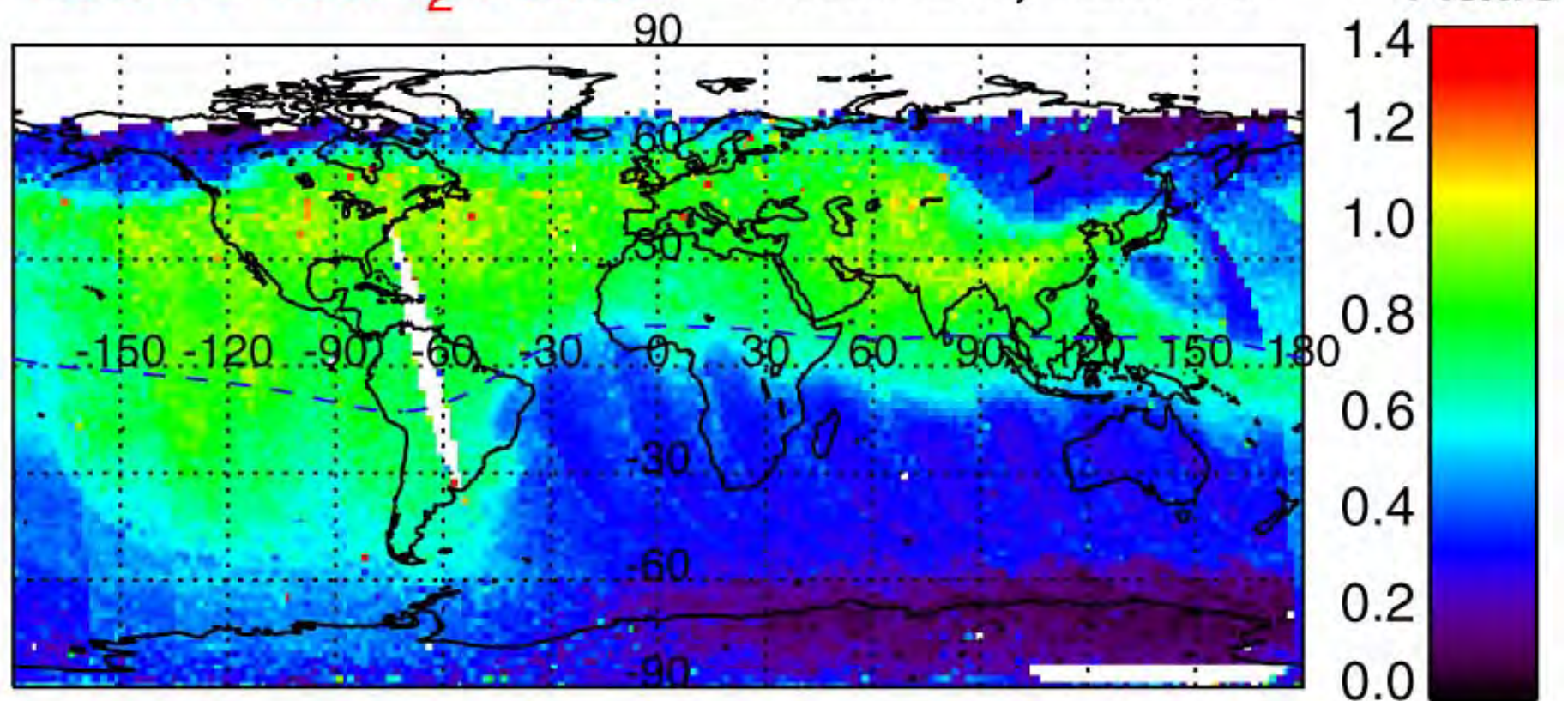
Nov 20, 2003

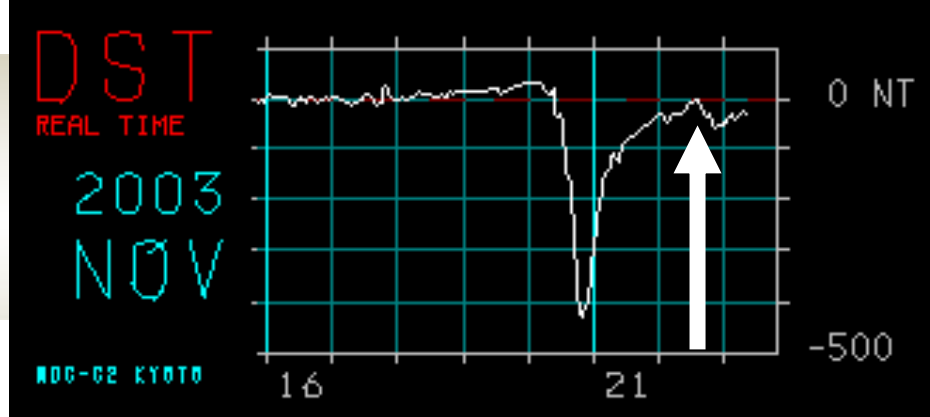




GUVI O/N₂ Ratio

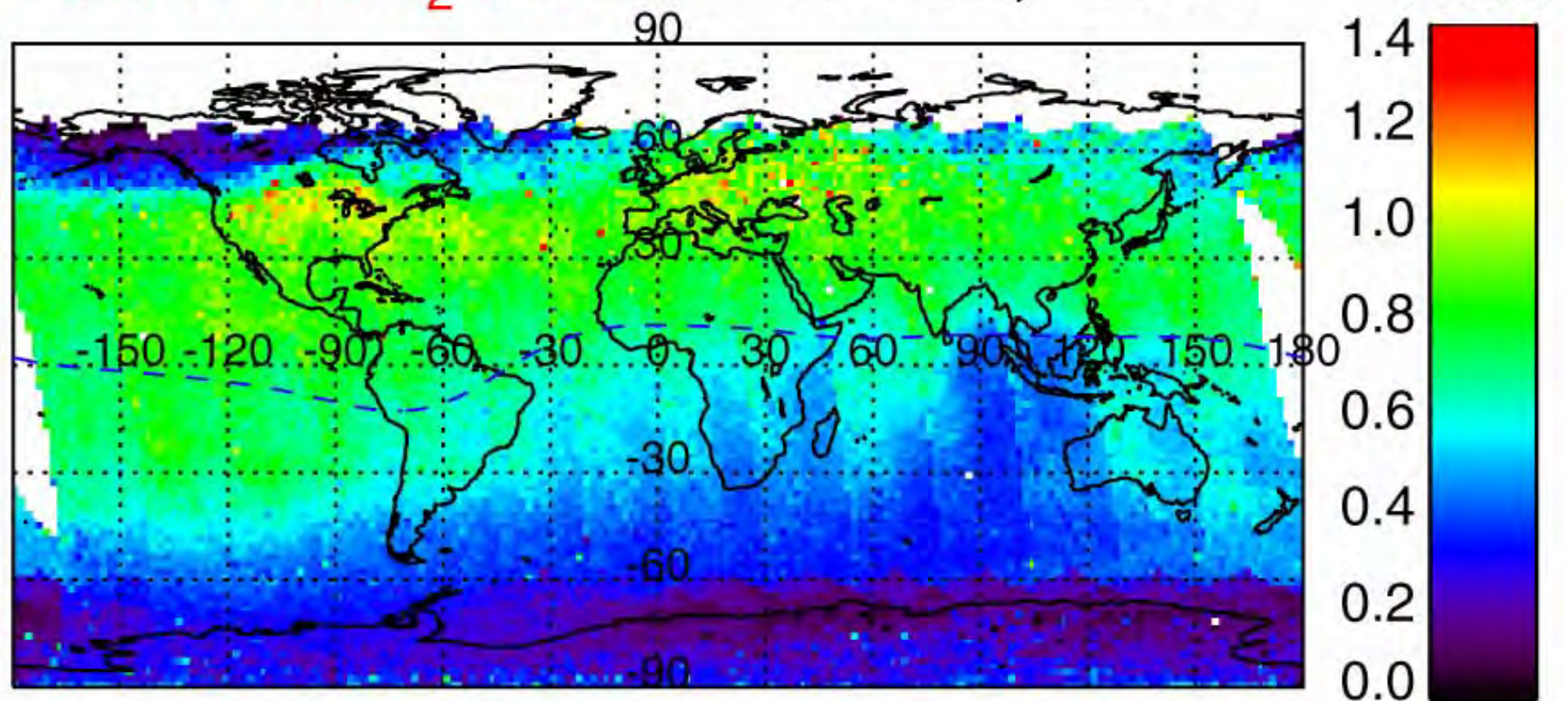
Nov 21, 2003





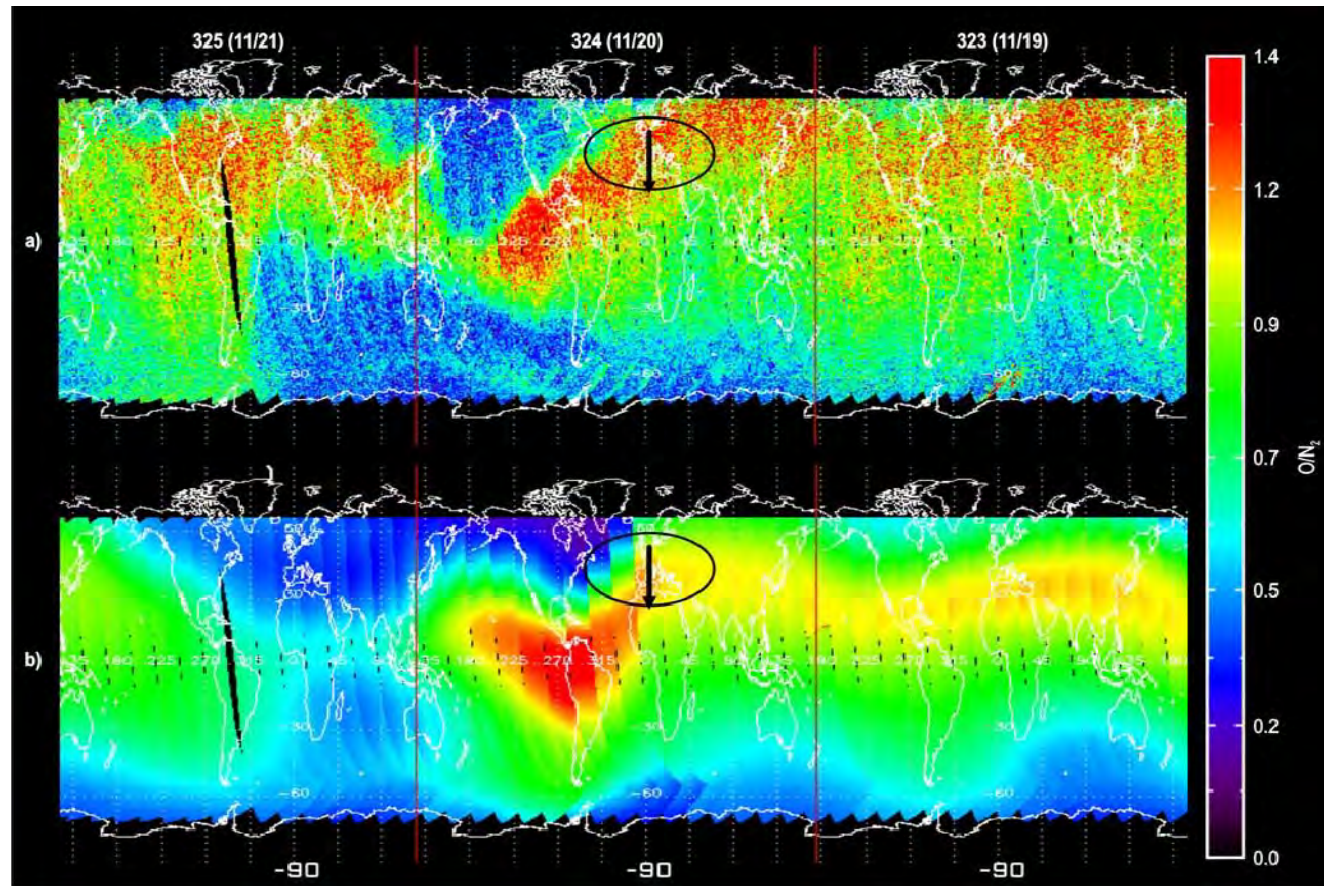
GUVI O/N₂ Ratio

Nov 22, 2003



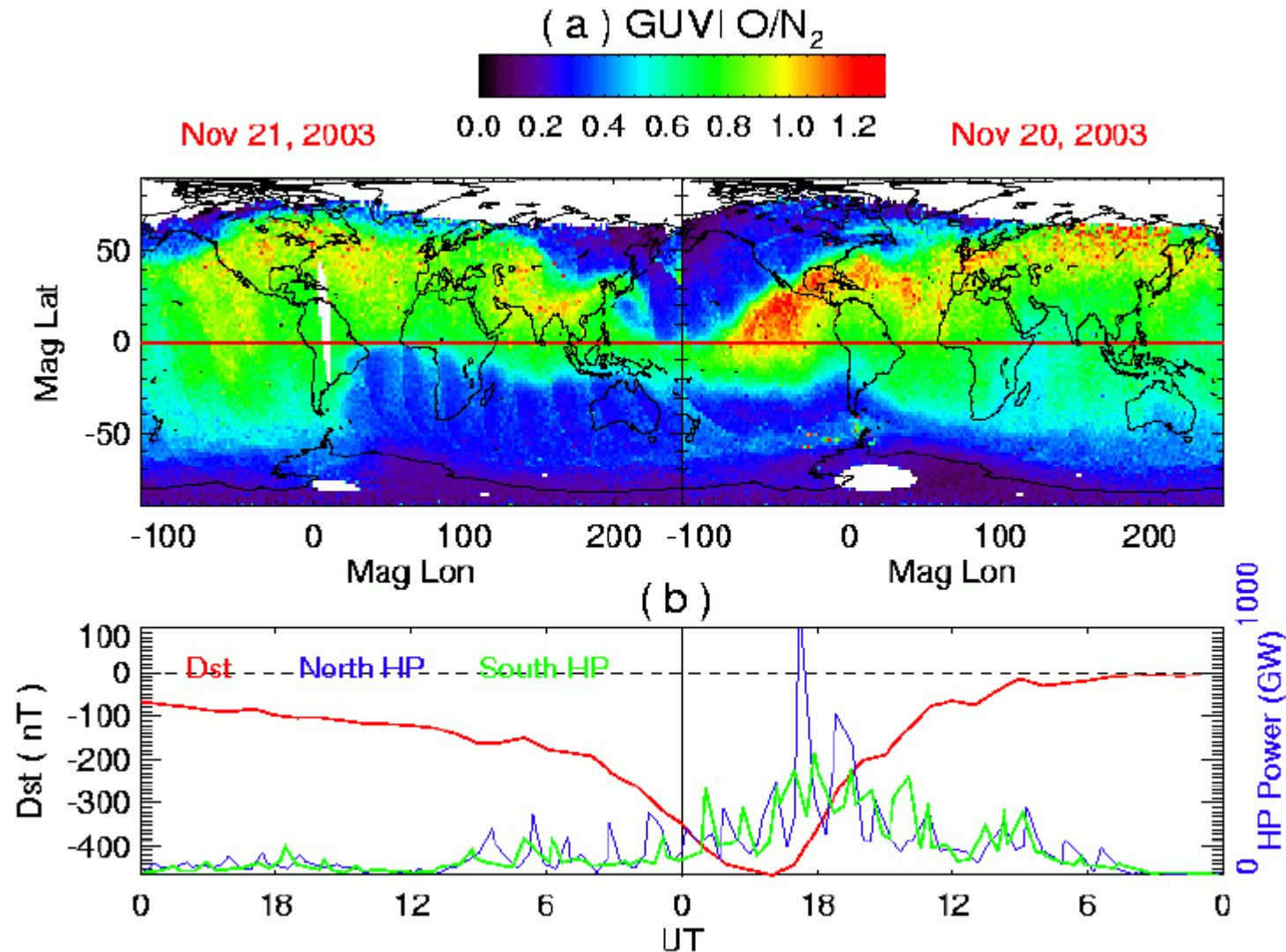
Storms Provide Useful Test Cases

The comparison of a dynamically driven quantity, such as O/N_2 , between observations and models allows us to test whether we have the onset and recovery phase of storms correctly modeled.



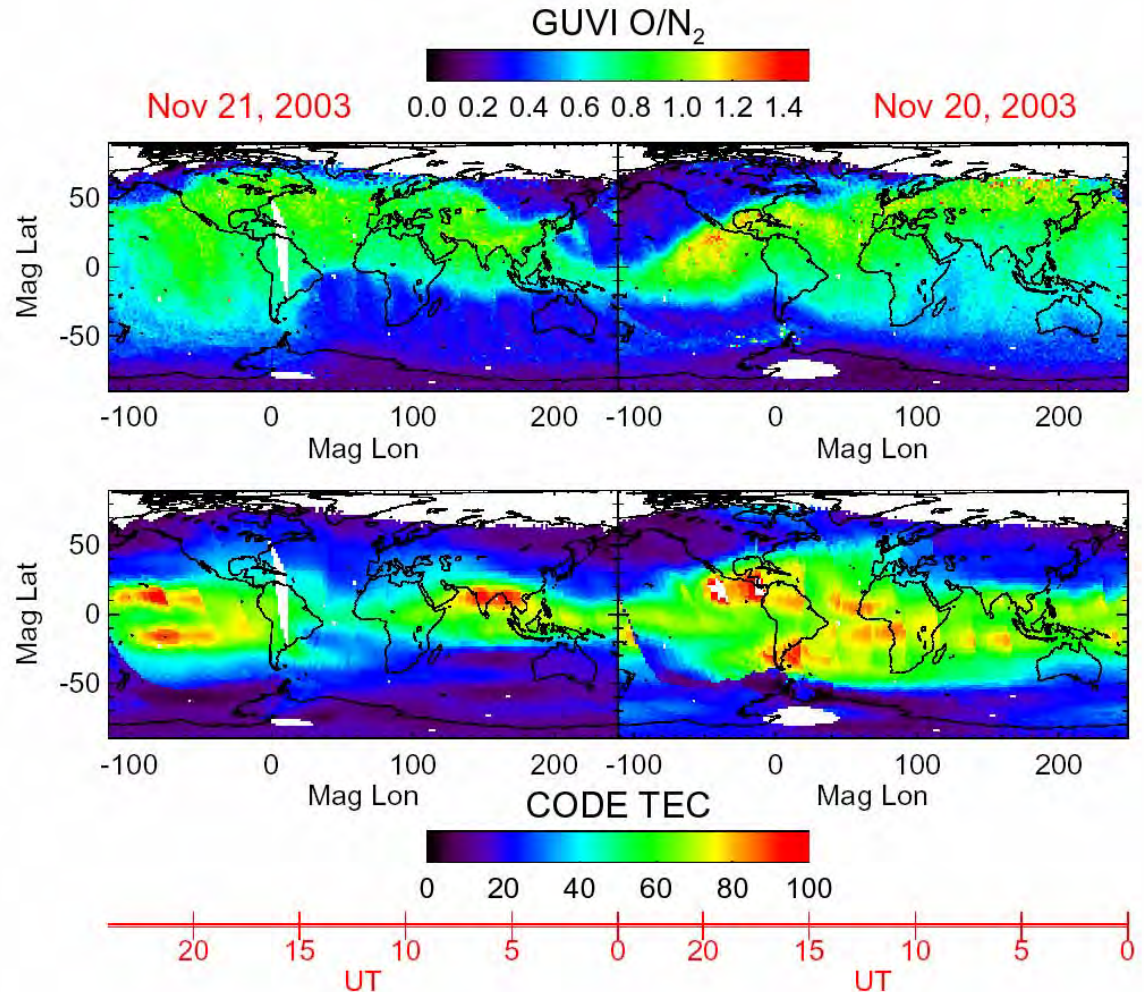
From Geoff Crowley's initial comparison with TIMEGCM

Was there an Effect Due to the Asymmetric Inputs?



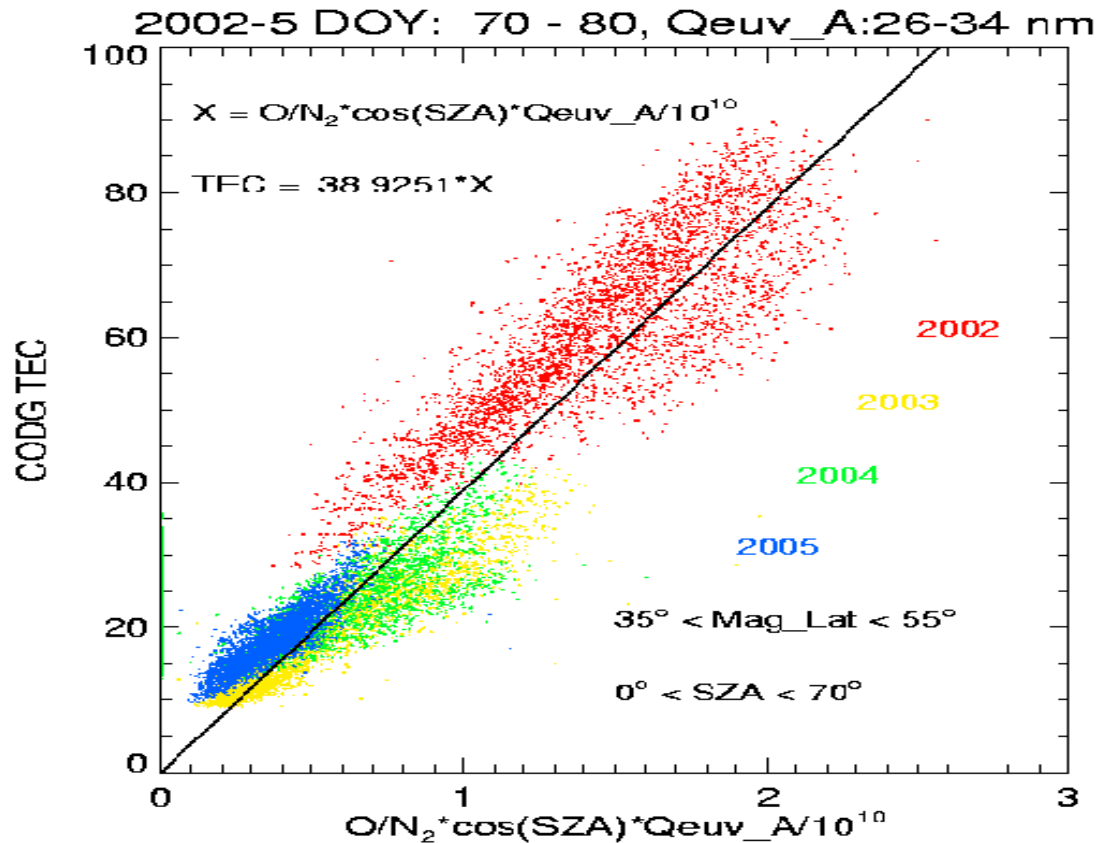
What Drives the Differences?

- Superstorms are particularly difficult to model and, more importantly, it is difficult to validate the model with observations
- There are coupling pathways that tie the ions and neutrals.
- We are just beginning to explore these pathways by using coordinated data analysis.

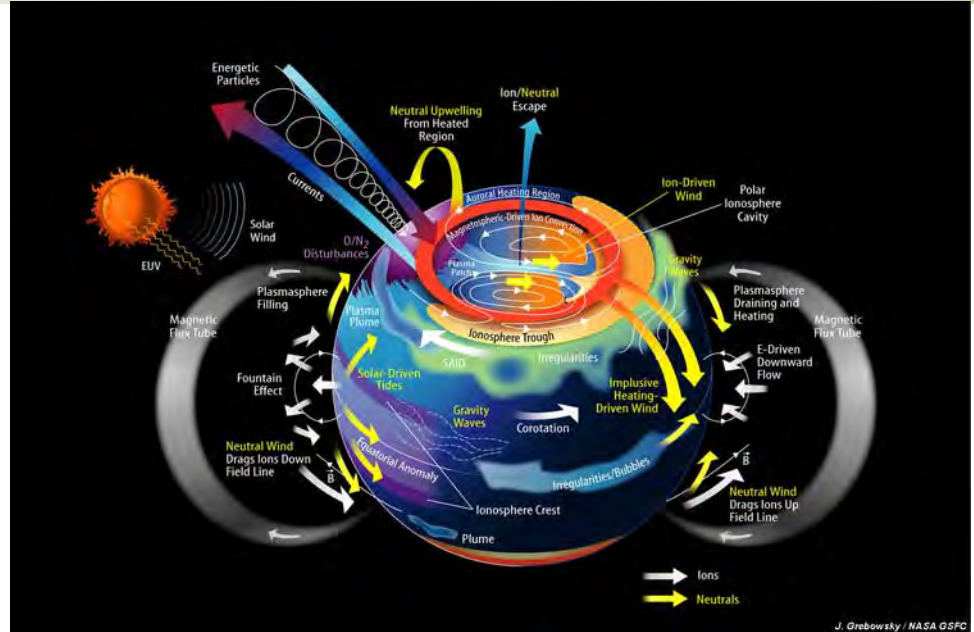
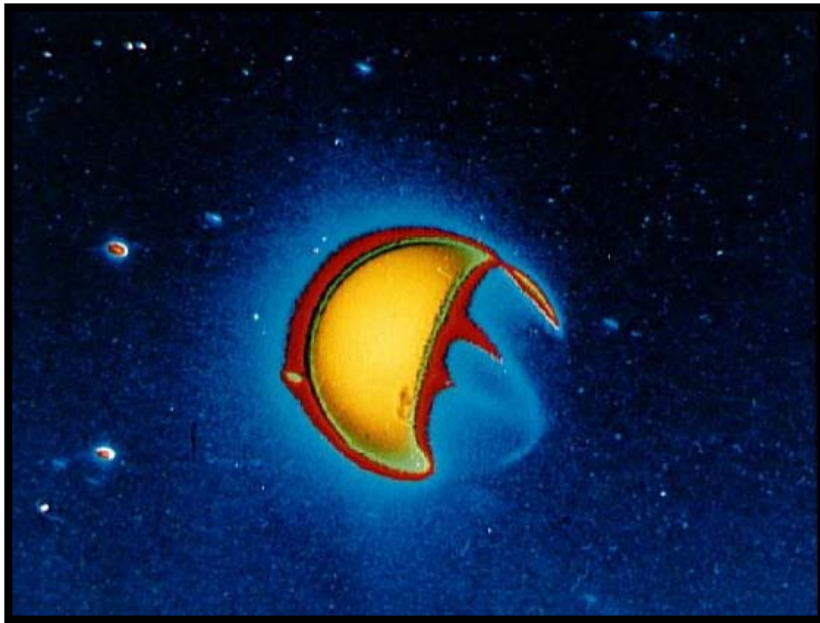


GUVI Observations of Midlatitude O/N₂ may help us understand the Relative Roles of Composition and Dynamics in Determining TEC

- Now that we have a large database of O/N₂ and GPS TEC measurements for quiet and disturbed times, for all seasons and all local solar times we can do a simple comparison between TEC and O/N₂.



We've Talked About Many of The Processes in the Coupled IT System and How UV Remote Sensing Can Be Used to Inform Our Exploration of Geospace



FUV remote sensing is a tool that has evolved over the last 35 years.

We have the tools and means in place to address the fundamental processes that shape the ionosphere-thermosphere system and connect the IT to the rest of geospace and the lower atmosphere.

What I would have liked to have told you about...

- The exciting work being done using GUVI and SuperDARN
- The use of UV imagery in AMIE
- Using two H Lyman α channels to determine the flux and energy of precipitating protons.
- Using all-reflection UV interferometers to determine velocities and outflow rates.
- How we might be able to determine the O/N₂ and O₂/N₂ in the aurora.
- How the OI 130.4 nm and 164.1 nm emission could be used to probe O and O₂ in the lower thermosphere.
- More about the use of UV imagery to investigate the morphology of ionospheric bubbles and tides/waves in the ionosphere
- More about how we might be able to extract effective meridional winds and ExB drifts from nightside ionospheric imagery
- The use of multicolor limb retrievals to constrain, O, O₂, N₂, and O⁺ on the dayside
- And more....

Where are the data?

GUVI Global Ultraviolet Imager - Microsoft Internet Explorer

Address: http://guvi.jhuapl.edu/

GUVI Global Ultraviolet Imager

HOME

- SCIENCE OBJECTIVES
- FACT SHEET
- WHATS NEW

OVERVIEW

EXTENDED MISSION

USING GUVI DATA

GUVI DATA PRODUCTS

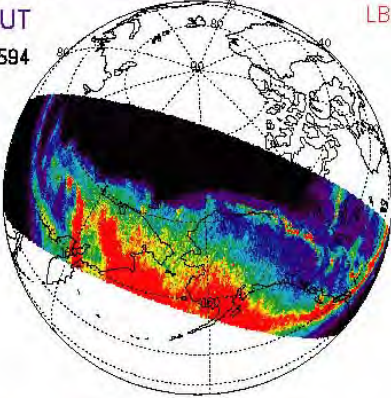
SUMMARY IMAGES

PUBLICATIONS

EDUCATION

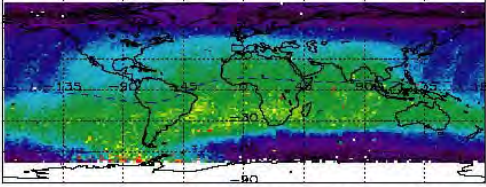
May 15, 2005
0653:00 UT
Orbit #: 18594

GUVI L1B
LBHS Data
kR



12
10
8
6
4
2
0

GUVI O/N₂ Ratio **May 16, 2005**



Ratio

1.4
1.2
1.0
0.8
0.6
0.4
0.2
0.0

12:34	12:35	12:37	12:39	12:40	12:42
19:45	16:30	13:16	10:02	06:48	03:34

LT
UT

The Johns Hopkins University Applied Physics Laboratory

The Last Updated: October 12, 2005

Done Internet

Where are the data?

GUVI.jhuapl.edu

GUVI Global Ultraviolet Imager - Microsoft Internet Explorer

Address: http://guvi.jhuapl.edu/

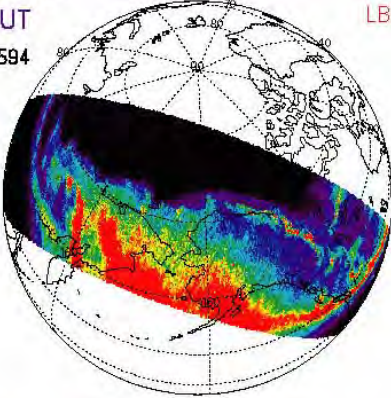
GUVI Global Ultraviolet Imager

HOME

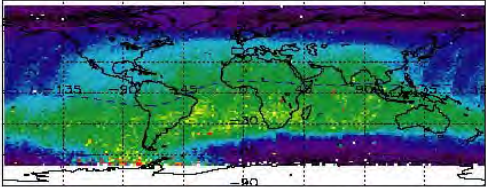
- SCIENCE OBJECTIVES
- FACT SHEET
- WHATS NEW
- OVERVIEW
- EXTENDED MISSION
- USING GUVI DATA
- GUVI DATA PRODUCTS**
- SUMMARY IMAGES
- PUBLICATIONS
- EDUCATION

May 15, 2005
0653:00 UT
Orbit #: 18594

GUVI L1B
LBHS Data
kR



GUVI O/N₂ Ratio May 16, 2005



12:34	12:35	12:37	12:39	12:40	12:42
19:45	16:30	13:16	10:02	06:48	03:34

LT
UT

The Johns Hopkins University Applied Physics Laboratory
The Last Updated: October 12, 2005

Data and Images are Available

GUVI Global Ultraviolet Imager

GUVI Data Products

LEVEL 1A Data Products
[Spectrograph](#)

LEVEL 1B Data Products (Current Version: *version 8*)
[Imaging](#) [Static Imaging](#)

LEVEL 1C Data Products (Current Version: *version 3*)
[Disk](#)

LEVEL 2B Data Products
[Day](#) [Limb](#)

LEVEL 3 Data Products

Aurora Data Products (E_0 and Q)	Summary Images	Data Files
Thermospheric O/N ₂	Summary Images	Data Files
Electron Density Profiles	Summary Images	Data Files
O/N ₂ and Total Electron Content (TEC)	Summary Images	CODE-TEC O/N₂ Data Files

Support Data Products
[GUVI Housekeeping](#)

The Johns Hopkins University Applied Physics Laboratory The Last Updated: October 21, 2005

- **Level 1B data are calibrated and geolocated**
- **Level 2B are gridded**
- **Level 3 are higher level data products**
 - **Available as pictures or as numbers!**

Data and Images are Available

GUVI Global Ultraviolet Imager - Microsoft Internet Explorer

Address: http://guvi.jhuapl.edu/guvi_accessdata.html

GUVI Global Ultraviolet Imager

HOME
OVERVIEW
EXTENDED MISSION
USING GUVI DATA
GUVI DATA PRODUCTS
ACCESS GUVI DATA
DATA USAGE
DATA AVAILABILITY
SUMMARY IMAGES
PUBLICATIONS
EDUCATION

GUVI Data Products

LEVEL 1A Data Products
[Spectrograph](#)

LEVEL 1B Data Products (Current Version: *version 8*)
[Imaging](#) [Static Imaging](#)

LEVEL 1C Data Products (Current Version: *version 3*)
[Disk](#)

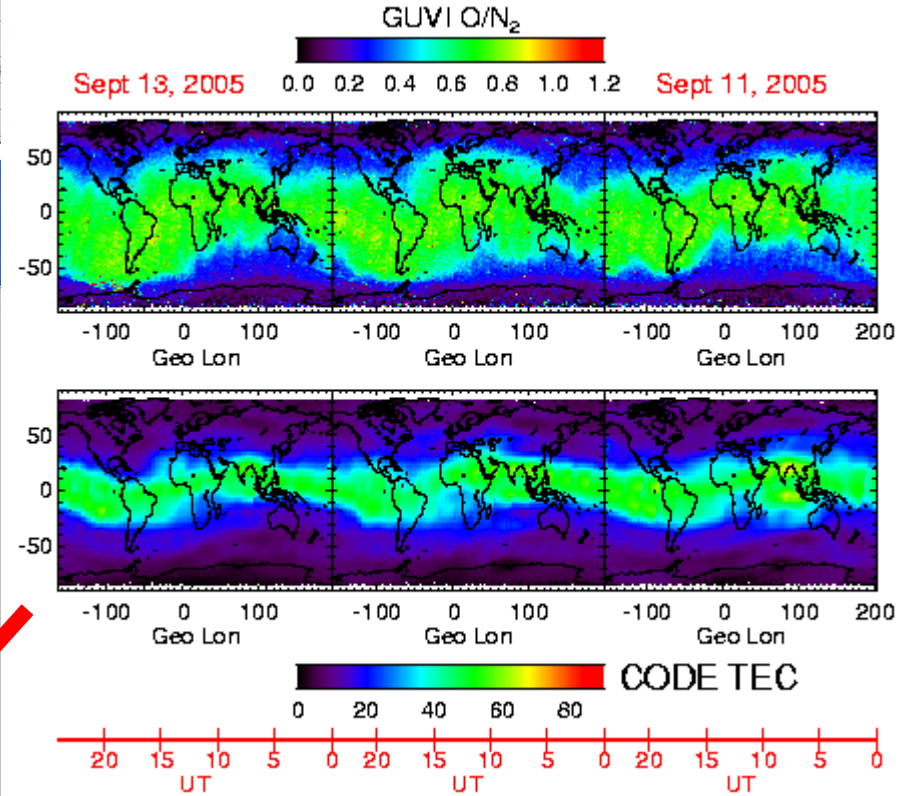
LEVEL 2B Data Products
[Day](#) [Limb](#)

LEVEL 3 Data Products

Aurora Data Products (E ₀ and Q)	Summary Images	Data Files
Thermospheric O/N ₂	Summary Images	Data Files
Electron Density Profiles	Summary Images	Data Files
O/N ₂ and Total Electron Content (TEC)	Summary Images	CODE-TEC O/N₂ Data Files

Support Data Products
[GUVI Housekeeping](#)

The Johns Hopkins University Applied Physics Laboratory The Last Updated: October 21, 2005



References

There are a number of references available that cover various aspects of UV/Vis phenomenology.

The seminal works are:

Barth, C.A., *Ultraviolet spectroscopy of planets*, Jet Propulsion Laboratory Tech. Rpt. 32-822, Pasadena, Ca, 1965.

The basic reference for much of UV/Vis backgrounds phenomenology is still:

Chamberlain, J.W., *Physics of the Aurora and Airglow*, Academic Press, New York, 1961.

even though some of the material is dated. Additional material can be found in

Chamberlain, J.W., and D.M. Hunten, *Theory of Planetary Atmospheres*, Academic Press, New York, 1987.

Auroral spectroscopy is discussed in

Vallance Jones, A., *Aurora*, D.Reidel Publ. Co., Dordrecht, 1974.

Omholt, A. *The Optical Aurora*, Springer-Verlag, Heidelberg, 1971.

The most recent attempt at a comprehensive review of UV phenomenology is

R.R. Meier, *Ultraviolet spectroscopy and remote sensing of the upper atmosphere*, *Space Sci. Rev.*, 1991.

Others include:

Meier, R.R., *Thermospheric aurora and airglow*, *Rev. Geophys.* 25, 471, 1987.

More of the forgotten lore...

Vallance Jones, A., R.R. Meier, and N.N. Shefov, Atmospheric quantal emissions: A review of recent results, *J. Atmos. Terr. Phys.*, **47**, 623-642, 1985.

Hunten, D.M., Airglow an introduction and review, in *The Radiating Atmosphere*, ed. B.M. McCormac, pp3-16, Springer-Verlag, New York, 1971.

Hunten, D.M., Spectroscopic studies of the twilight airglow, *Space Sci. Rev.*, **6**, 493, 1967.

A number of reviews covering the nightglow are available:

Forsyth, R.J., and P.C. Wraight, A survey of research on nightglow variability, *Planet. Space Sci.*, **35**, 1449-1461, 1987.

Kulkarni, P.V., Tropical airglow, *Ann. Geophys.*, **30**, 105, 1974.

The Rayleigh is defined in

RT References from the Dawn of Time

Radiative transport in planetary atmospheres is addressed at a basic level in many of the texts above. A number of techniques are discussed in:

Lenoble, J., *Radiative Transfer in Scattering and Absorbing Atmospheres: Standard Computational Techniques*, A. Deepak, 1985.

Mihalas, D., *Stellar Atmospheres*, W.H. Freeman and Co., San Francisco, 1978.

Ivanov, V.V., *Transfer of Radiation in Spectral Lines*, NBS Publ. 385, NBS, 1973.

Chandrasekhar, S., *Radiative Transfer*, Dover Publ., New York, 1952.

Chandrasekhar and Ivanov are primarily concerned with analytic approaches to the problem. The standard references for UV work are:

Strickland, D.J., and T.M. Donahue, Excitation and radiative transport of OI 1304Å resonance radiation- I. The dayglow, *Planet. Space Sci.*, 18, 661-689, 1970.

Strickland, D.J., and M.H. Rees, The OI 1304 and 1356 emissions in aurorae, *Planet. Space Sci.*, 22, 465-481, 1974.

The solution of the problem for a generalized spherical atmosphere is discussed in

Anderson, D.E., Jr., and C.W. Hord, Multidimensional radiative transfer: Application to planetary coronae, *Planet. Space Sci.*, 25, 563, 1977.

Inversions

Twomey, S., *Introduction to the Mathematics of Inversion in Remote Sensing and Indirect Measurements*, Elsevier, New York, 1977.

Menke, W., *Geophysical Data Analysis: Discrete Inverse Theory*, Academic Press, New York, 1989.

REFERENCES TO DAYSIDE DISK O/N₂ AND Q_{EUUV} ALGORITHMS AND APPLICATIONS

- Strickland, D.J., R. Link, and L.J. Paxton, Far Uv remote sensing of thermospheric composition, *Ultraviolet Technology IV, SPIE vol. 1764*, 117-131, 1992.
- Strickland, D. J., J. S. Evans, and L. J. Paxton, Satellite remote sensing of thermospheric O/N₂ and solar EUV: 1. Theory, *J. Geophys. Res.*, **100**, 12,217, 1995.
- Evans, J. S., D. J. Strickland, and R. E. Huffman, Satellite remote sensing of the thermospheric O/N₂ and solar EUV: 2. Data analysis, *J. Geophys. Res.*, **100**, 12,227, 1995.
- Strickland, D. J., R. J. Cox, R. R. Meier and D. P. Drob, Global O/N₂ derived from DE-1 FUV imaging dayglow data: Technique and examples from two storm periods, *J. Geophys. Res.*, **104**, 4251, 1999.
- Drob, D. P., R. R. Meier, J. M. Picone, D. J. Strickland, R. J. Cox, and A. C. Nicholas, Atomic oxygen in the thermosphere during the July 13, 1982 solar proton event deduced from far ultraviolet images, *J. Geophys. Res.*, **104**, 4267, 1999.
- Strickland, D. J., R. E. Daniell, and J. D. Craven, Negative ionospheric storm coincident with DE-1 observed thermospheric disturbance on October 14, 1981, *J. Geophys. Res.*, in press, 2000.

In the Case of Single Scattering Without Absorption the Equations are Very Simple

$$\text{Ch}\left(\chi, \frac{r_0}{H}\right) = \frac{\int_{r_0}^{\infty} n(r) V(\chi, r) dr}{\int_{r_0}^{\infty} n(r) dr} = \frac{\eta(\chi, r_0)}{\eta(\chi=0, r_0)}$$

$$4 \pi I(\chi, r_0) = g \text{Ch}\left(\chi, \frac{r_0}{H}\right) \int_{r_0}^{\infty} n(r) dr = g \text{Ch}\left(\chi, \frac{r_0}{H}\right) n(r_0) H$$

$$4 \pi I(\chi=90^\circ, r_0) = g \left(\frac{2 \pi r_0}{H}\right)^{\frac{1}{2}} n(r_0) H$$

